MEASUREMENT AND CHARACTERISATION OF MICRO/NANO-SCALE STRUCTURED SURFACES

---

by

Zhu Hao

A thesis submitted to The University of Huddersfield in accordance with the requirements for the degree of Doctor of Philosophy (Ph.D.)

EPSRC Centre for Innovative Manufacturing in Advanced Metrology

School of Computing & Engineering

University of Huddersfield

November 2012

Abstract

Micro/nano-scale structured surfaces play a critical role in precision engineering. For Microelectromechanical Systems (MEMS), they are key factors to ensure the system's functional performance. However, the measurement and characterisation of micro/nano-scale structured surface is still a great challenge for metrologists. As the size of structured surface features is in the range of nm-pm, the traditional measurement methods are no longer available for the micro/nano-scale structured surfaces. The reason is that the conventional measurement instruments often cannot reach the precision of the required measurement task. Moreover, the conventional characterisation and evaluation methods are not applicable for the micro/nano-scale structured surfaces due to their unique characteristics compared to macro engineered surfaces. Therefore, theoretical research of measurement and characterisation for micro/nano-scale structured surfaces needs to be carried out to meet the requirements for future inspection instruments.

The aim of this thesis is to establish a practical measurement guide and develop a methodology for characterisation and evaluation of micro/nano scale structured surfaces. The presented thesis has reviewed the definitions and classifications of structured surfaces. Their most significant applications in MEMS have been introduced. Measurement methods for structured surfaces based on different principles have been investigated. Measurement instruments employed throughout the research of the project have been summarized. To improve the evaluation efficiency, a new classification is given based on the surfaces' micro feature characteristics. Datum planes for structured surfaces have been established. Surface data pre-processing, including data enhancement and denoising techniques have been developed. To extract the primary form of the structured surface, a novel feature extraction algorithm based on active contours has been developed and compared with low-level feature extraction techniques. For micro structured steps, evaluation parameters and methods have been investigated with corresponding case studies.

Acknowledgements

The author would like to express his profound gratitude to his supervisor Professor Liam Blunt. This thesis would not have been complete without his continuous advice and encouragement throughout the course. Furthermore, the good advice, support and friendship of the author's second supervisor, Professor Jane Jiang, has been invaluable on both an academic and a personal level. The author is deeply grateful for their generosity in laboratory facilities, technical assistance and creating the wonderful environment which has made this project possible.

Moreover, the work was co-supervised by Dr. Shaojun Xiao, who as a colleague and friend. His guidance during the first half of the work is quite valuable.

Thanks are due to Dr. Tukun Li, Dr Wenhan Zeng and Dr. Qunfen Qi whose useful comments and guidance offered the author great help during his thesis writing-up.

The past and present members of the Centre for Precision Technologies (CPT) and the EPSRC Centre for Innovative Manufacturing in Advanced Metrology (Prof. Paul Scott, Dr.Feng Gao, Dr. Paul Bills, Dr. Leigh Fleming, Dr. Haydn Martin, Xiangqi Lan, Jian Wang, Hao Ding, Shengyue Zeng, Shan Lou and Hussam Muhamedsalih) have also a great help and their enthusiasm and inspiration enhanced the quality of the author's working life.

The author would like to thank all his friends in Huddersfield for helping him get over some of the lows of the last few years. Their encouragement helped author to complete his study.

Very special thanks are due to my wife, Ting Li for her unfailing support over the years. My profound gratitude also goes out to my family (mum, dad, grandma and MengMeng, my lovely daughter).

Contents

List of Figures

List of Tables

Abbreviations

MEMS:	Microelectromechanical systems
MST:	Micro Systems Technology
IC:	Integrated Circuit
MTSR:	Microsystems Technology Standardization Roadmap
NIL:	Nanoimprint Lithography
EDM:	Electric Discharge Machining
CVD:	Chemical Vapor Deposition
LPCVD:	Low-Pressure Chemical Vapor Deposition
SPM:	Scanning Probe Microscopy
ICT:	Information and Communication Technology
ITRS:	International Technology Roadmap for Semiconductors
RCHD:	Reflective Cylindrical Holographic Diffraction
WLI:	White Light Interferometry
PSI:	Phase Shifting Interferometry
VSI:	Vertical Scanning Interferometry
PZT:	Piezoelectric Transducer
CCI:	Coherence Correlation Iterferometer
SPM:	Scanning Probe Microscopy
AFM:	Atomic Force Microscopy
MM:	Mathematical Morphology
DTCWT:	Dual-tree Complex Wavelet Transform
DWT:	Discrete Wavelet Transform
HT:	Hough Transform
LP:	Linear Primitive
GAC:	Geometric Active Contours
ISO:	International Organization for Standardization
NIST:	National Institute of Standards and Technology
PEB:	Post Exposure Bake
LER:	Line Edge Roughness
LWR:	Line Width Roughness
RMS:	Root Mean Square
NPL:	National Physical Laboratory

List of Related Publications

Zhu H, X Jiang and S Xiao (2006). "*Metrology and testing technology of Micro-Electro-Mechanical-System (MEMS) annual report 2006: PartⅣ*". National Natural Science Foundation of China Key Project: 50535030. pp. 103-129.

Zhu H, L Blunt, X Jiang and S Xiao (2006). "*Measurement and Characterisation of Micro/nano-scale Structured Surfaces*". In: Proceedings of Computing and Engineering Annual Researchers' Conference 2006: CEARC'06. Poster. University of Huddersfield, Huddersfield.

Zhu H, X Jiang and S Xiao (2007). "*Measurement & Chraterisation of Micro-Electro-Mechanical-System (MEMS) progress report: PartⅣ*". National Natural Science Foundation of China Key Project: 50535030. pp. 87-98.

Zhu H, L Blunt, X Jiang and S Xiao (2007). "*Measurement and Characterisation of Micro/nano-scale Structured Surfaces*". In: Proceedings of Computing and Engineering Annual Researchers' Conference 2007: CEARC'07. Best Poster. University of Huddersfield, Huddersfield.

Zhu H, S Xiao, X Jiang and L Blunt (2008). "*MEMS Microstructured Surface Characterisation Based on Wavelet Transform Techniques*". In: Proceedings of Computing and Engineering Annual Researchers' Conference 2008: CEARC'08. University of Huddersfield, Huddersfield, pp. 87-92. ISBN 978-1-86218-067-3

Zhu H, X Jiang and S Xiao (2008). "*Metrology and testing technology of Micro-Electro-Mechanical-System (MEMS) annual report 2008*". National Natural Science Foundation of China Key Project: 50535030. pp. 163-216.

Zhu H and L Blunt (2009). *"An Active Contour Based Algorithm for Micro-scale Surface Feature Extraction"*. In: The Swedish Production Symposium, 2-3 December 2009, Göteborg, Sweden. pp: 190-196.

Zhu H, L Blunt, X Jiang and S Xiao (2009). *"Recognition of Features from Micro Scale Patterned Surfaces"*. In: The 9th International Symposium on Measurement Technology and Intelligent Instruments. (ISMTII-2009), 29 June - 2 July 2009, Saint-Petersburg, Russia.

Zhu H, L Blunt, X Jiang and S Xiao (2009). *"Measurement and Charaterisation of Micri/Nano Scale Stuctured Surfaces"*. In: University of Huddersfield Research Festival, 23rd March - 2nd April 2009, Poster. University of Huddersfield. 2009.

Zhu H, L Blunt and X Jiang (2009). *"Flexible Shape Extraction for Micro/nano Scale Structured Surfaces"*. In: Proceedings of Computing and Engineering Annual Researchers' Conference 2009: CEARC'09. University of Huddersfield, Huddersfield, pp. 190-194. ISBN 978-186218-085-7

Chapter 1 Introduction

1.1 Background

Surface metrology is a science of measurement that plays a very important role in industrial fields. From an engineering standpoint, it is the measurement of the deviations of a workpiece from its intended size and shape (Whitehouse 2003). In recent years, the role of surface metrology on a broader front has been explored. There are many new challenges confronting the surface metrologists nowadays, in particular, where surface metrology fits into nanometrology [1].

From a point of view of specific function, '*structured surfaces*' can be defined as the surfaces have a deterministic structure, with high aspect ratio geometric structure [4,122]. As a sub-dived category of "*engineered surfaces*", all structured surfaces are designed to meet a specific functional requirement [6].

Structured surfaces are one of the most important new range of engineered surfaces with significant industrial applications. Especially in Microelectromechanical systems (MEMS), micro/nano scale structured surfaces have the advantages to make the systems more compact and economical. Along with the rapid development in fabrication technologies of structured surfaces, various newly designed surfaces have been developed with numerous applications [1,2,7]. Large amounts of experimental achievements have now transformed MEMS devices into a commercial success. The global market for micro/nano structured surfaces with special properties will reach US$240 billion by 2011-2015 [2], this is due to the fact that MEMS have the advantages of reliable performance and reduced the cost. MEMS have successfully replaced conventional devices in many industrial areas [14].

However, as the size of the structured surface features reduces to the micro- and nanoscale, traditional measurement and characterisation methods are incapable of measuring and characterising the newly designed geometries. Conventional contact surface measurement instruments are designed for macro work pieces with micro scale topography. Their inherent limitations of contact make them incapable of meeting the measurement needs of structured surfaces' evaluation requirements.

Meanwhile, as the size of micro feature goes down to nanoscale, the classical physical principles of the materials are changed. The molecular forces at the surface become significant. This not only changes the physical properties of materials but also brings about great challenges for the surface geometry measurement and its characterisation. Therefore, measurement instruments based on new principles are a key factor for metrology. Without a practical measurement and characterisation method, the quality and functional performance of micro/nano scale structured surfaces cannot be ensured. Thus, new surface measurement instruments and characterisation methods need to be developed.

In this thesis, the research work is focused on the characterisation and evaluation of micro structured surfaces associated with surface measurement. As structured surfaces are an emergent scientific application, there is still a debate among the metrologists about their definitions and classifications. An accurate and clear definition of structured surface needs to be defined to avoid any confusion during the research. The definitions of surfaces need to be reviewed. Materials and fabrication techniques of structured surface have a close relationship with the associated measurement. It is difficult to develop a practical measurement tragedy without knowledge of structured surface materials and fabrication techniques. The background knowledge of structured surface materials and their physic properties and applications need to be taken into consideration. Due to the limitations of conventional metrology instruments, now, a variety of surface measurement systems with improved measurement capability have been developed by metrologists [3,7,10]. As the instruments are based upon different principles, it is necessary to investigate the measurement capabilities, and compare their merits and limitations. Developing a practical measurement method according to the specific properties of micro- and nanoscale structured surfaces is an important part of this research.

To have a clear overview of micro/nano scale structured surfaces and improve the research efficiency, it is necessary to classify the structured surfaces based on their characteristic surface features. Therefore, some of the most representative structured surfaces and MEMS devices need to be selected as the research objects and the results must have reference value for the other surfaces with similar micro structures. In MEMS, structured surfaces are designed to have several certain regions according to

different functions. An effective region segmentation and feature extraction technique is a key to the subsequent analysis. Due to the fact that MEMS devices are highly integrated systems, some of the surface micro features have complex shapes. The conventional methods are not capable. Additionally, new feature extraction techniques need to be developed. These methods need to have flexible initial scope and be set up to meet the requirements of both single and multiple feature extraction with complex shapes. According to the new classification, typical structured surface applications need to be investigated to seek the commonness and differences of the characteristic features. Due to the inconvenience of the conventional evaluation system of macro device, geometrical parameters and evaluation methods for the micro/nano structured features need to be investigated based on the proposed classification.

1.2 Aim and objectives

This project aims to establish a practical measurement guide and develop a methodology for corresponding feature extraction, characterisation and evaluation of micro- and nanoscale structured surfaces.

The specific objectives are given below in detail to fulfill the above aim, and include:

- Development of a thorough understanding of requirements and measurement preparing for structured surfaces, and investigate effects of the surface materials, feature shape and dimension on measurement.

- Development of a practical guide of measurement of micro- and nanoscale structured surfaces.

- Development of a classification method of micro structured surfaces according to their characteristic features. To classify all the structured surfaces with similar nano/micro structures to improve the efficiency of characterisation.

- Establishment of the geometric fundamental for typical structure characterisation, according to the classification.

- Development of geometrical parameters and evaluation methods for micro structured surfaces associated with experimental analysis for representative MEMS devices.

The major work of this project is concerned the theories of characterisation and evaluation of micro/nano scale structured surfaces. Therefore, the thesis focuses on the measurement, analysis, extracting and chracterisation of surface characteristic structures and providing a practical guide for most structured surfaces. This thesis does not cover the evaluation of structured surface displacement, deformation, as well as the static and dynamic performance characteristics.

1.3 Thesis layout

This thesis is organised as follows. Chapter 2 presents a review of the definitions and classifications of surfaces and the current state of structured surfaces, including materials, fabrication techniques and their major applications in MEMS. Chapter 3 presents the measurement of micro- and nanoscale structured surfaces and corresponding instrumentations. In Chapter 4, a classification of structured steps and structured pattern arrays is proposed. The methods of establishing evaluation references for structured surfaces are presented. Chapter 5 is devoted to the characterisation of micro structured step surfaces. Evaluation parameters and characterisation methods are given associated with case studies of typical MEMS devices and micro fluidics. Chapter 6 is concerned with the pre-processing of surface measurement data, including denoising, data enhancement and feature extraction techniques. Chapter 7 summarizes major research work with contributions and future work.

The major contribution to knowledge of this work is outlining below:

- Development of a novel flexible method of feature extraction. It can successfully extract specific micro features from structured surfaces. It is more flexible than the traditional low-level feature extraction methods.

- Development of geometrical parameters and evaluation methods for the micro structured steps based on a proposed classification of structured surfaces.

Chapter 2 Structured surfaces and MEMS

This chapter reviews the definitions of structured surfaces. It presents a discussion on surface classification systems with the focus on structured surfaces. The materials and fabrication techniques for micro/nano scale structured surfaces are presented. As the most significant applications of micro/nano scale structured surfaces, this chapter gives an overview of MEMS. The objective of this review is to clarify the scope of the work to be undertaken in future chapters, and to demonstrate a clear and thorough understanding of structured surfaces and MEMS.

2.1 Definitions and classifications of structured surfaces

Since the early days of engineering, it has been recognized that all surfaces have "*texture*", and all manufactured surfaces are can be considered as "*engineered surfaces*" [4]. As the interest in the past has mainly focused on the conventional machining processes such as turning, milling and grinding, the concepts of roughness, waviness and lay were defined in international standards and are in widespread use in industry [4,6]. In addition, there has been a great deal of research about the influence of the materials, machine tools and process parameters on the development of a given surface [8,9].

As technology has advanced and the understanding of surfaces has increased, a great deal of products have emerged where the surface has been specifically designed to provide a particular function [5,10]. For example, the structured surface of a modern dimpled golf ball is specifically designed to improve its functional performance. The flying distance has been regarded as one of the most important specifications of a golf ball. Due to the speed of its fast-flight, the distance is influenced by the aerodynamics of the dimple on its surface. A specifically designed concave surface can improve the aerodynamic characteristics to meet its functional requirements [39].

The impact of nanotechnology on manufacturing, as well as the new fabrication techniques processes have been widely accepted [5]. Most of these products utilise non-conversional manufacturing techniques such as masking and chemical etching. Consequently, it is necessary to define all class of such surfaces and update the classification system for the convenience of design, manufacture and metrology. For example, the nanoimprint lithography (NIL) is one of the developed nanofabrication techniques for producing structured surfaces. The principle of NIL is using a stamp to create designed micro/nano features on the surface. The surface is composed of two parts, an upper polymer layer and a silicon-substrate. The first step is to bring pre-made stamp and heated sample into contact under certain pressure. Then, cool down the stamp and surface, make them separated to from the micro/nano features. This method has the advantage of making large variety of different structures. Figure 2-1 shows the principles of the NIL [20-22].

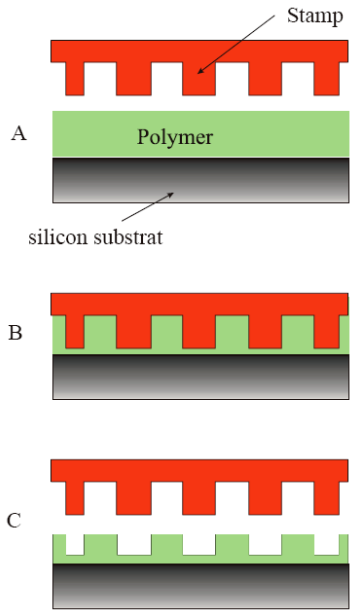

Figure 2-1 Schematic of principles of NIL

In 1989-1990s, Suh, Saka [46] and Stout [47] tried to divide surfaces into "*engineered surfaces*" and "*structured surfaces*".

In the 1990s, Evans and Bryan [4] suggested the definition of "*engineered surfaces*" and "*structured surfaces*" should be adopted using the following terminology. "*Engineered surfaces*" are surfaces where the manufacturing process is optimized to

generate variation in geometry and/or near surface material properties to give a particular function".

"*Structured surfaces"* are surfaces with a deterministic pattern of usually high aspect ratio geometric features designed to give a specific function.

Later in 1998, Scott and Blunt [6] offered the further amended definitions for some manufactured surfaces. "*Engineered surfaces"* are produced in specific ways that alter the surface and sub-surface layers to give required performance. "*Structured surfaces"* are those where the surface structure is a design feature intended to give particular functional performance.

Stout and Blunt proposed eight surface classifications, presented with their sub-classes in Figure 2-2.

In the schematic diagram below, all the surfaces have been classified into two major groups, one is the non-engineered surface, and the other is the engineered surface. The former group has been divided into two further sub-classes, random surface and systematic surface. Meanwhile, the engineered surfaces have been classified into structured surface and unstructured surface. This project focuses on the structured surfaces. The structured surfaces include two major parts, non-directional and directional surfaces [6]. In Chapter 4, the author proposed a new micro structured surface classification system according to structured surface functional properties and evaluation requirements.

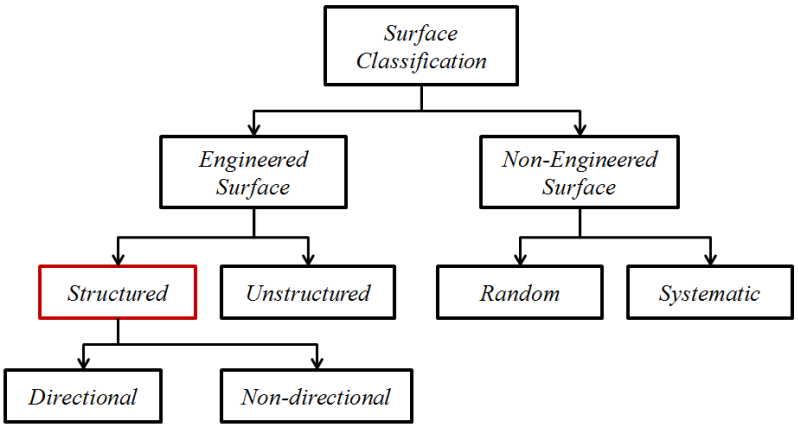

Figure 2-2 Surface classification schematic diagram [6]

"Engineered Surfaces": surfaces produced in specific ways that deliberately alter surface and sub-surface layers to give a specific functional performance.

"Non Engineered Surfaces": surfaces produced as a direct consequence of the manufacturing process where little or no attempt is made to influence surface character.

"Structured Surfaces": surfaces with a deterministic pattern of usually high aspect ratio geometric features designed to give a specific function.

"Directional Surfaces": surfaces with a deterministic pattern which exhibits specific directionality.

"Non Directional Surfaces": surfaces with a deterministic pattern but without specific directionality.

"Unstructured Surfaces": surfaces where a deliberate attempt has been made to impart texture through semi-control of the manufacturing process without achieving a deterministic pattern.

"Random Surfaces": surfaces produced by random and psuedo-random processes often with the specific intention of removing systematic features.

"Systematic Surfaces": surfaces exhibiting some repetitive features which are a consequence of the natural constraints of the process by which they have been produced [6].

In 2012, Jiang and Whitehouse [34] proposed a modified surface classification which can be straightforward to update and more convenient to build "toolboxes" fitted for specific usages. The hierarchical structure is shown in Figure 2-3.

In this classification, surfaces are classified based on *"surface texture"* and *"surface shape"*. For the former, it composed of two parts, *"stochastic surface"* and *"structured surface"*. *"Structured surface"* can be sub-divided into *"tessellation"*, *"linear pattern"*, *"rotational invariant pattern"* and *"multi-patterns"*. The proposed classification also takes surface shapes into account. This classification system combines surface features with their specific functions. In this way, it can cope with surface design specification according to the duality principle [42].

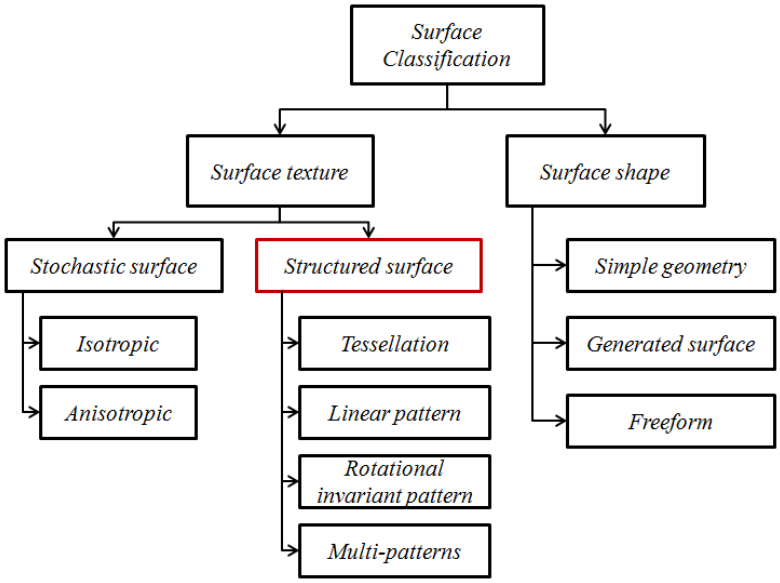

Figure 2-3 Surface classification hierarchy by Jiang and Whitehouse [34]

The definition of structured surfaces is concerned with the specific functional performance. For example, one of the early applications of structured surface is the road sign surface, whose functional requirement is to reduce the diffuse reflections, so that it could be seen in dim light. It has a reflective sheet with square or rectangular micro-prisms under the top layer to form a retroreflector of dim light. These micro-structures make the road signs clearer to read in a low-light environment. The structure of the road sign and the micro-structures on the reflective sheet surface are shown in Figure 2-4.

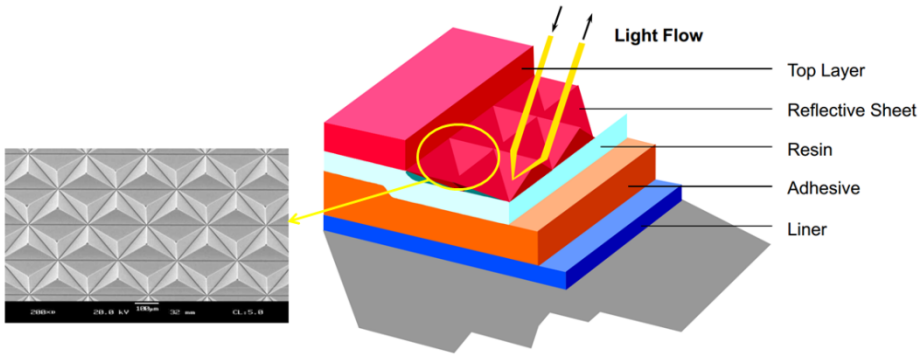

Figure 2-4 The structure of retroreflection road sign [43]

For micro/nano scale structured surfaces, the classification system is also needed to take account of their functional performance.

2.2 MEMS

"MEMS" is a loosely defined term for man-made mechanical components that are characterised by small size [16]. The exact definition of MEMS is difficult to formalize. Most scientists agree on the idea that MEMS should have dimensions in the micron-scale and have both electrical and mechanical components that form a system [68]. Generally, MEMS integrates mechanical components, sensors, valves, gears, and mirrors into a microsystem. Meanwhile, it also referred to micro machines, or Micro Systems Technology (MST). Figure 2-5 shows the general size of the MEMS devices with a generic comparasion.

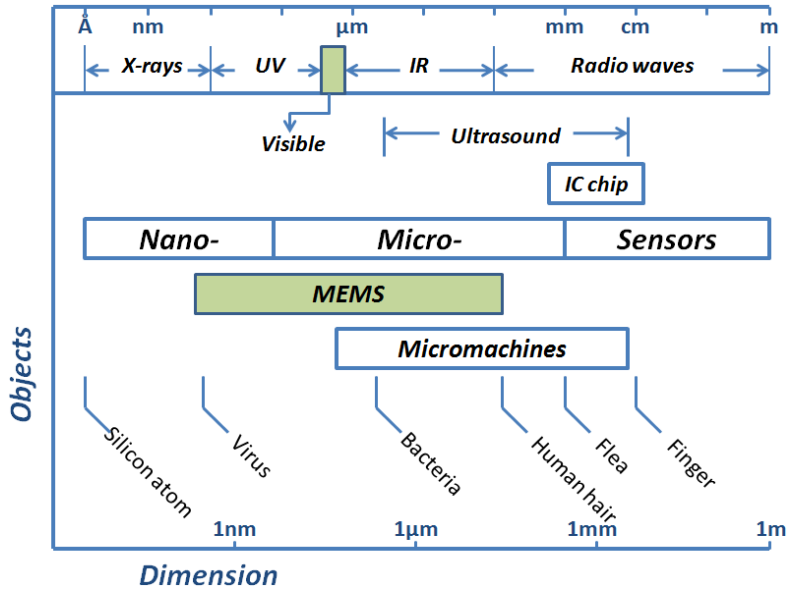

Figure 2-5 Dimensions of micro-sensors, MEMS and micro-machines, compared with some everyday objects [1,2]

The development of MEMS has led to a paradigm shift in manufacturing and applications. In MEMS manufacturing, batch fabrication processes have been utilized to make products more economical. For example, miniature inertial sensors have largely replaced the costly macroscopic components in automotive industry significantly reducing the manufacturing costs [16].

Starting in the 1960s, the development of integrated circuit (IC) technology has been used to make experimental mechanical structures [16].

In the 1970s, two of the significant applications of MEMS, pressure sensors and accelerometers chieved commercial success [9]. Figure 2-6 shows the picture of a pressure sensor.

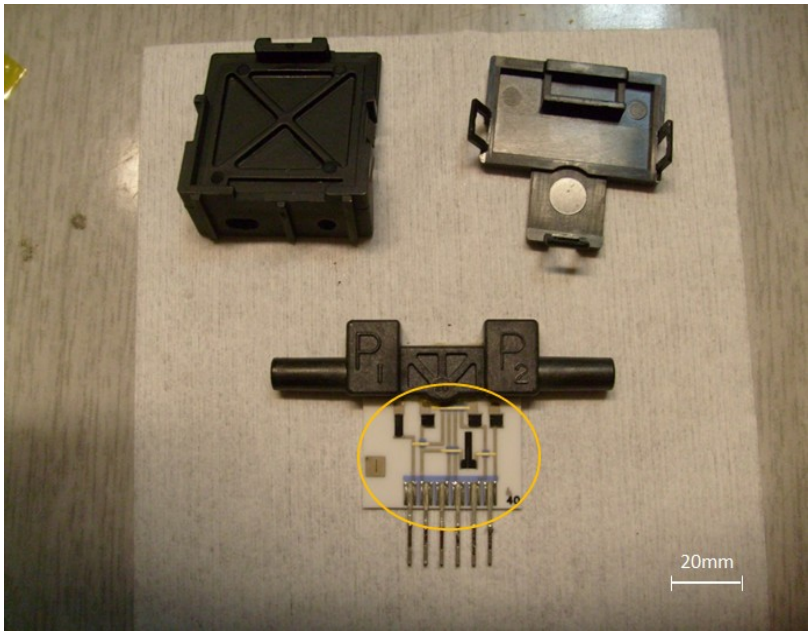

Figure 2-6 A disassembled MEMS pressure sensor

In the 1980s and 1990s, new fabrication technologies led to a great development in MEMS. Highly compact MEMS devices combined mechanical components with the integrated circuits. The applications and the market for MEMS developed rapidly. Some of the products have been used widely in industry. For example, micro switches, pressure sensors, micro-mirror arrays and micro fluidics [9,16]. Figure 2-7 shows the major applications of MEMS devices.

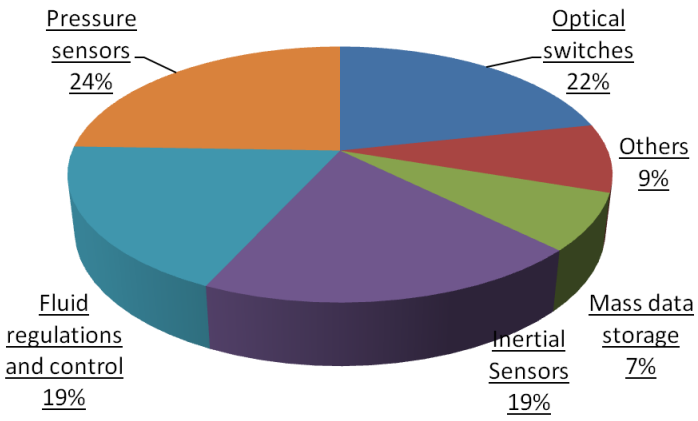

Figure 2-7 Major applications of MEMS devices [1,8]

From 2000 to the present, the MEMS have become a more integrated micro system with not only micro sensors but also actuators. This technology will depend on the

Microsystems technology (MST), and more importantly, micro/nano structured surface will play a significant role in these systems. Structured surfaces have been wildly used in almost all kinds of MEMS products. The quality of structured surface will be a great influencing factor for MEMS. Figure 2-8 provides an overview of MEMS together with some of the application areas. Micro/nano structured surfaces ensure the performance of MEMS, and work as the foundation of the whole system.

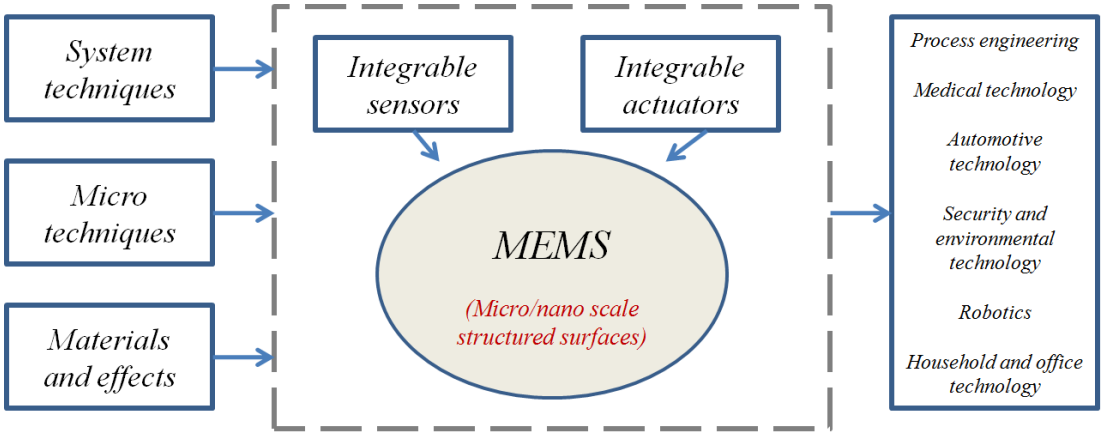

Figure 2-8 Overview of MEMS and application areas

In summary, the MEMS development potential is enormous in many industrial and technical fields. There are many companies have devoted to MEMS research and development. As the market of MEMS continuously is expanding and the price continuously decreased, MEMS will most likely become more and more important in the future. With the applications of micro/nano structured surfaces, for the miniaturization of many portable devices will become possible. Structured surfaces are key issue in MEMS development, lack of quality evaluation will result in a low rate of finished product. Therefore, establishing an effective evaluation system and developing a methodology for preparing and conducting the measurement of structured surface is imperative [8].

2.3 Materials of micro/nano scale structured surface

As has been discussed above, one of the most exciting technological developments of micro/nano scale structured surface has been MEMS. Generally, MEMS are composed of both micro-fabricated mechanical and electrical structures which range in scale from the micro to nanoscale. In order to have a thorough understanding of

structured surfaces, especially MEMS surfaces, knowledge concerning the materials used to construct these systems is indispensable.

The materials for micro/nano scale structured surface can be classified as metals materials, semiconductors materials, polymers materials and composites materials. In this section, a brief introduction to the basic nature of each type of material will be presented.

2.3.1 Metals

Metals play an important role in MEMS manufacturing and processing. It has been wildly used in many different capacities. Applications of metals ranging from hard etch masks to structural elements. One major application is the thin film which provides conducting interconnects and structural elements in micro-sensors and micro-actuators in MEMS systems. Table 2-1 provides some information on 11 selected metals.

Table 2-1 The properties and applications of common metals in MEMS

Metal	Resistivity (Ω·m) at 20 ℃	Applications
Silver (Ag)	1.59×10^{-8}	Electrochemistry
Aluminum (Al)	2.82×10^{-8}	Elect interconnects Optical reflection
Gold (Au)	2.44×10^{-8}	High T elect interconnect Optical IR Electrochemistry
Chromium (Cr) Titanium (Ti) Titanium tungsten (TiW)	1.20×10^{-7} 4.23×10^{-7} $7.5\times10^{-7}-2.0\times10^{-6}$	Intermediate adhesion layer
Copper (Cu)	1.72×10^{-8}	Elect interconnects
Indium tin oxide (ITO)	$3.0\times10^{-6}-3.0\times10^{-5}$	Transparent interconnects
Iridium (Ir) Platinum (Pt)	5.12×10^{-8} 1.07×10^{-7}	Electrochemistry Bio-potential sensors
Tungsten (W)	5.62×10^{-8}	High T elect interconnects

There are a number of deposition methods, for example, evaporation, sputtering and chemical vapor deposited (CVD). The electroplating metal makes thin films one of the most wildly used components in MEMS devices [7].

Copper is one of the important materials used in MEMS. It has a high ductility and excellent electrical conductivity. Due to MEMS commonly having an electrical system, it has been used for electrical interconnects wildly. Also, copper structures at both nanometer and micron size scales play a key role in MEMS. They have been used in MEMS switches and resonators [7,13].

Aluminum is also a widely used metallic material in micro-fabricated devices. Due to the fact that aluminum thin film can be sputter deposited at a relatively low temperature, it is appropriate to be used in conjunction with polymers in MEMS. In most cases, aluminum is used as a structural layer, and sometimes a sacrificial layer. Aluminum has also been proven as an effective material for surface micro-machining. Finally, because Al can be processed at a temperature below 400℃, this property brings Al advantage in applications of the integrated circuits (ICs) [7].

Tungsten, nickel and copper can be used as a structural material for surface micro-machining. In this case, metals are the structural layer and silicon dioxide is often used as a sacrificial layer.

Overall, metals are good thermal and electrical conductors in MEMS. As a structural layer, metals are easy to deposit and maintain good strength to meet the design requirements.

2.3.2 Semiconductors

Semiconductor has been wildly used in MEMS. Differ from a conductor and an insulator, it has an electrical-conductivity normally in the range 1×10^{3} s/cm to 1×10^{-8} s/cm. Semiconductor is an inorganic material. It made from elements in the fourth column of the periodic table [8]. To a certain extent, semiconductor materials play a fundamental role in the modern electronics. The applications of semiconductors are including ICs, sensors, actuators and MEMS devices.

Due to the rapid development of semiconductor materials, a large number of productions become more compact and reliable. Especially in the areas of compact mobile devices, micro sensors and MEMS, the development of semiconductor materials increases the level of production integration. This leads to higher demands of the material. Semiconductors are applicable to a variety of manufacturing processes, including deposition, patterning and etching.

Among all the semiconductor materials, silicon (Si) is one of the most commonly used materials used to create integrated circuits. Silicon is attractive for the rapidly developing fields of MEMS and nano-fabrication, because it is a cheap high-quality material, and it has an ability to incorporate electronic functionality. Elemental semiconductors are made from single elements. Elemental semiconductors are composed of the elements in the group Ⅳ of the periodic table, for example, silicon and germanium (*Ge*) [8]. Since the 1960s and 1970s, with the development of technology, *Si* has been applied to the field of both mechanical and chemical micro machining. Flexible mechanical structures were fabricated, which led to commercial high-volume of Si-based productions becoming viable. During the 1980s, *Si* micro-

fabrication technology became popular in the areas of IC technologies. Later with the rise of MEMS technology, *Si* became a primary material for such devices [7].

Single-crystal *Si* has a diamond-like crystal structure. Similar to other semiconducting materials, the conductivity can be altered by doping other materials. Single-crystal *Si* plays a significant role in micro bulk fabrication.

For surface micro-fabrication applications, single-crystal *Si* has been used as a mechanical platform. Therefore, the device structures made from Si or other materials can be built on it. As more and more Si-based integrated MEMS applications have achieved commercial success, single-crystal Si has become more important in MEMS.

Solid-phase oxides (SiO_2) is another important semiconductor material. It remains a stable chemical property under most conditions. In micro/nano structured surfaces, structures made from Solid-phase oxides can be grown or deposited on the substrates. In polysilicon surface micro-machining, (SiO_2) are normally applied as a sacrificial layer, as it can be easily dissolved during the procedure. Therefore, it will not damage the polysilicon layer [7]. Another important application of silicon dioxide is the (SiO_2) film. It can be manufactured by a low-pressure chemical vapor deposition (LPCVD) process.

Compound semiconductors are made up of special combinations like gallium arsenide (*GaAs*) which are commonly used in fabricating optical devices [8]. Table 2-2 lists the mechanical, electrical, and thermal properties of several semiconductor materials.

Table 2-2 Properties of common semiconductor materials in MEMS technology [8]

Material	Property					
	Density ρ_m (kg/m^3)	Melting point T_{mp}(℃)	Boiling point T_{bp}(℃)	Electrical conductivity σ $(10^3\ S/cm)$	Thermal conductivity κ(W/m/K)	Young's modulus E_m(Gpa)
Si	2330	1410	2355	4×10^{-3}	168	190
Ge	5350	937	2830	3×10^{-5}	60	N/A
GaAs	5316	1238	N/A	$\sim 10^{-5}$	370	N/A
SiO_2	2200	1713	230	N/A	1.4	57-85

2.3.3 Ceramics

Ceramics are inorganic materials which consist of metallic and nonmetallic elements that are chemically bonded together. Normally, ceramic has a crystalline structure, or may be amorphous [9]. Typical engineering ceramic materials include alumina Al_2O_3, silicon carbonitrides (*Si-C-N*), zirconium dioxide (ZrO_2) and silicon nitride (Si_3N_4).

Ceramic materials have some unique properties, which make them highly suitable for certain MEMS applications. Ceramic materials can be made for durable biological micro components due to their resistance to corrosion. In the extreme industrial conditions, for example, at an extreme high-temperature environment ceramic materials resist corrosion and remain stable chemical properties. That unique advantage of ceramics is suitable in fixing the friction problems in micro high-speed motorized systems. It also has a low density mechanical property to reduce weight of the whole system. Therefore, in most micro turbines, a number of components are made of ceramics. Another advantage of ceramic materials is their relatively low cost and conventional manufacturing processes. However, ceramic materials need to improve their reliability and reduce the flaw-size sensitive in MEMS applications [18].

In order to achieve better exposition of the attributes of ceramic materials and their applications, an example, carbonitrides (*Si-C-N*) will be introduced.

Si-C-N is predominantly an amorphous ceramic. It is composed of silicon, carbon and nitrogen. Therefore, in general, *Si-C-N* can be written as $Si.nSi_3N_4xC$.

The obvious glass-transition temperature of *Si-C-N* material is about 1500°C, and it can go up to 1800°C by adding boron element. Compare to pure chemically vapor deposited (CVD) *SiC*, the oxidation resistance property of *Si-C-N* is even better. Due to its low modulus and high strength, *Si-C-N* has a high figure-of-merit value for thermal shock resistance. It also has the advantages of low-cost fabrication. In most multi layer ceramic MEMS devices, components are made of *Si-C-N* materials [9,15].

Table 2-3 shows properties of *Si-C-N* and compared to other Silicon-based materials.

Table 2-3 Properties of *Si-C-N* as compared to other silicon-based materials [9]

Property	Si-C-N	SiC	AL_2O_3
Density (g/cm^3)	2.35	3.17	3.19
E modulus (Gpa)	80-225	405	314
Poisson's ratio	0.17	0.14	0.24
CTE(10^{-10}/K)	3	3.8	2.5
Hardness(GPa)	25	30	28
Strength(MPa)	500-1200	418	700
Toughness($MPa \cdot m^{1/2}$)	3.5	4-6	5-8

2.3.4 Polymers

A polymer is typically a large carbon molecule composed of repeating structural units typically connected by covalent chemical bonds [10]. In MEMS, polymer materials are being actively used, including elastomers, plastics and fibers. There are many advantages of polymer materials due to their characteristic physical and chemical properties [10]. For example, polymer materials are low-cost and easy to process. In terms of applications, polymer materials are being developed for displays, memory, circuitry and micro actuators and form the basis of flexible electronic.

The term polymer covers huge range applications. It can be dived into three classifications, including plastics, fibers and elastomers. Since the early 90s, polymer materials have become popular in MEMS. There are five major reasons to explain why polymers can be successful in MEMS. First of all, compared to silicon polymer materials provide greater mechanical yield strain. Silicon has a large Young's modulus. Therefore, it has the advantage of mechanical strong. However, it is brittle in some of the MEMS applications. Polymer can sustain a much greater deformation

compared to silicon. In MEMS devices, some components are directly in contact with other materials, for example, micro pressure sensors. The robustness of material will effetely reduce the possibility of system failure, and polymer is suitable for such applications.

Secondly, polymer materials can significantly reduce the cost of manufacturing. The circumstance of polymer processing is not costly. Some MEMS based polymer components can be processed without clean room control. Therefore, the cost of polymer fabrication is lower compared to other materials.

Thirdly, silicon-based substrates can only be manufactured in the wafer format. Meanwhile, polymer-based substrates are not limited to wafer format. This makes polymer components of MEMS devices have unlimited sizes.

Fourthly, the silicon micromachining process is relatively strict. The fabrication of polymer-based MEMS is more flexible. A number of novel techniques can be applied to the polymer-based MEMS fabrication, for example, molding, CVD, embossing and lithography.

Fifthly, compared with other materials have been introduced above that polymers have the unique chemical functionality [10]. For example, it can change volume as the temperature changes. This property makes polymer-based films more durable. Micro/nano structures can be manufactured on these films by energetic ion track etching technique [8,14]. Polymer materials have been wildly used in micro sensors and actuators [11].

The number of polymer materials available is enormous. More and more polymer-based components can be applied to MEMS or other compact devices. As the development of processing techniques, the polymer micromachining will become more convenient and more reliable. A huge variety of polymer materials will be available in the future. Table 2-4 shows some polymer materials and their applications [17].

Table 2-4 Representative polymer MEMS materials and applications [14]

Material	Processing methods	Applications
Parylene	Chemical vapor deposition	1. Micro pumps and valves 2. Pressure and shear stress sensors 3. Micro air vehicle wings 4. Microfluidics 5. Reduced friction coatings
Polyimide	Spin coating, extrusion	1. Sensor substrates 2. Microfluidics
Acrylics	Molding	1. Microfluid channels
PDMS	Molding	1. Microfluidic channels 2. Pumps and valves
Liquid crystal polymer	Chemical etching	1. Flow sensors
Biodegradable polymer	Molding	1. Drug delivery devices
SU-8 epoxy	Photo patterning, spin casting	2. Artificial haircell sensors
Polyurethane	Molding	3. Microstructures
Nano-composite elastomers	Screen printing, molding	1. Conductors 2. Sensors 3. Actuators

2.3.5 Composites

The last type of MEMS material is a composite material, which is a combination of two or more materials [10]. Most composites consist of a selected filler or reinforcing material and a compatible resin binder to obtain the desired material characteristics [12,13]. Usually the component materials of a composite do not easily dissolve in one another and are physically identifiable by an interface between the components. For example, nanocomposite materials are developed to improve the contact reliability of MEMS switches. The material of MEMS switches contact components requires good conductivity and rough surfaces to reduce adhesion force. Gold and copper are good conductor material, but both of them are soft. They will creeps under the contact and cause stiction, that leading to a failure of the device. Composite material has both good conductivity and hardness. It makes MEMS switches achieve more than 10 billion cold contact cycles without any adhesion failure [17,33].

2.4 Micro/nano fabrication techniques

With the rapid development of nanotechnology, there is now a wide range of techniques that are capable of creating micro/nano scale structures. Each technique has its own advantages and disadvantages and various degrees of quality, speed and cost [15,17,19]. Most of these fabrication techniques can be categorized into 'bottom-up", and "top-down" approaches. Figure 2-9 shows the use of bottom-up and top-down techniques in manufacturing. The diagram illustrates some of the types of materials and products using these two approaches.

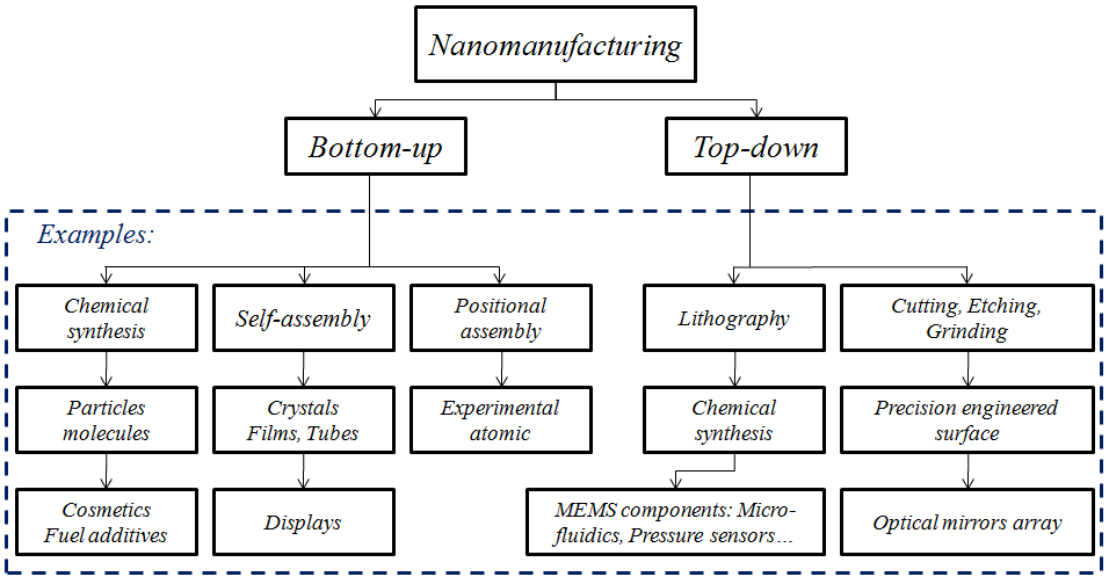

Figure 2-9 Use of bottom-up and top-down techniques in manufacturing [16]

The basic idea behind the bottom-up involves the building of micro/nano structures, atom-by-atom or molecule-by-molecule [16]. There is a number of techniques can achieve this goal. In this section, three major parts of the bottom-up techniques will be discussed and they are chemical synthesis, self-assembly, and positional assembly. Among these techniques, positional assembly is the only technique in which single atoms or molecules can be placed [13,14]. As a more practical technique, chemical synthesis can create a desired structure using large numbers of atoms, molecules or particles.

Compared to the bottom-up methods, the idea of top-down manufacturing is essentially material removed. Top-down manufacturing starts with a larger piece of material, and then material is removed using etching, milling or machining to form a

desired nanostructure by removing material. The approaches of this method can be split into two categories: lithography and precision machining which has been developed and refined by the semiconductor industry over the past decades. Because of their reliability, top-down methods can produce the more complex micro devices, like MEMS, micro structured surfaces and circuits on microchips. Compared to bottom-up method, techniques using top-down are higher in energy usage and are associated with more waste of material [18,20]. However, it is undeniable that top-down techniques are more reliable and practical, especially in the industrial field [16].

2.4.1 Chemical synthesis

In chemistry, chemical synthesis is a purposeful execution of chemical reactions to get a product or several products [21]. Chemical synthesis is a method of producing raw materials, including molecules and particles [23]. This technique can be used either directly in products in their bulk disordered form, or as the building blocks of some materials.

A more intuitive description of chemical synthesis, a typical fabrication process of nano-particles by using chemical synthesis technique is shown in Figure 2-10. The whole process starts with precursor phase, and the material can be in three physical state, including solid, liquid or gas [27]. Then nano-particles can be formed by a chemical method. The new creation can be changed in other physical states, like liquid and vapour. Once the circumstances are created, nano-particles can be made by chemical reaction. At last, a further phase transformation may be needed to produce the final product [23,24].

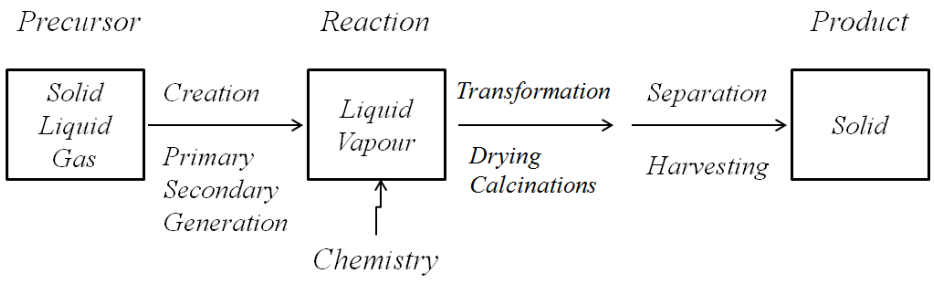

Figure 2-10 Fabrication process of nano-particles by using chemical synthesis technique

However, nano-particles have a tendency to agglomerate. Therefore, nano-particles are normally manufactured from a liquid phase. This ensures a better control of

surface energies and reduces the agglomeration [26]. Processing and handling ability is a key factor for nano-materials. Mixing nano-scale particles together before agglomerating can generate wholly new complex nano-phase materials which could not be made by any other methods [22]. However, most techniques of chemical synthesis method can be only applied at laboratory scale due to their strict manufacturing process.

2.4.2 Self-assembly

Self-assembly is a specified process in which a disordered system of pre-existing components' forms an organized structure or pattern as a consequence of specific, local interactions among the components themselves, without external direction [11]. Like chemical synthesis, self-assembly is also a bottom-up production technique. Through a series of chemical or physical interaction atoms or molecules arrange themselves into ordered nano-scale structures. Therefore, to form the final product, there is a need for a designed accurate interaction [25]. For example, the formation of salt crystals with their complex structures is the result of self-assembly.

In the industrial field, self-assembly is relatively new. There are some advantages of self-assembly. First of all, it carries out many of the most difficult steps in nano-fabrication, including atomic level modification of micro/nano scale structures using highly-developed chemical techniques [12]. Secondly, the whole process of self-assembly should inherently create less waste and use less energy. Thirdly, self-assembly is one of the most important strategies used in biology for the development of complex, functional structures. Fourthly, it can incorporate biological structures directly as components in the final systems [27].

However, there are still many details need to be improved. For example, computer modeling is expected to aid the development of more complex systems. Slow self-assembly process needs to be accelerated by using an external forces or fields, e.g. electric or magnetic.

2.4.3 Positional assembly

Positional assembly is the last bottom-up technique discussed in this section [28,30,31]. Using positional assembly techniques, atoms, molecules or clusters are

deliberately manipulated and positioned one-by-one. To achieve this, Scanning Probe Microscopy (SPM) or optical tweezers are used. Figure 2-11 shows the most famous experimental demonstration of molecularly precise positional assembly of individual atoms, achieved by Eigler and Schweizer at IBM Almaden in 1989 [29]. In this case the authors used an STM to position 35 xenon atoms on a nickel surface to spell out the corporate logo "IBM".

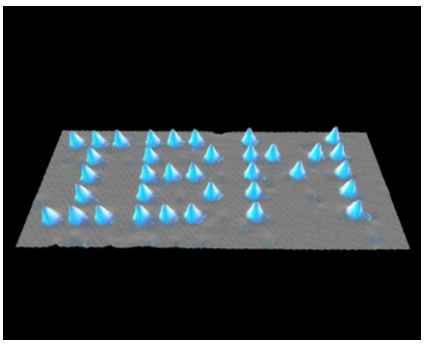

Figure 2-11 Experimental demonstration of molecularly precise positional assembly of individual atoms

However, positional assembly is an extremely slow and laborious technique, and it is unsuitable as an atomic-scale industrial process.

2.4.4 Lithography

In micro/nano fabrication, lithography is a transfer of a pattern into a photo-sensitive material by selective exposure to a radiation source [14]. There are three different components used during the fabrication process, including the mask layer, the photosensitive layer and the substrate layer. Both mask layer and substrate layer are not sensitive to the radiation. It means the physical properties will not change after being exposed to the radiation source [31]. The photo-sensitive layer will be etched under the radiation. During the fabrication process, both photo-sensitive layer and substrate are covered with the mask with designed slots [32]. So the micro steps or slots remain after the material is exposed. The vertical height of slots is controlled by the exposure time. Figure 2-12 shows the principle of lithography.

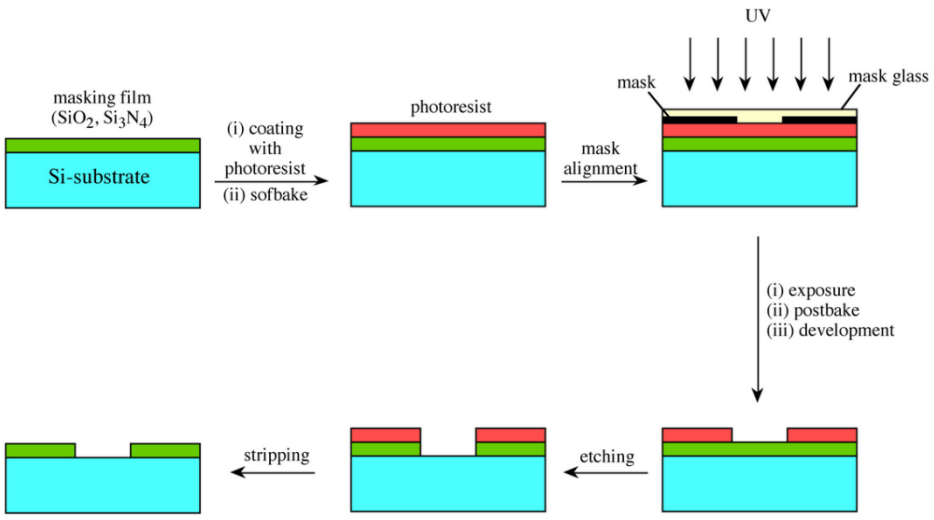

Figure 2-12 Principle of lithography method

The lithography method was, firstly, used in semiconductor manufacturing to pattern semiconductor wafer. The radiation sources of lithography methods, include light, ions and electrons, and then subsequent etching or deposition of material on to that surface to produce the desired device [22]. The main lithographic tools use a focused beam of electrons or ions to write patterns, and those that rely on the projection of light through a mask to define a pattern over a complete semiconductor wafer [46]. The lithography method has an ability to pattern features in within nanometer range. When using a beam of electrons or ions as the radiation source to write patterns, the greatest routine resolution can reach sub-10nm, but both are too slow to be used directly in production. Compared to beam-based techniques, optical lithography has clear advantages. It provides rapid throughput, and it is cost effective. However, the beam-based techniques have a higher resolution. So in semiconductor manufacturing, beam-based techniques such as electron-beam lithography used to fabricate the masks, and the final production is made by optical lithography technique. Furthermore, lithographic patterning techniques enabled the miniaturization of small mechanical moving devices, and now are wildly used in the field of MEMS manufacturing.

2.4.5 Precision machining /cutting

Precision machining for MEMS is an important technique. It is suitable for metal materials, this technique aims to make structured surfaces with high tolerances [21,23]. For example, a number of important applications are fabricated by this method, like microlens arrays and the landing zone of the computer hard disks.

Compared to the macro engineering, the specific processing methods, including cutting, laser machining and burnishing are similar and based on the same principle.

Precision is the key factor of the machining processes. A large number of structured surfaces are fabricated by precision machining. For example, ultra-precision machine tools nowadays can achieve a very high precision at nano scale [27,44]. For structured surfaces with different applications, a machining process needs to be carefully chosen. The scale and specifications of the micro features are key factors [45]. Optical components, like microlens arrays commonly use the diamond machining method to fabricate a lens mould prior to injection moulding. A large portion of the structured surfaces with rotationally symmetric features can use the same method.

The landing zone of the hard disk uses Ultra-short UV to create small pits on its surface according to a certain arrangement [44]. The wavelengths of the Ultra-short UV are commonly 157,193 or 248nm [4]. The principle of this method uses the light to focus on the surface. Mask projection technique is applied in manufacturing process. The designed micro features can be created by the heat of light beams. Some adjacent regions use metals, ceramic or glass as the martial, so it will not be affected by the heat.

The precision engineering methods have been applied in many MEMS manufacturing. Compared to chemical synthesis and self-assembly, it is a more practical method for batch production.

2.4.6 Convergence of top-down and bottom-up techniques

The relationship between top-down and bottom-up technique is illustrated in Figure 2-13. The figure shows the development in the accuracy of an artifact from 1940 to 2010 [44, 49]. The bottom-up processes have evolved to create large structures by chemical processing. The difficulty is to ensure the structure size to meet the design requirements and production efficiency. The top-down processes, on the other hand, aims to make smaller structures by using precision machining and lithography method. It is more suitable for mass production of the practical structured surface production. With the rapid development of fabrication techniques, the quality of micro structures

is continuous improving. From the figure below, it is clear that the two methods start to converge in both fabrication scale and precision [50].

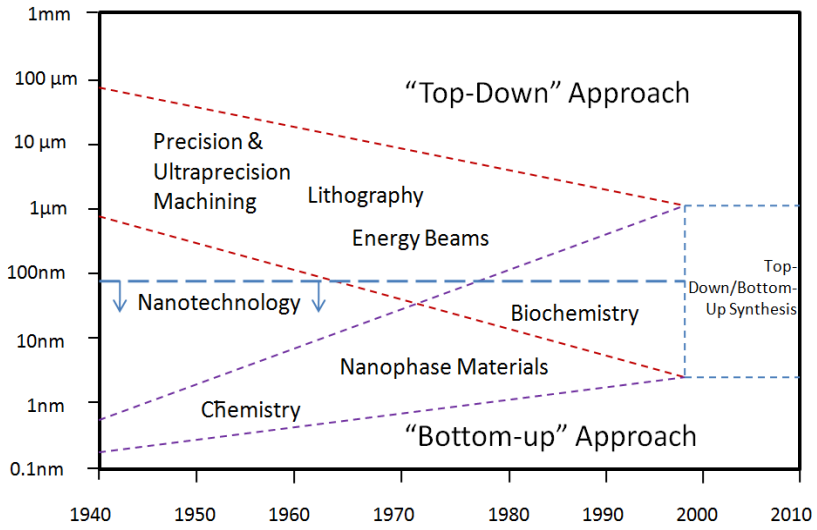

Figure 2-13 The convergence of top-down and bottom-up fabrication techniques

2.5 Applications of micro-structured surface

The number of MSMS applications is increasing every year. Due to their unique advantages, MEMS are applied in many mechanical, electrical and industrial production areas. In this section, some of the most important applications have been reviewed. The structured surfaces of these applications are considered to be representative e.g. MEMS pressure sensor surface, microlens array surface, landing zone surface of a hard disk, pin grid array surface and micro fluidic chip surfaces.

2.5.1 Micro accelerometer sensors and pressure sensors

The MEMS micro accelerometer sensor is an example which successfully replaced the tradition accelerometer in the automobile industry. Due to the small size of the MEMS micro accelerometer sensors, it is possible to make the air bag compact. Furthermore, it has a simple structure to ensure it reliable performance. On its surface, there are several micro channels with a certain distance, and two electrodes on the both sides of the sensor, as shown in Figure 2-14. Once the acceleration of the automobile is exceeded the threshold, there will be a deformation of the micro channels, i.e. the distance of the channel sidewall will be changed [46]. The electrical capacitance will also change. The impact signal is transferred to the electrical signal,

and air bag is activated. It is clear the micro feature size and geometry of the surface in MEMS micro accelerometer sensor is a key factor to ensure the performance.

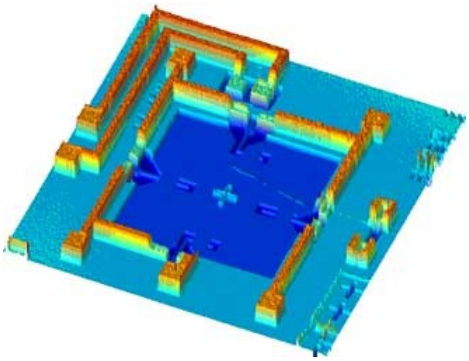

Figure 2-14 Optical profiler image of part of a MEMS PZT pressure sensor

MEMS pressure sensors are based on the same principle. It has more applications in industry. Commonly, the surface in MEMS pressure sensors has the similar structures but the smaller distance between micro channels and also the thickness of sidewalls. Therefore, the sensor is very sensitive to the pressure [57].

2.5.2 Microlens arrays

The microlens array is a breakthrough in optical technology and has many applications, including optical switches, amplifiers, and isolators [53]. The advantage of impact size and low cost make cameras of mobile devices possible. Compared to the traditional optical lens, the microlens arrays use multiple lenses to replace single lens, as shown in Figure 2-15. The microlens are arranged on the surface according to a designed grid. Both single microlens and the grid arrangement are important to ensure the quality of the microlens array [43, 52].

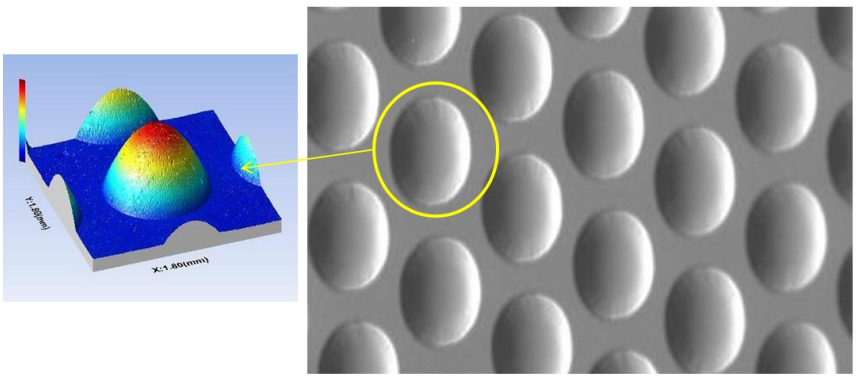

Figure 2-15 Microlens array surface

The fabrication of the microlens array mainly uses the hot embossing technique. A thin piece of plastic material is set between a designed mold produced using diamond turning techniques and a smooth backing plate, ensure the embossing tool fully contact material. The material will be heated to a specific temperature called softening temperature (T_g) to make the material melting. Meanwhile, pressure is put on the embossing tool to form the microlens array. Once the plastic material is cooled down below the softening temperature, the pressure is released. The material can be separated from the mold to give a microlens array. Figure 2-16 shows the process of the hot embossing technique.

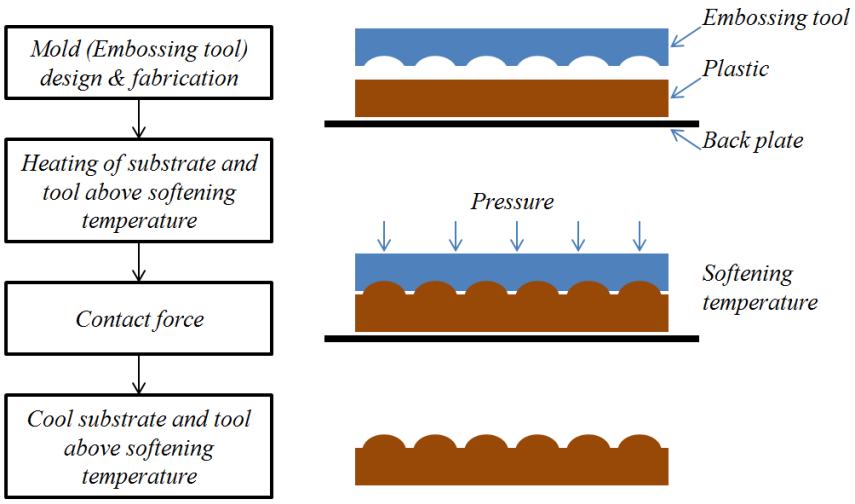

Figure 2-16 Procedures for fabricating microlens array [17]

Compared to lenses, micro lenses are much smaller that normally have diameters of less than 1mm. In order to characterise the microlens array, it is important to measure both parameters of the single lens and the array arrangements. For example, the lens

width, radius, vertical/horizontal deviation, etc. Both the lens and the array arrangement evaluations are key factors to ensure the performance of micrelens array.

2.5.3 Micro fluidic chip surface

Micro fluidic chip technology emerged in the early 1990s as a novel approach to the high-speed separation of biological compounds, including DNA and proteins [43,50]. Since the early development within this area, growth in the research field has exploded and now includes chemists and engineers focused on developing new and better microchips [42]. Figure 2-17 shows one of the micro fluidic chips and measurement data.

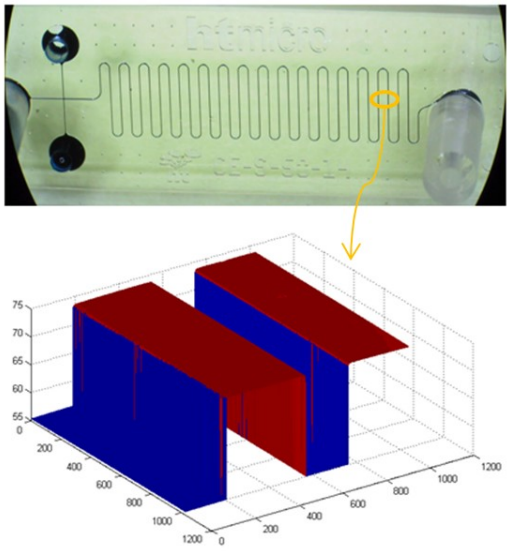

Figure 2-17 Micro fluidic device and measurement data concerning channel geometry

The micro channels and steps geometry/size are the most important characteristic features on the surface [45]. To design the microfluidic device architecture, the characteristics of testing sample need to be well investigated. For example, a microfluidc device for biological cell trapping, consists of parallel connected microchannels. It is designed to establish different flow resistances in different section, therefore when testing the fluid flow through some specific curved sections, target cells will be trapped in the connecting channels, as illustrated in Figure 2-18. The size of microchannels needs to be fabricated according to the target cell to meet the functional requirement.

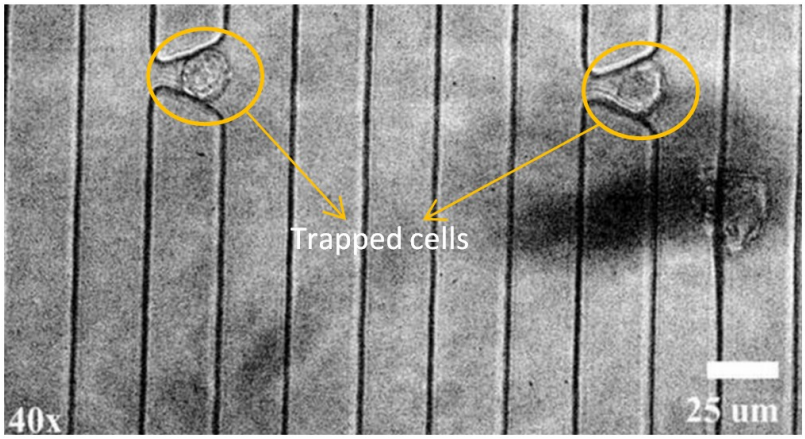

Figure 2-18 Trapped and arrayed cells by microfluidic [53]

2.5.4 Landing zone surface of hard disk

Hard disk is an indispensable component of the computer. The landing zone surface of the hard disk is designed to have a certain patterned precision surface [48]. From Figure 2-19, it is clear the surface has the micro bumps.

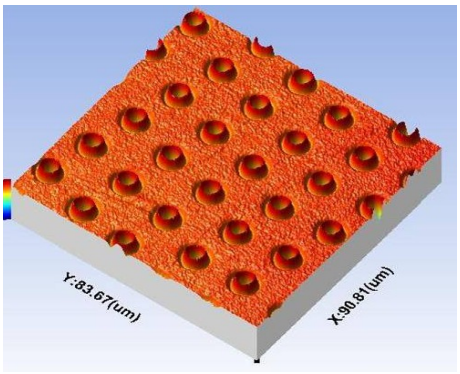

Figure 2-19 The landing zone of hard disk

During the fabrication process, a laser light beam is focused on the surface and melts the disk substrate martial rapidly. As the shape and location of these micro bumps require high precision, the energy, processing time and laser wavelength need to be precisely controlled [41].

The landing zone of hard disk ensures the reading/writing head to park on the disk surface accurately. The key evaluation parameter includes: height, diameter and density.

All the MEMS devices outlined above are examples of the most wildly used applications. The surface features of these MEMS devices are representational, so in the future chapters the different analysis, extraction and characterization methods will be used for these structured surfaces.

2.6 Summary

In this chapter, the definitions and classifications of structured surfaces are firstly reviewed. Furthermore, an introduction of MEMS is given. MEMS devices are the most significant applications of structured surfaces. The schematic diagrams in this chapter will be helpful to understand classification of surfaces and some specific properties of structured surfaces and MEMS. Materials are another important issue of surface measurement, understanding the properties of materials before measurement is significant and also will affect the measurement instrument choice and following analysis. There are plenty of materials applied in MEMS. Five major types of materials have been introduced. Different properties and applications of materials are summarized. Related parameters of different materials are listed in the tables in each section. Then micro/nano fabrication techniques, including two commonly used approaches "bottom-up" and "top-down" techniques have been introduced. At last, five representative applications of MEMS have been introduced. All these MEMS devices have a close connection with the structured surfaces.

Chapter 3 Metrology strategy

This chapter presents the challenges for metrology when measuring micro/nano scale structured surfaces. Three major types of surface instrumentation based on different principles are presented with corresponding specifications.

3.1 Metrology in micro/nano scale structured surfaces and challenges

Measurement of micro/nano scale structured surfaces is one of the main challenges for surface metrology in the coming years. Effective measurement of the micro/nano-scale structured surfaces is important for evaluating functional properties [52]. The balance lies between the available instruments and their abilities for a fast and reliable measurement. Rigorous metrology at the nanoscale has played an important role in industry in recent decades. It has focused on the field of surface topography characterisation through development of new instruments, micro/nano-scale traceable artifacts and surface parameters. For various structured surfaces with different properties, a practical measurement will facilitate useful characterisation and functional evaluation.

In any case, measurement and characterisation are important for any manufacturing process. Regarding nano-technologies, it has been shown that there is a major challenge in measurement capabilities [1,47]. Instruments are being used at the limits of their resolution to measure and characterise a range of nano-products. In addition,

when materials have some nanoscale dimension, their properties are different, compared to the traditional components and require different measurement disciplines and quantities [57]. There are new technological requirements necessary to meet the needs of nano-scale measurement and characterization [57,61].

For micro/nano structured surfaces, the manipulation of matter at the molecular level to create microstructures with unique properties is the key [54]. Metrology and instrumentation is an underpinning need for structured surface evaluation. Advances in fundamental structured surfaces and manufacturing of new micro/nano scaled products will depend on the capability to measure accurately and reproducibly properties and performance characteristics at nano scale. Micro/nano scale structured surfaces and related products require high performance, cost effective, reliable instrumentation and improved measurement methods [55,56]. The currently available suite of metrology tools is capable of meeting the needs of laboratory research. However, there are many technical challenges that must be addressed to successfully develop the instrumentation and metrology needed to support the future nano-technology industry [51]. These challenges include the development of standards, calibration methods, modeling, quantitative instrumentation, 3D characterisation of structures and measurement under real application conditions, as listed in Table 3-1.

Table 3-1 Key challenges for metrology in micro/nano scale structured surfaces

Metrology	Challenges
Standards and calibration	1. International collaboration to establish common standards 2. Traceable force and displacement calibration 3. Methodologies based on reliable data and models 4. Understanding of nanometer scale forces and contact mechanics
Instruments	1. Resolution, sensitivity and speed 2. Measurement environments (temperature, frequency) 3. Measurement limitations 4. Material specific issues 5. Non-destructive measurement
Modeling	1. Spatial resolution 2. Models to describe complex micro structure
3D Characterisation	1. Spatial and spectral resolution and specificity 2. Data computation speed 3. Accuracy and traceability
Measurement under real application conditions	1. Real-time measurement capabilities 2. Robustness 3. Large area capabilities

3.2 Instrumentation

Generally, all surface metrology instruments for micro/nano structure surface measurement can be categorised into three major types according to their different physical principles [59]. These three categories are contact-based instruments, optical instruments and scanning probe microscopy, each with different advantages, disadvantages and scope of application, as shown in Table 3-2.

Table 3-2 Surface measurement instruments and their applications

Principle	Merits	Limitations
Contacting measurement	1. Traceability 2. Large measurement range	1. Mechanical contact force (surface damage) 2. Tip geometry 3. Slow in 3D measurement
Non-contacting optical measurement	1. Fast measurement 2. High vertical resolution (0.1nm)	1. Limited detectable slope 2. Limited lateral resolution
Scanning probe microscope	nm resolution in X, Y and Z dimensions	1. Slow measurement 2. Limited measurement range

The stylus-based instruments are representative examples of the contacting method. Confocal instruments and optical interferometers use non-contacting method. In addition, scanning probe microscopy techniques use both contacting and non-contacting methods, as shown in Figure 3-1.

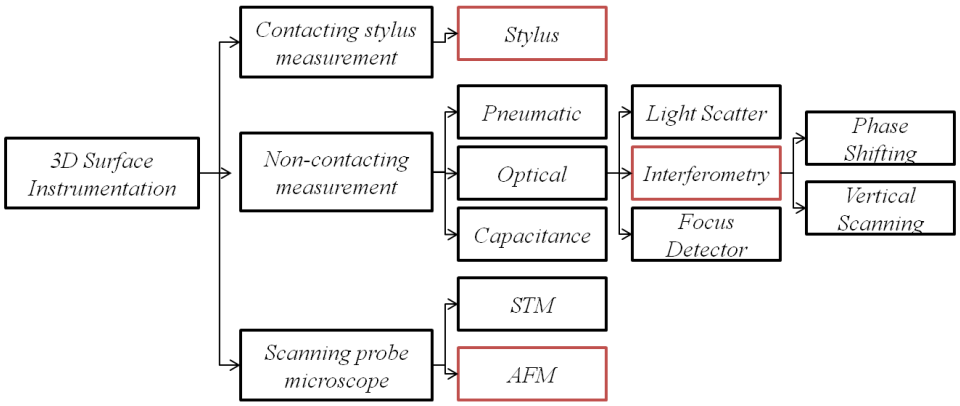

Figure 3-1 Classification and representative instruments of surface metrology

For different surfaces, the choice of the appropriate instrument is the first element of successful measurement. Both measurement range and resolution of instruments play a critical influence on measurement results. Therefore, it is necessary to understand the range and resolution of these three major types of instruments [58,60].

In Figure 3-2, a Stedman diagram is given. Stedman diagram was first proposed by Margaret Stedman (National Physical Laboratory, UK). It is a useful method to characterise these instruments capabilities. Both measurement range and resolution can be demonstrated and compared by this diagram. In this figure, the two axes respectively represent a log/log plot the minimum/maximum spatial distance and the minimum/maximum height the instruments can resolve and scan. Three blocks show the scope of applications of stylus-based instruments (blue), optical instruments (green) and scanning probe microscope instruments (grey). The red blocks show the approximate scope of the structured surfaces. The small block at the left side shows the structured surfaces applications like carbon nanotubes, inorganic nanotubes and nanowires. The large block at the right shows the applications like micro/nano steps, micro lens arrays, micro/nano fluidics, etc [2,56]. To compare the red blocks presenting the structured surfaces with other blocks, the limitation of instruments is shown in the diagram marked with arrows. From left to right, the first part is carbon nanotubes, the diameter of these nanotubes is normally 1-2 nm, and the length is from 0.2μm. The second part presents structured surfaces like micro-needle arrays. The heights of these micro needles are about 500μm, and the distance among them is less than 100μm. The third part presents structured surfaces like microlens arrays, the diameters of these microlens are about 800μm and the height is 2nm. All the structured surfaces in these three parts cannot be effectively measured by the existing surface instruments.

Although, there are other methods can improve the scopes of these existing surface measurement instruments. For instance, digital image stitching can effectively improve the measurement range of optical instruments. It combines multiple surface measurement data with overlapping fields. However, there are still many challenges

in measurement, especially for the many applications which have the nanoscale in two dimensions, like nanotubes [56].

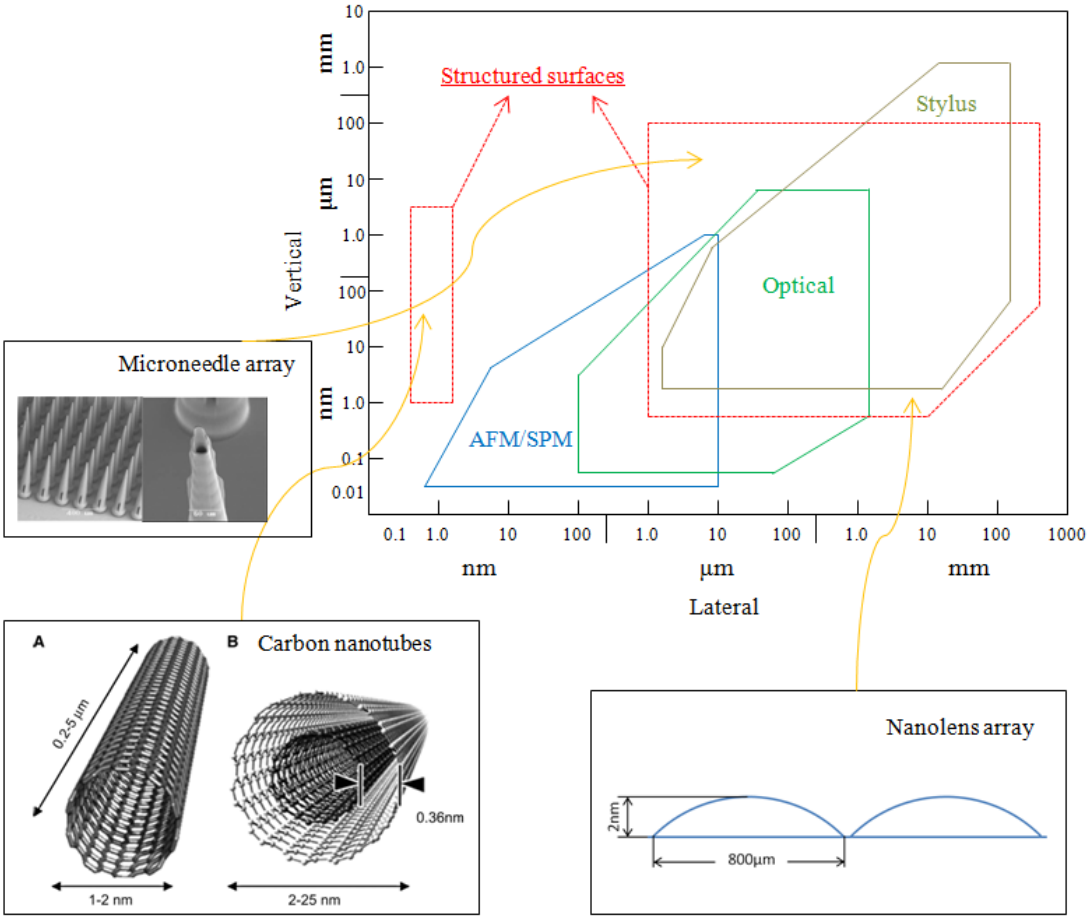

Figure 3-2 Measurement range and resolution of 3D surface instruments [2,56]

In this project, three instruments have been employed throughout the research. They are Talysurf PGI Series 2, Talysurf CCI 3000 and Veeco Dimension 3100 AFM, respectively, based on contacting stylus-based method, non-contacting optical method and scanning probe microscopy.

3.2.1 Stylus-based instruments

Among all three types of instruments, stylus-based instruments have the longest history in industry surface measurement. Stylus-based instruments have been widely

used in automotive industry. Most of the surface finishes standards in the world follow the prescribed methodology of stylus-based instruments. Furthermore, the contacting method gives the stylus-based instruments an advantage in dirty environments. Compared to the non-contacting optical method or scanning probe microscope, it won't greatly be influenced of environment. Therefore, this approach is particularly suitable for industrial field measurement.

For stylus-based instruments, a stylus is firstly moved into contact with a specimen and then moved across the surface laterally for a pre-defined distance and specified contact force [70]. The small surface variations in vertical direction can be measured by the displacement of the stylus. In recent decades, most stylus-based instruments are based on computers. An analog signal representing the height position of the stylus can be generated and converted into a digital signal by an analog-to-digital converter. Furthermore, all the measurement results and figures can be analysed and displayed. Generally, a stylus-based instrument can measure very small features in vertical direction ranging in height from 10 nanometres to 1 millimetre. The radius of diamond stylus ranges from 20 nanometres to 25 μm, 60° or 90° cone [70]. The stylus tracking force can range from less than 1 to 50 milligrams, as shown in Figure 3-3.

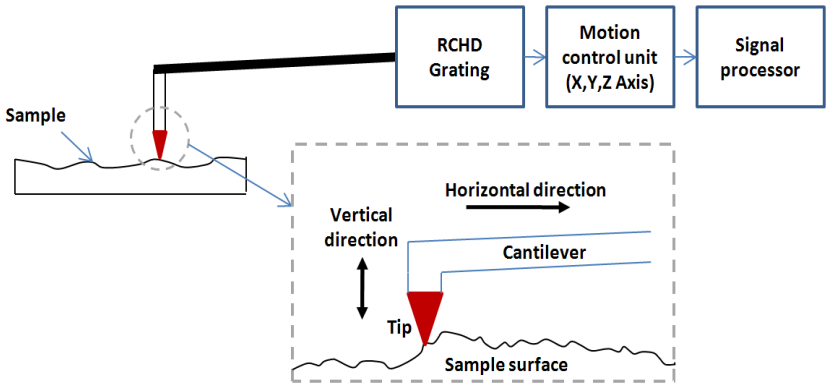

Figure 3-3 A schematic diagram of stylus-based instruments

Talysurf PGI Series 2 is a metrology instrument ideal for precision form and surface finish measurement [61]. The sample can be measured by moving the stylus contacting the surface. The vertical displacement of the stylus is transferred to a digital signal processor. All the measurement results are calculated and displayed by Talysurf PGI software. Motion control unit allows a user to control movement of stylus and during the measurement process. It can automatically control the stylus movement path according to the initial settings. Furthermore, for the PGI system a reflective cylindrical holographic diffraction (RCHD) grating monitors the vertical movement of the stylus. Stylus-based instruments have the advantages of high vertical resolution and large measurement range. Meanwhile, it has the limitations. It will damage the surface of the sample due to mechanical contact. Compared to optical instruments, it has slower measurement speed in 3D measurement.

The stylus-based instruments can use a laser interferometer to measurement the displacement of the stylus tip. Calibration of the X/Y-axis is an important procedure to define the cut-off wavelength and sampling length. Z-axis calibration of stylus-based instruments uses a calibration artifact with a known radius, after that the correction for the actuate movement of the stylus can be calculated. It has the

advantages of simple, quick and accurate. For example, the Talysurf PGI Series 2 calibration procedure consists of measuring a sphere standard block with a known radius, as shown in Figure 3-4 [61].

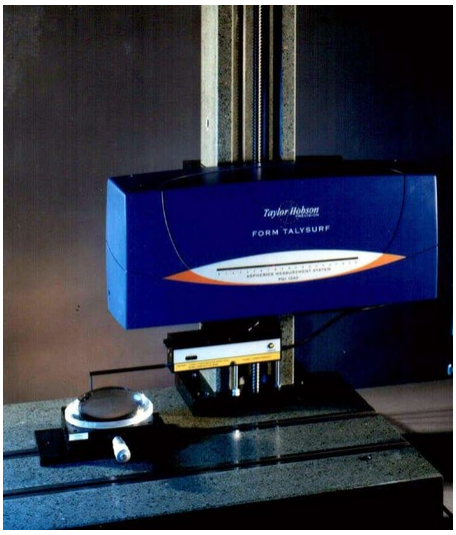

Figure 3-4 Gauge calibration using a spherical artifact [61]

The stylus Typical specifications are summarized in Table 3-3.

Table 3-3 The specifications of Talysurf PGI Series 2

Talysurf PGI Series 2	Specifications
Vertical resolution	12.8nm
Lateral resolution	0.25μm
Vertical range	10mm
Lateral range	120mm
Traverse speed	0.5mm/s 1.0mm/s
Stylus force	1mN

3.2.2 Non-contacting optical measurement

Non-contacting optical measurement instruments have some clear advantages over the stylus-based instruments. The instrument does not touch the sample, so the surface cannot be damaged during the measurement processes. The measurement speed of

optical instruments is also much higher [60]. An areal measurement of the surface can be obtained by optical instruments. Optical instruments can measure surfaces though the transparent medium such as glass or plastic film. This feature is ideal for some MEMS devices' measurement.

Optical interferometry is a powerful technique for non-contact measurement of surface topography at high vertical and moderate lateral resolution. It combines two light waves to give interference. Currently, both laser and white light are used as the light source of the interferometry. For example, ZYGO's Verifire™ Series of phase-shifting interferometers use laser as the light source. The advantage of laser light source is the interference fringes can be easily obtained, but any stray reflections will give spurious interference fringes. This will lead to incorrect measurement result.

White Light Interferometry (WLI) uses white light as the light source. As shown in Figure 3-1, there are two major types of interferometry, Phase Shifting Interferometry (PSI) and Vertical Scanning Interferometry (VSI) [62].

The basic principle and structures of PSI are shown in Figure 3-5. In PSI mode, a white-light beam from the light source is filtered by a set of the lens before it passes through the interferometer objective to the specimen surface. Half of the white-light beam can be reflected by the interferometer beam splitter to the reference surface. Therefore, interference's fringes can be formed and observed by combining two groups of beams. One is from the specimen surface, and the other is from the reference surface. The fringes appear darker bands and lighter bands alternating when it focuses on the specimen surface. During the measurement process, a piezoelectric transducer (PZT) moves the reference surface a known distance linearly to cause a phase shift between the test and reference beams. The instrument records the intensity

of the resulting interference pattern at a number of different relative phase shifts, and then the intensity can be transferred to wave front data by integrating [46,63].

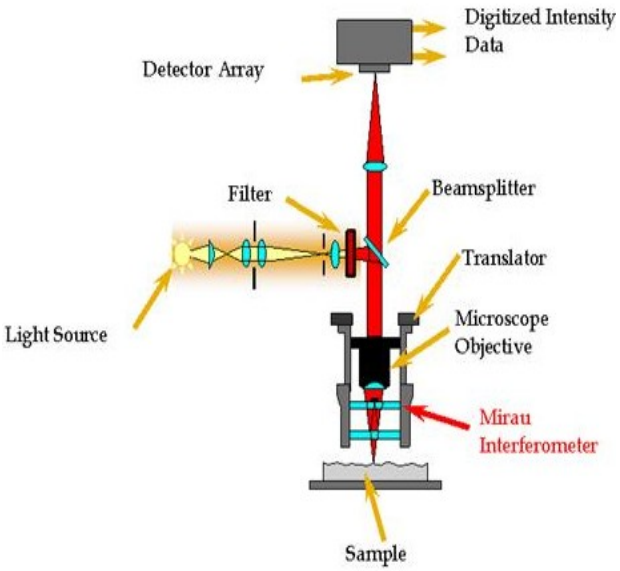

Figure 3-5 The basic principle of Phase Shifting Interferometry

The PSI mode of WLI is suitable for measurement of relatively "smooth", continuous specimen surfaces. Once the surface-height difference between adjacent measurement points is greater than λ/4, height errors in multiples of λ/2 may be introduced, and the wave front data cannot be reliably reconstructed [63]. Thus, there is necessary to improve the technique for the relatively "rougher" specimen surface.

The basic interferometer principles of VSI are similar to PSI. The interference fringes can be produced also by recombining two beams. One is the light reflected from a reference mirror, and the other is the beam from a specimen surface. Compared to the PSI mode, the VSI mode uses a neutral density filter to preserve the short coherence length of the white light. The instrument does not measure the phase of the interference fringes like PSI mode. The degree of fringe modulation or coherence will be measured in VSI mode. During the measurement, the microscope objective moves

in the vertical direction to scan the specimen surface. The motion can be controlled precisely by the instrument. Due to the short coherence length of white light, interference fringes can be appeared and observed at the focus positions. The focus positions change while the vertically distance changes. Fringe contrast at a single sample point reaches a peak as the sample is translated through focus [66]. The camera captures frames of interference data as the whole system scans vertically. The measurement data at each point of the specimen surface can be recorded by the instrument. Finally, the vertical position corresponding to the peak of the interference signal is extracted for each point on the surface [64,69]. A summary and differences between PSI and VSI is shown in Table 3-4.

Table 3-4 Operational differences between VSI and PSI

VSI	PSI
Neutral density filter for white light	Narrow bandwidth filtered
Vertically scans, the objective actually moves through focus	Phase-shift at a single focus point, the objective doesn't move
Processes fringe modulation data from the intensity signal to calculate surface heights	Processes phase data from the intensity signal to calculate surface heights

Talysurf Coherence Correlation Iterferometer (CCI) 3000 is an advanced type of measurement interferometer. It uses a selectable bandwidth light source to produce the interference pattern. A patented correlation algorithm has been applied to find the coherence peak and phase position of an interference pattern. This method provides both high resolution and high sensitivity to returning light. TalySurf CCI 3000 can reach 0.1Å (10 pm) resolution for both step height and micro roughness measurement [65]. Talysurf CCI 3000 uses artifacts to calibrate the instrument in both vertical and lateral axes. It is traceable to ISO standards. It is suitable for MEMS and micro/nano scale structured surfaces where the ultimate in high precision 3D profiling is required.

Meanwhile, it has a good data resolution in X and Y axes combined with a very low missing data rate. Lateral resolution can reach 0.36 μm. Almost all types of materials having reflectivity between 100% and 0.3% can be measured. It also has a $300mm \times 200mm$ height capacity, components up to $300mm^2$ in size and specimen areas up to $7.2mm^2$ can be measured and analysed without data stitching [16]. The typical specifications of TalySurf CCI 3000 are summarized in Table 3-5.

Table 3-5 Typical specifications of TalySurf CCI 3000

Talysurf CCI 3000	**Specifications**
Vertical range	100 μm
Vertical resolution	0.01nm
RMS repeatability	3pm
Vertical scanning speed	7mm/second
Measurement rang	$0.36mm \times 7.2mm$
Number of measurement points	1,048,576 (1024×1024 pixel array)
Lateral resolution	0.36μm
Step height repeatability	0.1nm (25mm step)
Linearity	0.03% of measured value
Pixel noise	0.2nm
Surface reflectivity	0.3%~100%
Component size	X,Y=300mm Z=200mm
Component weight	10kg
Measurement Time	10~20 seconds

Beside optical interferometry, confocal microscopes are also important non-contacting optical measurement instruments. The confocal microscope was first invented by Marvin Minsky in 1955 at Harvard University [49]. Confocal microscope is a point by point measurement instrument. It consists with of two major parts, a stationary optic part and a moving specimen stage. This design has the advantage of keeping the sensitive alignment of moving optics. Light focus on the surface by a pinhole aperture. As the specimen on the stage moving, an image of surface can be

illuminated by collecting the returning rays. The principle of confocal microscope is shown in Figure 3-6.

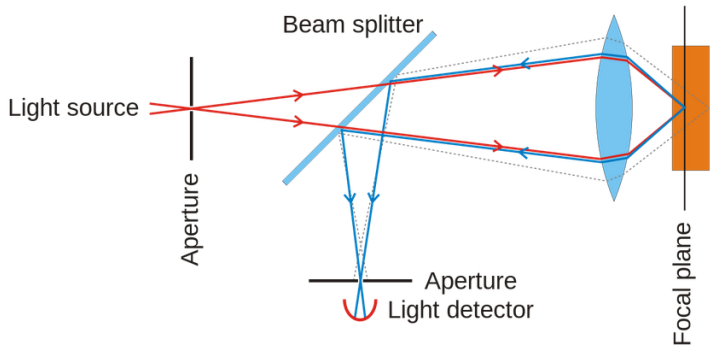

Figure 3-6 Principle of confocal microscopy

Compared to the conventional microscopes, confocal microscopy will only collect the returning light from the microscope's focal plane. Therefore, the measurement result of confocal microscopy can avoid the influence of the unwanted scattered light. The image has better contrast and makes confocal microscopy better observation of surface details.

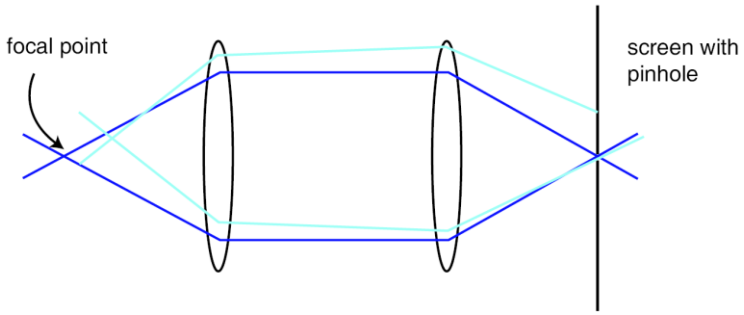

Figure 3-7 Rejection of light not incident from the focal plane

Figure 3-7 demonstrates the rejection of light not incident from the focal plane. The dark blue lines represent the light from the focal plane and light blue represents the light not from the focal plane (different colours just for demonstration, not present different wavelength). From the picture, the light blue lines do not focus at the

location of the screen. Therefore, most of the light collected not from the instrument's focal plane will be excluded. It ensures the quality of measurement results. The image will appear blurred as the results from a conventional microscope.

3.2.3 Scanning probe microscopy

Scanning Probe Microscopy (SPM) forms images of sample surfaces based on a probe scanning the specimen. By moving the probe in both X and Y directions on the surface, line by line, an image can be obtained. It records the probe-surface interaction as a function of position [67]. The resolution of SPM varies. Some techniques reach an atomic level. The resolution of microscopes is not limited by diffraction, but only by the size of the probe-surface interaction volume, that means it can be down to a few pm. So, SPM has the ability to measure small local difference in height, especially micro step height of MEMS and structured surfaces. Compared to electron microscope methods, measurement samples don't need a partial vacuum. However, SPM has its drawbacks, for example, the maximum image size is small, and relatively slower in measurement speed.

As an important established type of SPM, Atomic Force Microscopy (AFM) is also a very high resolution instrument [65]. It consists of a cantilever and tip used to scan the surface. The cantilever is normally silicon with the very sharp tip made of Si , SiN or diamond. The tip can be obtained by both acid etching and cutting. Figure 3-8 shows an image of AFM cantilever and tip.

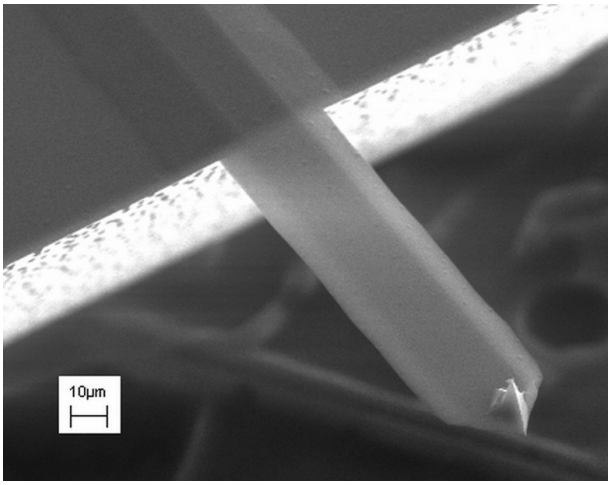

Figure 3-8 Typical AFM cantilever and tip

During the measurement, the tip is brought into proximity of a specimen surface. Force between the tip and surface leads to a deflection of the cantilever according to Hooke's law. Forces measured in AFM, including mechanical contact forces, van der waals forces, electrostatic forces, etc. [17]. Normally, the deflection is measured by a laser spot reflected from the top surface of the cantilever into the photodiode. If the tip was scanned at a constant height, a risk would exist that the tip collides with the surface, causing damage [68]. Hence, in most cases, a feedback mechanism is employed to adjust the tip-to-sample distance to maintain a constant force between the tip and the sample.

The AFM can be operated in several different modes, including contact mode, non-contact mode and tapping mode. In contact mode, the tip is so close to the specimen surface, therefore, that the attractive forces can be very strong. The force between the tip and the surface is kept constant during scanning by maintaining a constant deflection. Figure 3-9 shows a schematic diagram of the AFM contact mode operation.

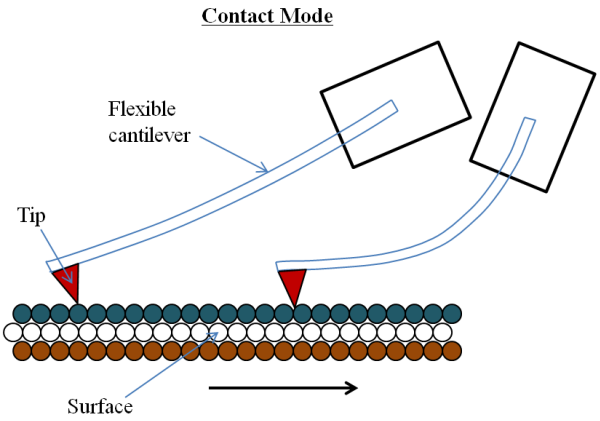

Figure 3-9 Schematic diagram of the AFM contact mode operation

In non-contact mode, the tip does not contact the specimen surface [70]. The distance between them is usually a few nanometers. The flexible cantilever oscillated at a resonant frequency. Due to the extremely short distance between tip and surface, the internal force will modify the frequency. Compared to the reference resonant, the characteristic information of the surface can be obtained. As the cantilever and tip move along the surface, the Measuring the tip-surface distance at each point allows the AFM to construct a topographic image of the sample. Figure 3-10 shows a schematic diagram of the AFM contact mode operation. Compared to contacting mode, non-contacting mode will do less damage to the sample, so it is suitable for the soft specimens. In the case of rigid samples, the measurement data will be almost same.

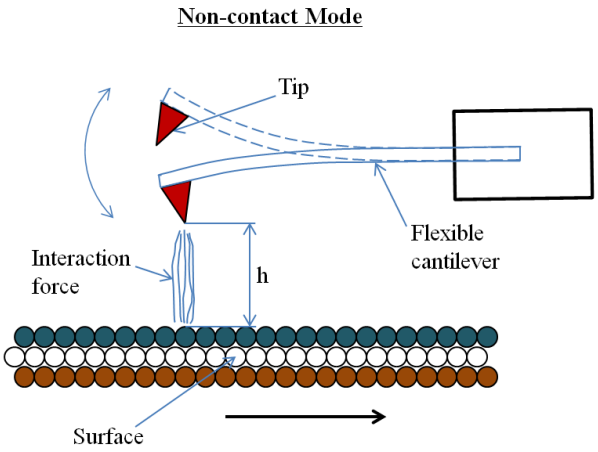

Figure 3-10 Schematic diagram of the AFM non-contact mode operation

Tapping mode can be seen as a combination of both contacting and non-contacting modes. The probe tip is placed close enough to the surface, so the short-range forces can be detectable. Also it will prevent the tip from sticking to the surface. Therefore, tapping mode can reduce the damage of samples. Figure 3-11 shows a schematic diagram of the AFM contact mode operation.

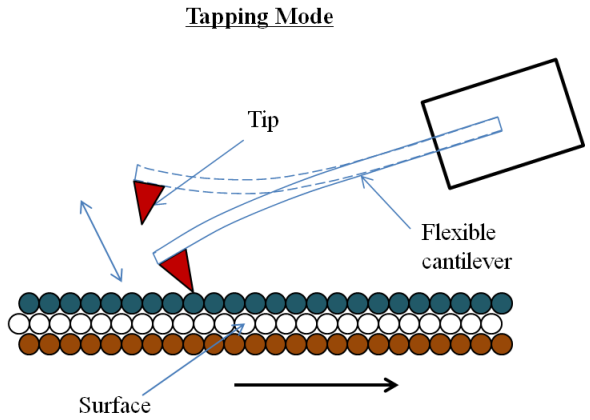

Figure 3-11 Schematic diagram of the AFM tapping mode operation

Block diagram of atomic force microscope and details of an AFM tip are shown in Figure 3-12.

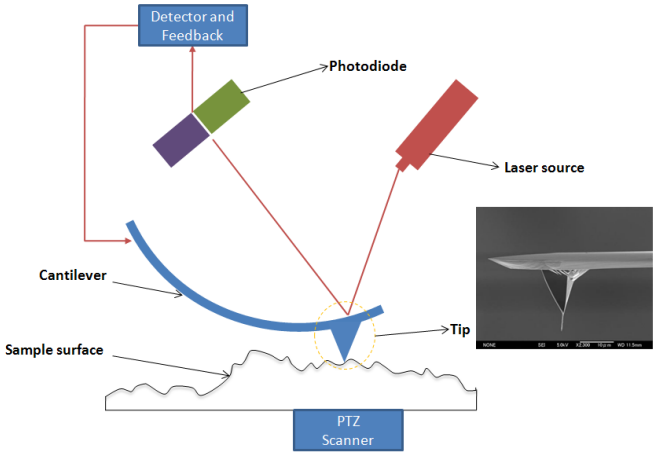

Figure 3-12 Block diagram of atomic force microscope and details of an AFM tip

The Dimension 3100 AFM is an instrument capable of imaging specimen surfaces with both horizontal and vertical resolution down to nanometers [69]. The instrument uses a sharp tip on the micro-scaled cantilever to measure the specimen. The tip contacts with the surface and scans across it horizontally. It has the ability to measure samples from small pieces to 150 mm diameter wafers. The probe is the most important component of the instrument. These are two types of probes have been commonly used. One is the RTESP probe, and the other is DNP-20 probe. The former type of probe is normally used for the tapping mode while the latter is used for contact mode. The typical specifications of Dimension 3100 are summarized in Table 3-6.

Table 3-6 The typical specifications of Veeco Dimension 3100 AFM

Veeco Dimension 3100 AFM	Specifications
X-Y Scan Range	~90 μm^2 Lateral accuracy typically within 1%, max. 2% 16-bit resolution on all axes
Z Range	$\leq 6\mu m$
Sample Size	$\leq 150mm$ diameter $\leq 12mm$ thick
Sample Holders	150mm vacuum chuck Magnetic holder
Stage	$125mm \times 100mm$ inspectable area 2μm resolution Repeatability unidirectional: 3 μm in X, 4 μm in Y Repeatability bidirectional:8 μm in X, 10 μm in Y
Tip/Cantilever Holders	Tapping/contact modes
Microscope Optics	150 μm to 675 μm viewing area 1.5 μm resolution
Tip Viewing	On-axis real-time
Vibration Isolation	Silicone vibration pad

3.3 Summary

In this chapter, it is firstly introduced the significance of surface measurement and then the challenges of metrology in micro/nano scale structured surfaces including Standards and calibration, instruments, modeling and 3D characterization. A classification of instruments based on different physical principles is given. Three major types are summarized as contacting stylus instruments, non-contacting optical measurement and scanning probe microscopes. Their respective measurement range, resolution, advantages, disadvantages and applications are summarized. Later in this chapter, three instruments are employed throughout the research of the project. They are Talysurf PGI Series 2, TalySurf CCI 3000 and Veeco Dimension 3100 AFM. Finally, the principles and specifications of three instruments are introduced.

Chapter 4 Feature description of micro structures and establishment of evaluation reference

This chapter presents a classification according to structured surfaces' micro characteristic structures. The objective of this classification is to find the optimum classification of micro characteristic structures based on previous investigation of representative structured surfaces and MEMS. Furthermore, the mathematical process to establish a datum plane for characteristic microstructures has been established as the identification of characteristic functional regions.

4.1 Structured steps and structured pattern array

As mentioned in chapter 2, structured surfaces can be divided into directional surfaces and non-directional surface. For MEMS devices, due to the fabrication techniques, most of them can be defined as structured surfaces having structured steps. A further type of structured surface is structured pattern arrays. The following section will discuss these two major types and their definitions.

In chapter 2, several applications of MEMS have been introduced. Among these applications, most MEMS devices have a similar surface, such as micro pressure sensors, accelerometers, gyroscopes and RF MEMS resonators, as shown in Figure 4-1. These MEMS commonly use structured steps as their dominate structural feature.

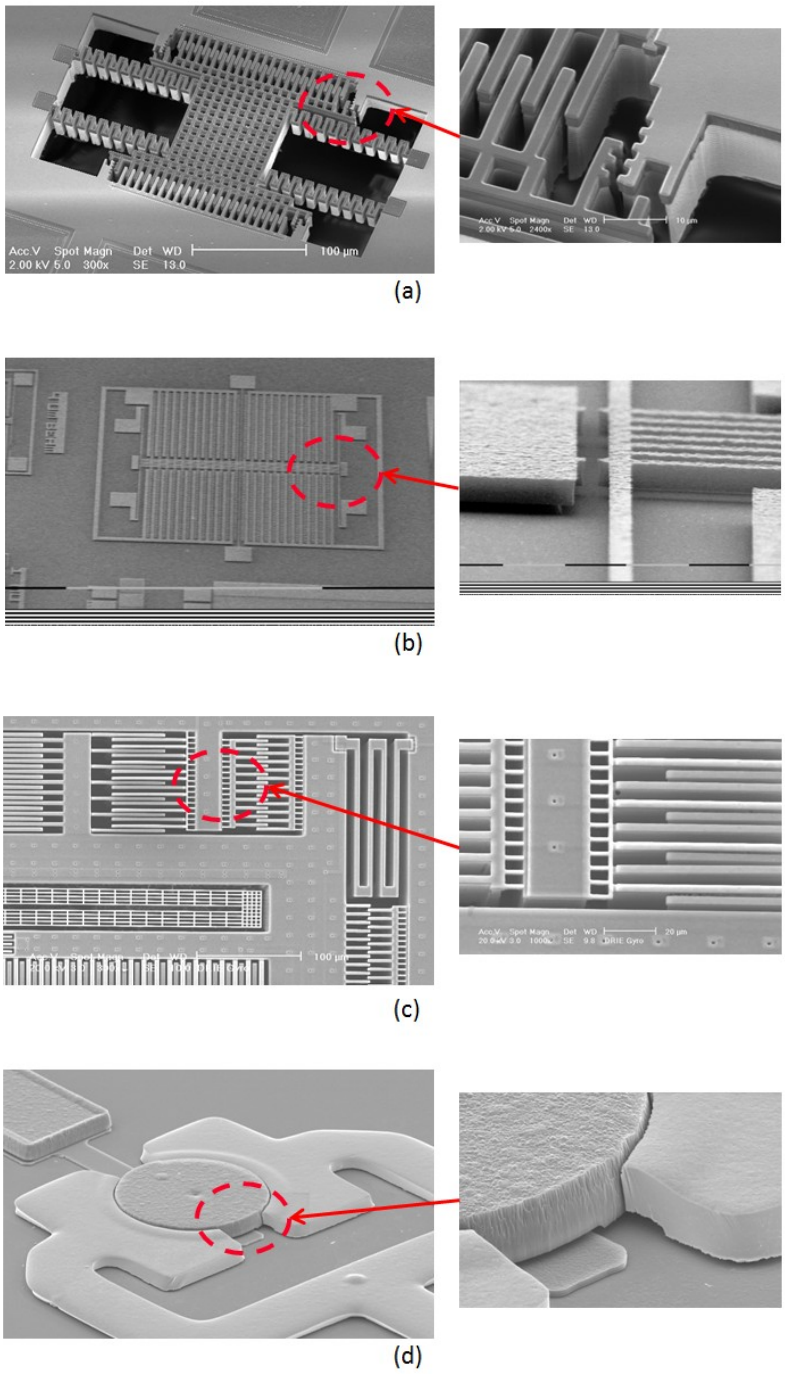

Figure 4-1 (a) Accelerometer (b) Micro sensor (c) Gyroscope (RF MEMS Resonators) and (d) local amplifications of micro structures [9]

The structured steps can be defined as the following descriptions:

1. Characteristic structures of the surface are planar steps and grooves at the micro scale. Meanwhile, its geometric parameters and relationships between them are key factors to ensure that device performance.

2. Cross sections of the surfaces at the micro/nano scale have micro step/groove feature regions.

The other major structured surface type is the structured pattern array. In general, the surface of this type is composed of many similar elements (micro structures). The distance between these elements are commonly small (from 100μm to several nm). Meanwhile, all these elements are arranged in a periodic arrangement, as shown in Figure 4-2.

The definition of the structured pattern array is as follows.

1. All elements or primitives are arranged on the surface according to certain rules, and form a periodic array or tessellated pattern.

2. From a mathematical point of view, if the images function of the surface is approximately periodic or constant. Then, the certain areas of the surface can be considered as the repeating structured pattern.

In Figure 4-2, there are three devices with structured pattern array surface.

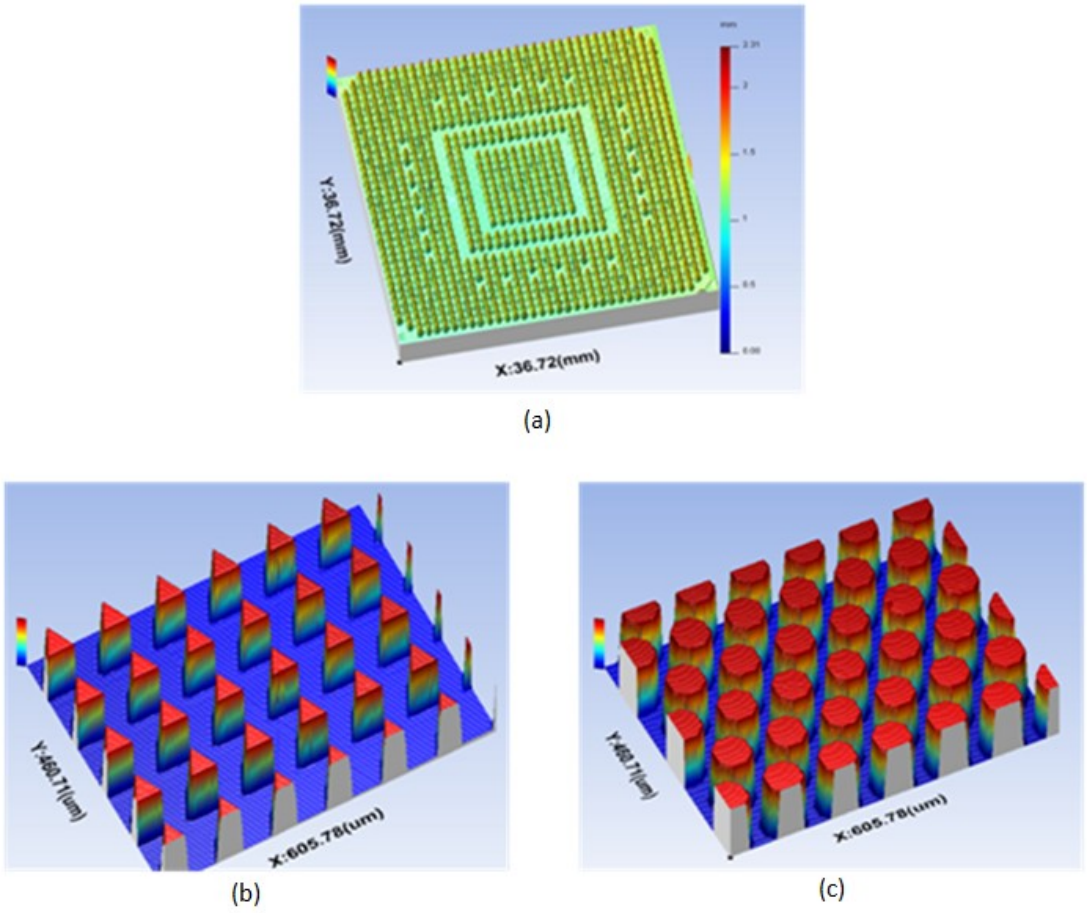

Figure 4-2 Three devices with structured pattern array surface (a) Chip pin surface (b) Structured surface with etched Si triangular structured features (c) Structured surface with etched Si octagonal structured features

To define the structured pattern, a mathematical expression of a two-dimensional image is given:

$$I = f(i,j), \quad i,j \geq 0 \tag{4.1}$$

$f(i,j)$ is measurement data in Z direction of row x and column y, suppose m is the horizontal minimal period of the array structures, otherwise n is the vertical minimal period. As most of structured surfaces have a similar periodicity, suppose a sufficiently small threshold value σ, if the inequality (4.2) can be satisfied, then it can be considered as a micro array surface.

$$\left| f(i+m,j+n) - f(i,j) \right| < \sigma \tag{4.2}$$

4.2 Establishment of datum plane for structured surface

Datums are planes, points, lines, or axes from where measurements are made [70]. A datum feature is an actual feature on a part, such as a structured surface, that is used to establish a datum to which dimensional geometrical measurement are compared. A datum plane is a geometric part of the whole specimen. For example, for micro/nano scale structured surfaces, all the location and size dimensions are depended on the datum plane. Datum plane is the foundation for structured surface characterisation. It also affects the further analysis, like feature segmentation and evaluation [82]. The former on the parts themselves are referred to as datum feature simulators.

The establishment of datum plane is significant for the following structured surface characterisation. A micro-structure, such as a step and micro optical lens is considered as a datum feature. A least squares and B-spline fitting method will be applied to simulate a datum plane. The datum plane will be a reference plane of the structured surface, then all the parameters such as the step height, width, flatness, roughness...etc. can be obtained with reference to the datum plane.

4.2.1 Plane fitting

The least squares method is a standard approach to the approximate solution of over determined sets of data. For establishing a datum plane, the definition of the plane needs to be defined. So, a plane in 3D space may be defined as:

$$Ax + By + Cz + D = 0 (C \neq 0) \tag{4.3}$$

A, B, C and *D* are parameters of X-Y-Z in three dimensional space, hence,

$$z = -\frac{A}{C}x - \frac{B}{C}y - \frac{D}{C} \tag{4.4}$$

$$z = a_0 + a_1 y + a_2 \tag{4.5}$$

Let

$$a_0 = -\frac{A}{C}, a_1 = -\frac{B}{C}, a_2 = -\frac{D}{C} \tag{4.6}$$

Assuming there are n points, $(n \geq 3)$ for these points, $(X_i, Y_i, Z_i), i = 0,1,...n-1$ to fit the above plane equation:

$$S = \sum_{i=0}^{n-1} (a_0 x + a_1 y + a_2 - z)^2 \tag{4.7}$$

Must meet

$$\frac{\partial S}{\partial a_k} = 0, k = 0,1,2 \tag{4.8}$$

Which,

$$\begin{cases} \sum 2(a_0 x + a_1 y + a_2 - z_i) x_i = 0 \\ \sum 2(a_0 x + a_1 y + a_2 - z_i) y_i = 0 \\ \sum 2(a_0 x + a_1 y + a_2 - z_i) z_i = 0 \end{cases} \tag{4.9}$$

Thus,

$$\begin{cases} a_0 \sum x_i^2 + a_1 \sum x_i y_i + a_2 \sum x_i = \sum x_i z_i \\ a_0 \sum x_i y_i + a_1 \sum y_i^2 + a_2 \sum y_i = \sum y_i z_i \\ a_0 \sum x_i + a_1 \sum y_i + a_2 n = \sum z_i \end{cases} \tag{4.10}$$

Which is equivalent to:

$$\begin{vmatrix} \sum x_i^2 & \sum x_i y_i & \sum x_i \\ \sum x_i y_i & \sum y_i^2 & \sum y_i \\ \sum x_i & \sum y_i & n \end{vmatrix} \begin{pmatrix} a_0 \\ a_1 \\ a_2 \end{pmatrix} = \begin{pmatrix} \sum x_i z_i \\ \sum y_i z_i \\ \sum z_i \end{pmatrix} \tag{4.11}$$

By the linear equations above, the coefficients a_0, a_1, a_2 can be found. Therefore, a datum plane can be established [23,46].

4.2.2 Curve fitting

Curve fitting is the process of constructing a curve or a mathematical function that has the best fit to a series of data points, possibly subject to constraint. There are two different approaches of curve fitting, or smoothing, in which a smooth function is constructed that approximately fits the data [93].

The first approach is an interpolation method, where an exact fit to the data is required [57]. Interpolation methods use measured cloud points to determine a fitting surface. The error of fitting a surface, to a great extent, depends on the measurement data. If there are enough points, the fitted surface will be more accurate. In contrast, if measurement data is limited, interpolation methods will lead to an inaccurate result.

The second approach to fitting is regression analysis. It mainly focuses on the statistical inference. For example, the uncertainty of a curve fitted to data [61]. The curves can be applied for the data visualization. It can infer the values for the regions where no effective data has been measured. Furthermore, it presents the relationships between the variables. In some cases, extrapolation can be applied for the fitted curve beyond the range of reliable measurement data, for example, for the edge region of micro step structured surfaces [63,72].

4.2.3 Least squares quadric surface fitting

Among all the boundary surfaces, quadric surface fitting is relatively simple [52]. Assuming $a_1, a_2, a_3, ...a_9$ are the coefficients of the quadric surface under X-Y-Z coordinate system, then, the equation of the quadric surface is;

$$a_1x^2 + a_2y^2 + a_3z^2 + a_4xy + a_5yz + a_6xz + a_7x + a_8y + a_9z + 1 = 0 \quad (4.12)$$

And in matrix form,

$$V = Ax - f \tag{4.13}$$

And,

$$A = \begin{bmatrix} x_1^2 & y_1^2 & z_1^2 & x_1y_1 & y_1z_1 & x_1z_1 & x_1 & y_1 & z_1 \\ x_2^2 & y_2^2 & z_2^2 & x_2y_2 & y_2z_2 & x_2z_2 & x_2 & y_2 & z_2 \\ . & . & . & . & . & . & . & . & . \\ . & . & . & . & . & . & . & . & . \\ . & . & . & . & . & . & . & . & . \\ x_n^2 & y_n^2 & z_n^2 & x_ny_n & y_nz_n & x_nz_n & x_n & y_n & z_n \end{bmatrix} \tag{4.14}$$

$$V = \begin{bmatrix} V_1 \\ V_2 \\ . \\ . \\ . \\ V_n \end{bmatrix}, f = \begin{bmatrix} -1 \\ -1 \\ . \\ . \\ . \\ -1 \end{bmatrix}$$

V is an objective function of distance from each measurement point and fitting curve, according to least squares method. Furthermore, $V^TV = \min$ then, the normal equation is,

$$NX = b \tag{4.15}$$

In the equation above, $N = A^TA; b = A^Tf$

Then, the quadric surface can be expressed by the inversion of above equation,

$$X = N^{-1}b \tag{4.16}$$

As fitting parameter X found, the sum of squares of fitting residual is,

$$\begin{aligned} [v \cdot v] &= \sum_{i=1}^{n} (a_1x_i^2 + a_2y_i^2 + a_3z_i^2 + a_4x_iy_i + a_5y_iz_i \\ &+ a_6x_iz_i + a_7x_i + a_8y_i + a_9z_i + 1)^2 \end{aligned} \tag{4.17}$$

Therefore, fitting precision of quadric surface is,

$$\delta_s = \pm\sqrt{\frac{[v \cdot v]}{n-3}} \tag{4.18}$$

However, from the expression for the quadric surface the shape of the surface is not intuitive. If the species of the curved surface is obvious and intuitive, then it is more convenient to compare the measured surface and the fitting surface and also more convenient to obtain the display of entity shape [73]. Meanwhile, some of the geometrical parameters, such as radius, thickness, arc length may be obtained. So equation 4.12 is transferred to an expression of an implicit function, the species of curved surface becomes intuitive.

$$f(x,y,z) = A_1x^2 + A_2y^2 + A_3z^2 + 2A_4xy + 2A_5yz + 2A_6xz + 2A_7x + 2A_8y + 2A_9z + A_{10} \tag{4.19}$$

The species of the curved surface are determined by the corresponding coefficients, assuming,

$$H = \begin{vmatrix} A_1 & A_4 & A_5 & A_7 \\ A_4 & A_2 & A_6 & A_8 \\ A_5 & A_6 & A_3 & A_9 \\ A_7 & A_8 & A_9 & A_4 \end{vmatrix} \tag{4.20}$$

$$D = \begin{vmatrix} A_1 & A_4 & A_5 \\ A_4 & A_2 & A_6 \\ A_5 & A_6 & A_3 \end{vmatrix} \tag{4.21}$$

$$w_1 = A_2A_3 - A_6^2, w_2 = A_1A_3 - A_5^2 \tag{4.22}$$

$$w_3 = A_1A_2 - A_4^2, w_4 = A_4A_5 - A_1A_6 \tag{4.23}$$

$$w_5 = A_4A_6 - A_2A_5, w_6 = A_5A_6 - A_3A_4 \tag{4.24}$$

If the coefficients of the quadrics surface equation satisfy the relations below,

$$\frac{A_4A_5 - A_1A_6}{A_6} = \frac{A_2A_5 - A_4A_6}{A_5} = \frac{A_3A_4 - A_5A_6}{A_6} \tag{4.25}$$

It can be considered as a cone surface.

Alternatively, if the coefficients of quadrics surface equation satisfies the relations below,

$$A_1 = A_2 = A_3, A_4 = A_5 = A_6 = 0 \tag{4.26}$$

It can be considered as a cylindrical surface.

4.2.4 Fitting B-Spline curves to point clouds

Fitting a curve to a set of data points is a fundamental problem in many applications like computer graphics and computer vision. To establish a datum plane for structured surface, B-spline fitting methods also provide an effective way to solve the problems [78]. Before the description of how to fit a set of data points with a B-spline curve using a least-squares algorithm, a definition of B-Spline curves is given. A B-spline curve is defined as a collection of n+1 control points $\{Q_i\}_{i=0}^{n}$ by.

$$X(t)=\sum_{i=0}^{n} N_{i,d}(t)Q_i \tag{4.27}$$

The control points can be any dimension, but must all be the same dimension. The degree of the curve is d and must satisfy $1\le d\le n$. The functions $N_{i,d}(t)$ are the B-spline basis functions, which are defined recursively and require the selection of a sequence of scalars t_i for $t_i \le t_i+1$. Each t_i is referred to as a knot, in the total sequence. For a knot vector, the basis function that starts the recursive definition is.

$$N_{i,0}(t)=\begin{cases}1, t_i < t < t_{i+1}\\ 0, otherwise\end{cases} \tag{4.28}$$

For $0\le i\le n+d$, the recursion itself is.

$$N_{i,j}(t)=\frac{t-t_i}{t_{i+j}-t_i}N_{i,j-1}(t)+\frac{t_{i+j+1}-t}{t_{i+j+1}-t_{i+1}}N_{i+1,j-1}(t) \tag{4.29}$$

For $1\le j\le d$ and $0\le i\le n+d-j$, the support of a function is the smallest closed interval on which the function has at least one non-zero value. The support of $N_{i,d}(t)$ is clearly $[t_i, t_{i+1}]$. In general, the support of $N_{i,j}(t)$ is $[t_i, t_{i+j+1}]$. This fact means that

locally the curve is influenced by only a small number of control points, a property called local control.

The main classification of the knot vector is that it is either open or periodic. If open, the knots are either uniform or nonuniform. Periodic knot vectors have uniformly spaced knots [71]. The use of the term open is perhaps a misnomer since one can construct a closed B-spline curve from an open knot vector. The standard way to construct a closed curve uses periodic knot vectors. Uniform knots are.

$$t_i = \begin{cases} 0, 0 \le i \le d \\ \dfrac{i-d}{n+1-d}, d+1 \le i \le n \\ 1, n+1 \le i \le n+d+1 \end{cases} \tag{4.30}$$

Periodic knots are

$$t_i = \frac{i-d}{n+1-d}, 0 \le i \le n+d+1 \tag{4.31}$$

The data points are $\{s_K, p_K\}_k^m$, where s_K is the sample spacing and p_K is the sample data. The sample spacing are assumed to be increasing. A B-spline curve that fits the data is parameterized by $t \in [0,1]$, so the sample times need to be mapped to the parameter domain by $t_K = (s_K - s_0)/(s_m - s_0)$.

4.3 Conclusions

In this chapter, a classification of structured surface has been defined. The two major types of structured surfaces can be classified into structured steps and structured pattern arrays. The datum plane for structured surfaces has been established for further characterisation and evaluation.

Chapter 5 Characterisation and evaluation of micro structured steps

The objective of this chapter is to study the evaluation parameters of micro structured steps associated with their functional performance. An evaluation system of MEMS structured surface needs to be established. Evaluation parameters for micro structured step features need to be studied. Step height calculation based on different methods needs to be investigated. Due to the difficulty in step sidewall measurement, method of step wall roughness estimation needs to be developed.

5.1 Evaluation parameters for micro structured steps

The most significant evaluation parameters for micro structured step samples are step height and groove depth, width of the step and approximate sidewall roughness. In Figure 5-1, the schematic diagram shows the geometric parameters of a micro structured step. In (a), H is the step height or groove depth, W is the width of the step and R_i is the approximate sidewall roughness. (b) is the cross-section of the step, it is perpendicular to the measurement reference plane and parallel to the machining direction. Six parameters are defined, a is the middle point of the sidewall edge, b is the average step width, c is the step height, d is the minimum step width, e is the maximum step width and h is the projective distance of the sidewall.

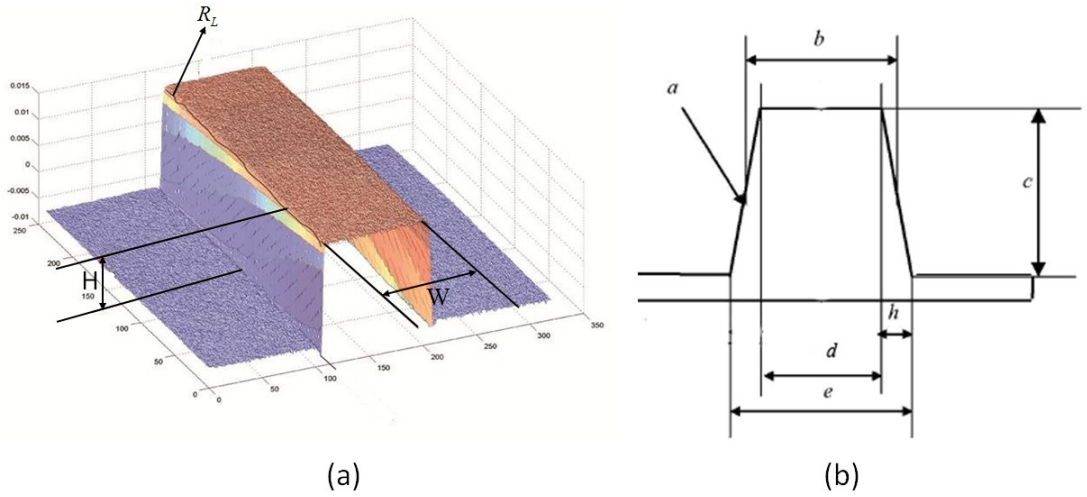

Figure 5-1 (a) Three major evaluation parameters of micro step (b) Cross-section of the step

5.2 Geometric dimensions of structured steps

Due to the small size of the structured surface features, any errors in geometry size of the surfaces can lead to serious loss of function. Most functional properties of structured surfaces depend on the precision of the structure size feature geometry and geometrical relationships between features, especially for most MEMS applications. This means, it is essential to have a strict control of the precision manufacturing process. For instance, atom filters which are used in space technology have tiny holes with the diameter normally under 45nm to keep out ultraviolet rays. The efficiency of the filters can be reduced to 10% when the diameter enlarges to 55nm [91]. In packaged MEMS systems, communication conduits including wire, fringing fields, optical waveguides and chemical transmitters are the important components to connect different functional regions. Their size and positional accuracy will directly affect the MEMS function. Due to the small size of MEMS and low fault-tolerance property, once the error exceeds allowable value, it can cause failure of the whole system. Consequently, the evaluation parameters step height H and step width W are based on the following definitions. Statistic sizes are considered in the light of

International Organization for Standardization (ISO) and National Institute of Standards and Technology (NIST). Local size is defined as the distance between two points or the local dimension of a certain range. Maximum and minimum size is respectively the maximum value and minimum value of the local dimension after removal of the noise points.

5.2.1 Topography of step sidewall

One of the most influential applications of structured surfaces with micro-step feature is micro fluidic chips. A key evaluation parameter of fluidic chips is the sidewall roughness. Micro fluidic chips are used for bio-samples analysis and DNA testing based on an electrophoresis technique [93]. Surface effect on fluid flow as a result of micro tunnel sidewall topography is an important issue as it will affect the function of the micro fluidic chip. Surface effects on micro fluidic function are classified into surface topography effects and surface force effects. Surface topography effect refers to the fluid-flow resistance by the tunnels' sidewall. Surface force effect refers to the surface friction force, surface adhesion, etc. For the conventional devices at the macro scale, topography of the sidewall has little effect on the fluid. However, for the micro fluidic chips, due to their small size the effect on the fluid is significant. Even small changes of sidewall roughness will affect the fluid flow in the whole chip.

The topography of micro structured step surfaces depends on both processing techniques and materials. For example, SU-8 photoresist is the major material for micro fluidic chips. Each processing step, including spin coat, soft bake, expose, post exposure bake (PEB) will cause physical or chemical reactions on the material surface and thus change the surface roughness. Meanwhile, internal stress changes during the knockout process. It causes deformation of the sidewalls or even collapse of the micro

tunnels. Hence, an effective surface measurement is necessary to ensure surface reaching design requirements [95].

Sidewall measurement, it is still a huge challenge in surface metrology. General surface instruments cannot handle sidewall roughness measurement, but it is an important evaluation parameter and impossible to be ignored. In this chapter, a novel method is applied to obtain the sidewall roughness by using line edge roughness. The advantage of this method is that there is no need for particular measurement instruments, so it is applicable for all the samples measured by existing conventional methods can be available. However, it also has the disadvantage that it is only an approximate roughness that can be obtained and significant of useful information may be neglected. Both the step top side edge and intersection edge of the micro tunnel bottom surface can be considered as the components of the sidewall roughness. Thus, the sidewall roughness is represented by the line edge roughness.

5.2.2 Slope angle of sidewall

Slope angle is another geometrical parameter, which affects the function of the step structured surface. It is the slope of sidewall and tunnel bottom surface. If the angle is less than 90 degrees, it indicates during the processing, the SU-8 photoresist has been overexposed by ultraviolet. The width of the tunnel bottom is larger than the designed mask. Conversely, if the angle greater than 90 degrees, the width of the tunnel bottom is smaller than the designed mask, as shown in Figure 5-2.

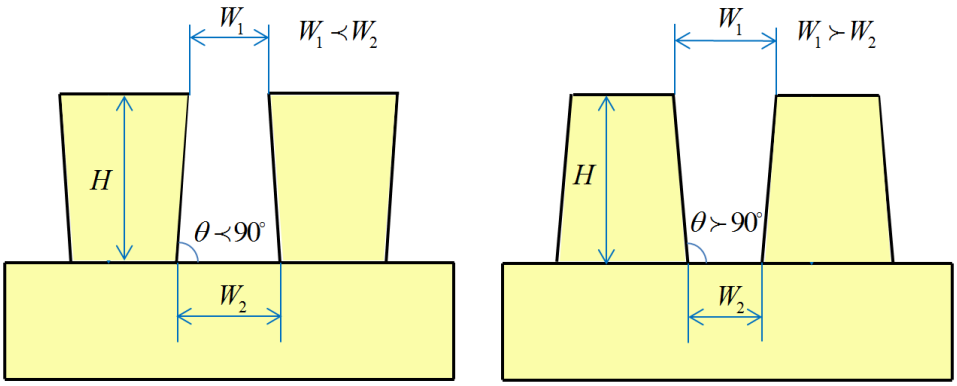

Figure 5-2 Slope angle of sidewall

5.3 Evaluation of micro structured step height

Height and width evaluation of micro steps is a key process parameter for structured surface characterisation. Up to now, there is still no complete operational standard for structured step height evaluation published by International Organization for Standards. In this section, three different methods are presented.

5.3.1 Point-to-point step height evaluation

The point-to-point method is a rapid way to calculate approximate step height. In this case, step height is represented by the vertical dimension from two sampling point from both the step top surface and the tunnel bottom surface, as shown in Figure 5-3. This method has the advantage of computation simplicity and is suitable for the step height rapid estimation. However, due to the randomness of two selected sampling points, the result generally contains the errors. For the specific cases which step height is the key parameter, this method is not recommended [52].

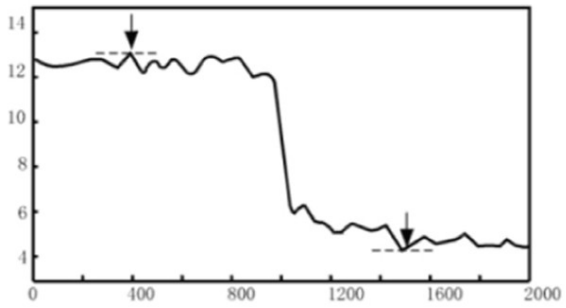

Figure 5-3 A schematic diagram of point-to-point method

Because only two sampling points are selected, therefore the result is responded to represent a single edge step height only. For many of the structured step surfaces, single edge step height is applicable. However, for some samples, though the steps are similar the heights on both sides may be quite different. Under such circumstances, single edge step height cannot represent height information of both sides, so a double side step height method is demanded, which will be discussed in following section. During the process, sampling points is a key issue of the evaluation, an effective selection of sampling points depends on the width of the steps, Figure 5-4.

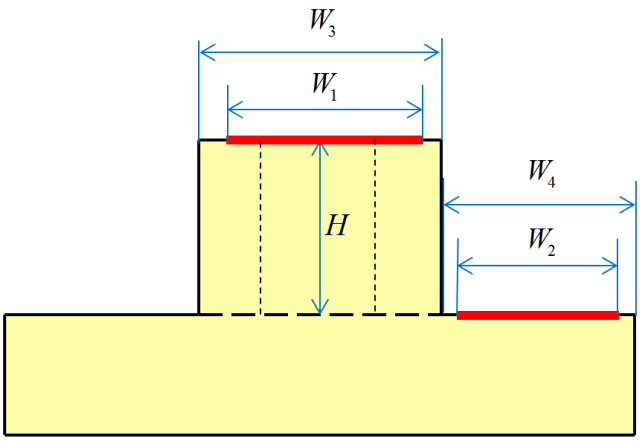

Figure 5-4 Single edge step height evaluation

From the figure above, two surfaces step surfaces are shown, one is the higher step top surface and the other is the lower tunnel bottom surface. Firstly, the edge of step

needs to be determined by the differential method. To reduce the influence of the step edge regions, the data of edge regions need to be neglected. The length of step edge regions W_1, W_2 depends on the width of step top/bottom surface (W_3, W_4). Then, respectively fitted the both step top surface and the tunnel bottom surface, shown as the red lines in the figure above. The step height H can be obtained by the distance between the top surface and bottom surface.

5.3.2 Evaluation based on ISO 5436 and NIST

Evaluation based on ISO 5436 is shown in Figure 5-5. In the middle is the higher step top surface and both sides are the lower tunnel surface. The width is all equal to W , and both sides are symmetric to the centre line of the step [75,105]. As mentioned in the last section, step edge regions need to be neglected. As the width of step W is known, the whole step surface can be divided into three parts respectively from left to right side the length of each region is $W/4$, $W/2$ and $W/2$ .So the effective region in the middle is $W/2$, the measurement data in this region will be used to calculate the step height. Data of both sides will be neglected. For the tunnel surface, the step edge region can be also defined as the region close to the step sidewall and the length of step the edge region is also defined as $W/4$. The data in the remaining part of $W/2$ is effective. Therefore, in this figure, all three parts are effective, represented by A, B, C , the width is $W/2$, then lengthening fitted lines to the step edge. The step height h is defined as the average vertical dimension between them.

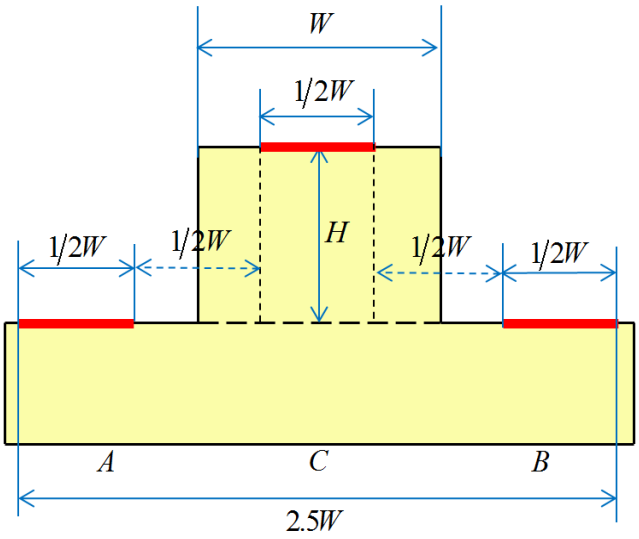

Figure 5-5 Step height evaluation based on ISO 5436

Differing from the method based on ISO 5436 is the method based on NIST. In this case, the step is divided into two parts, left side and right side, as shown in Figure 5-6. First of all, the step height of each side is calculated, then the average value of both sides is defined as the step height. As the method based on ISO 5436, it also needs to define the step edge regions, but more flexibly compared to the former. For each separate part, right or left, two-step edge regions on the step top surface are defined as a length of W/X. Furthermore, for the tunnel bottom surface, a region close to the step sidewall with a length of W/X is defined as the step edge region.

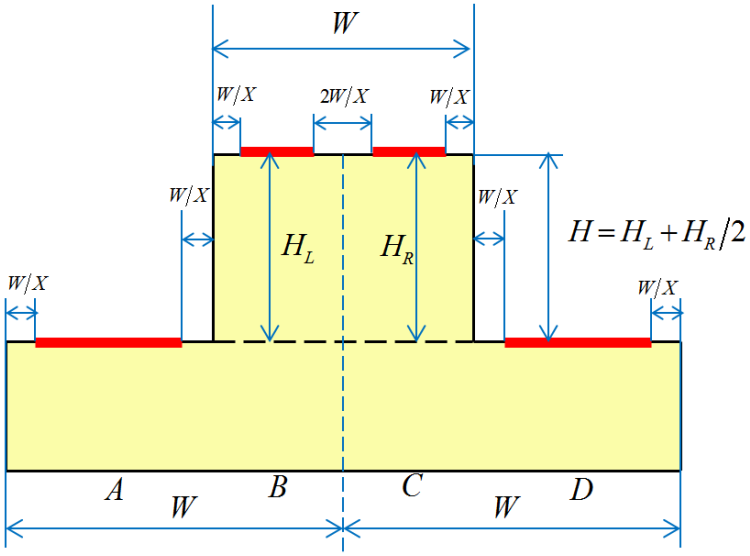

Figure 5-6 Step height evaluation based on NIST

In contrast to the method based on ISO 5436, the step edge regions are obtained by experiment. A specific W/X value is set for different measurement samples. In some cases, the width of the step top surface is quite small, if only a fixed $W/3$ width region is defined for step height evaluation this will lead to significant error. So, a flexible selection is more suitable under this circumstance. Both regions on the left and right side are shown as the A, B, C, D in the picture above. Lengthening two pairs of lines A, B and C, D, therefore, the step height H_L for the left part and step height H_R for the right part are obtained. The step height H is the average of these two parts.

5.3.3 Evaluation based on histogram method

Step height analysis is based on histogram method using a graphical representation by calculating a visual impression of the distribution of measurement data. This method is based on graphical statistics. It means histogram is an estimate of the probability distribution of the height values but cannot represent the location of specific pixels. For step height evaluation, it is important to consider the step edges. In this section,

the histogram used to find the threshold value of the edge. Suppose that the level histogram corresponds to an image, $f(x,y)$, composed of dark objects in a light background, object and background pixels have effective levels grouped into two dominant modes. To extract the objects from the background a threshold T is to be selected to separate these modes. Then any point (x,y) for which $f(x,y) \geq t$ is called an object point, otherwise, the point is called a background point. As the value of micro step surface is proportional to the step height, by this method, the top surface of micro steps, step sidewall and corners determined. So the step height can be calculated. A practical valve is shown in the figure below. p_1 and p_2 represent the corresponding heights z_1, the step top surface height and z_2, the tunnel bottom surface height.

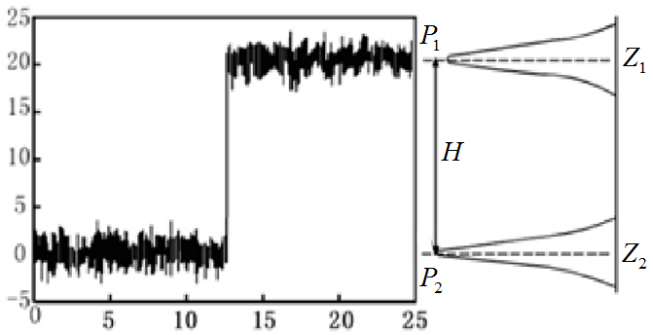

Figure 5-7 Step height evaluation base on histogram method

The height of micro step H is,

$$H = (Z_2 - Z_1) \times \frac{Z_{sr}}{Z_{gs}} \tag{5.1}$$

Z_{sr} is the scanning range in Z direction and Z_{gs} is the gray scale in Z direction.

The section area of micro step S is,

$$S = \left[\sum_{i=1}^{m}(Z_i - Z_1)\right] \times \frac{X_{sr}}{X_{gs}} \times \frac{Z_{sr}}{Z_{gs}} \tag{5.2}$$

Z_i is the height value of the points at the right side of $p_i, i = 1,2,...,m$. n_i is the number of points equal to Z_i. X_{sr} is the scanning range in X direction and X_{gs} is the resolution in X direction.

For the practical measurement samples, the histogram may contain multi extreme values. In this circumstance, the maxim extreme values are defined as the tunnel surface height. But, for the step top height, the average of extreme values is defined as the step top height. The section area of micro step S can be obtained not only from the histogram but also from the section profile.

$$S = \left[\sum_{i=1}^{P}(Z_i - Z_1)\right] \times \frac{X_{sr}}{X_{gs}} \times \frac{Z_{sr}}{Z_{gs}} \tag{5.3}$$

Once section area of micro step S and the height of micro step H are obtained, then the width W is,

$$W = \frac{S}{H} = \left[\sum_{i=1}^{m}(Z_i - Z_1) \times n_i\right] \times \frac{X_{sr}}{X_{gs}} \times \frac{1}{Z_2 - Z_1} \tag{5.4}$$

5.4 Evaluation of sidewall roughness

Due to the limitations of existing surface measurement instruments, it is impossible to measure the sidewalls of micro step surface. To evaluate sidewall roughness, Line Edge Roughness (LER) provides an indirect approach. It defines σ as the single-line edge roughness. Similar to the LER, Line Width Roughness (LWR) defines σ as the line width variation [86]. Figure 5-8 shows the principles of LER and LWR methods. In contrast to single line edge roughness, LWR uses the deviation of both sides of the edge to evaluate micro steps.

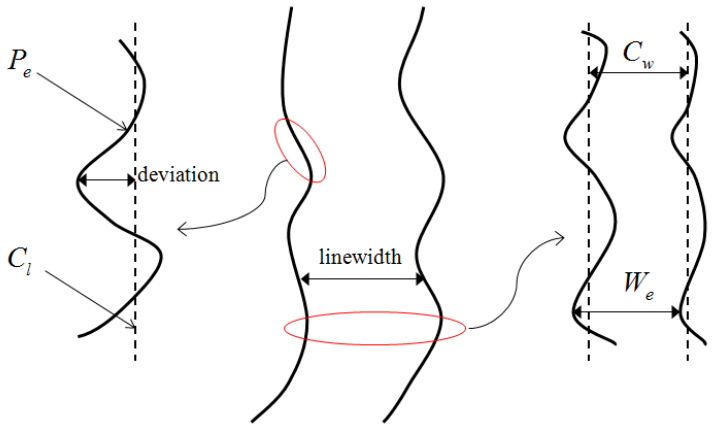

Figure 5-8 Schematic diagram of LER and LWR method

In the figure above, p_e is the line edge point, c_l is the centre line of edge, w_e is the distance between both sides of the edge point and the C_w is the average line width.

For the LER method, R_w is

$$R_w = 3\sqrt{\frac{\sum_{i-1}^{N}(W_e - C_w)^2}{N-1}} \tag{5.5}$$

For the LWR method, R_s is

$$R_e = 3\sqrt{\frac{\sum_{i-1}^{N}(P_e - C_l)^2}{N-1}} \tag{5.6}$$

Both two methods analyse the line roughness of the intersection between the sidewall contour and height section parallel to the measurement datum plane. The line roughness can be considered as a component of sidewall roughness. To satisfy the evaluation requirements, two-line roughness of a sidewall respectively extracted from the top and bottom position of the micro step sidewall is analyzed to evaluating the sidewall roughness.

Generally, statistical parameters, for example, Root Mean Square (RMS) cannot offer the detailed description of the sidewall roughness. Although, spectral methods based on Fourier transform can provide the frequency distribution but still cannot offer the details of an edge line. In addition, power spectral density is a wildly used parameter for sidewall roughness evaluation [99]. The central problem of extreme difficulty of measurement remains however.

5.5 Case study

A local measurement of data can be obtained using a step height standard gauge block from NPL (National Physical laboratory), as shown in Figure 5-9. The material of this sample is one of the most commonly used semiconductor materials, SiO_2. This gauge block is manufactured by lithography methods.

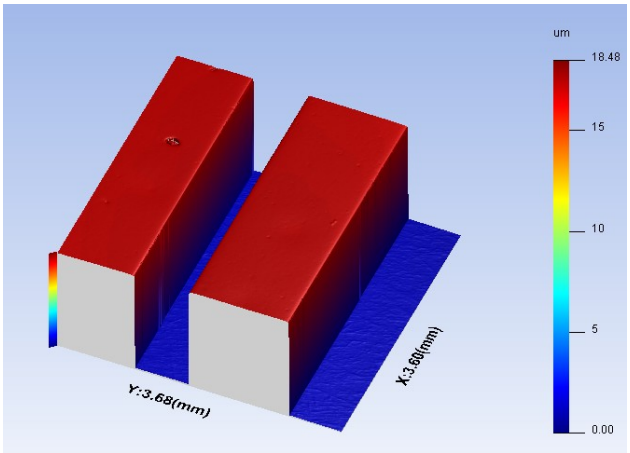

Figure 5-9 Local measurement data of step height standard gauge block

The nominal size of the step height standard gauge block is shown in the schematic diagram below, as shown in Figure 5-10.

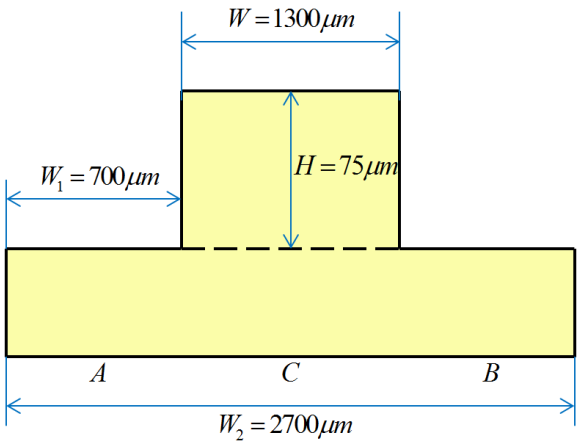

Figure 5-10 Nominal size of the step height standard gauge block

This sample was measured by a TalySurf CCI 3000. Due to the size of micro step, at least a $3.6\times3.6mm$ measurement area is needed to obtain the whole measurement data of standard gauge block without any stitching. Therefore, a $\times5$ lens is selected for measurement. In all, there are five lenses to choose with different resolutions, respectively, $\times2.5,\times5,\times10,\times20$ and $\times50$. Lens choice depends on the practical measurement need. The optical specification of Talysurf CCI 3000 system is listed below in Table 5-1.

Table 5-1 Optical specifications of Talysurf CCI 3000

Optical specifications					
Magnification	×2.5	×5	×10	×20	×50
Numerical Aperture	0.075	0.13	0.3	0.4	0.55
Working Distance (mm)	10.3	9.3	74	4.7	3.4
Optical Resolution(μm)	7.2	3.6	1.8	0.9	0.36
Maximum Slope(degrees)	2.0	4.0	7.7	14.6	27.7
Measurement Area(mm^2)	7.2×7.2	3.6×3.6	1.8×1.8	0.9×0.9	0.4×0.4
Lateral sampling Resolution(μm)	7	3.5	1.75	0.88	0.35

As described above, this sample was measured using a TalySurf CCI system. The instrument uses a white-light as the light source and a patented correlation algorithm to find the coherence peak and phase position of an interference pattern [97,100]. Batwing artifacts are usually associated with interferometry when measuring micro step surfaces [91]. The measurement height near the step edge appears higher than the actual value and at the bottom of step measurement height near the step sidewall appears lower than the actual value. Batwing effects are related to the wavelength. Shorter wavelength will narrow the width of the batwings. Meanwhile, batwing is related to the height of the micro steps, small step height will cause more batwing effect. For example, if the step height down to a few nanometers the measurement height near step edge will appear much higher than the actual value and also the width. For this sample, the step height is $75\mu m$, so the batwing effect is not abvious but still some false information or discontinuous points appear at the step edge [93]. To reduce the influence of the measurement error, the original measurement data needs to be

pre-processed. In Figure 5-11, (a) shows the original measurement data and (b) shows the data after denoising.

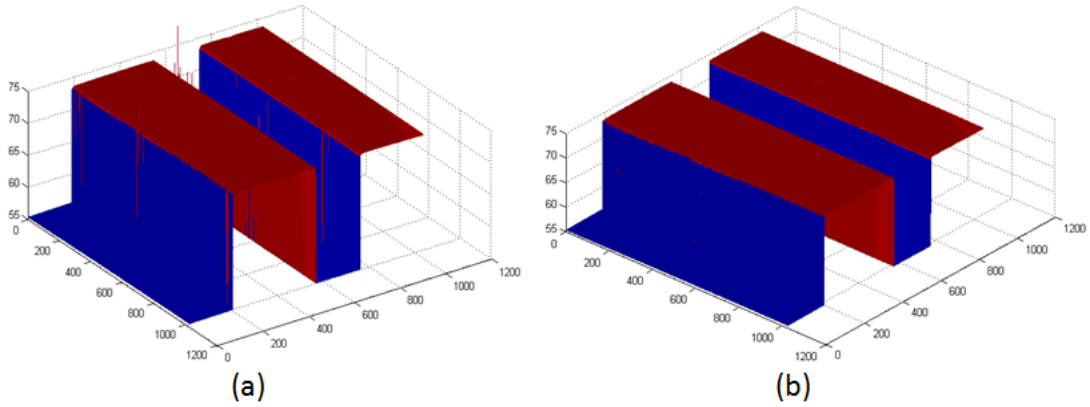

Figure 5-11 (a) Original measurement data (b) data after denoising

After pre-processing of the original measurement, a datum plane is established by least squares fitting. Due to the approximate step height being known, a threshold is determined based on the position of top and bottom edges of the step. Two edge lines are respectively at the position of 10% and 90% sidewall height and the all these edge lines are parallel to the datum plane, as shown in Figure 5-12.

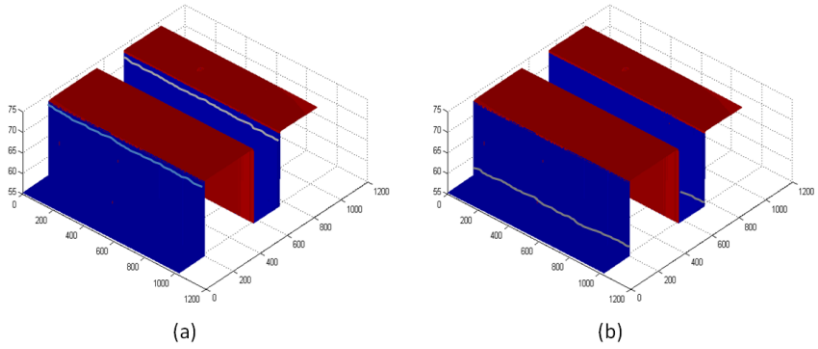

Figure 5-12 Line edge roughness of the micro step sidewall

In Figure 5-13, shows the results of step height evaluation based on ISO 5436, NIST and histogram method.

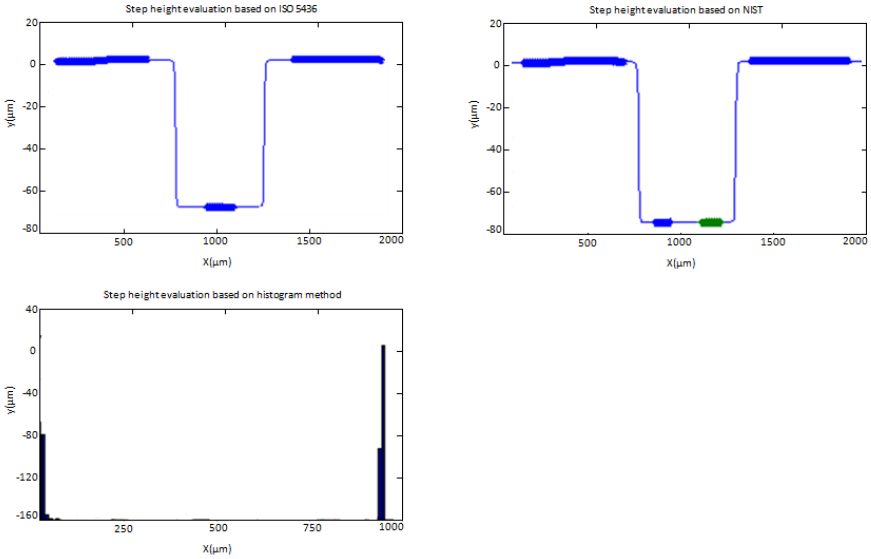

Figure 5-13 Sample step height evaluation based on ISO 5436, NIST and histogram method

Based on the three methods above, the step height and width of standard gauge block can be calculated, the results are shown in Figure 5-14 and Figure 5-15.

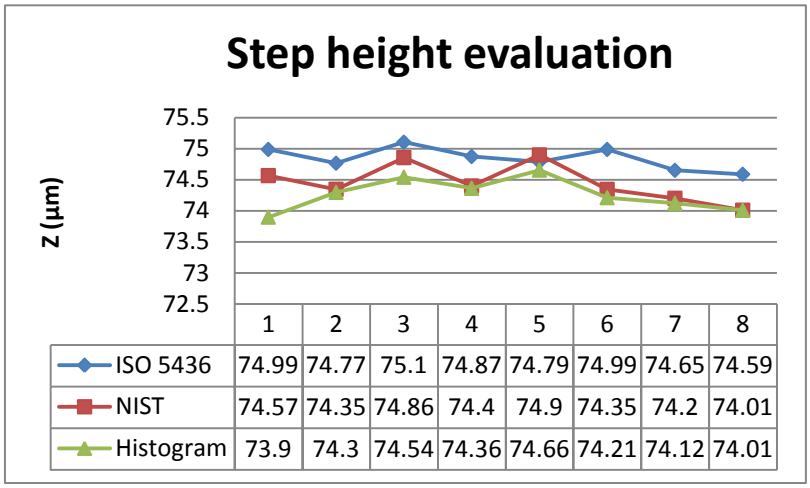

Figure 5-14 Results of step height based on ISO5436, NIST and histogram method

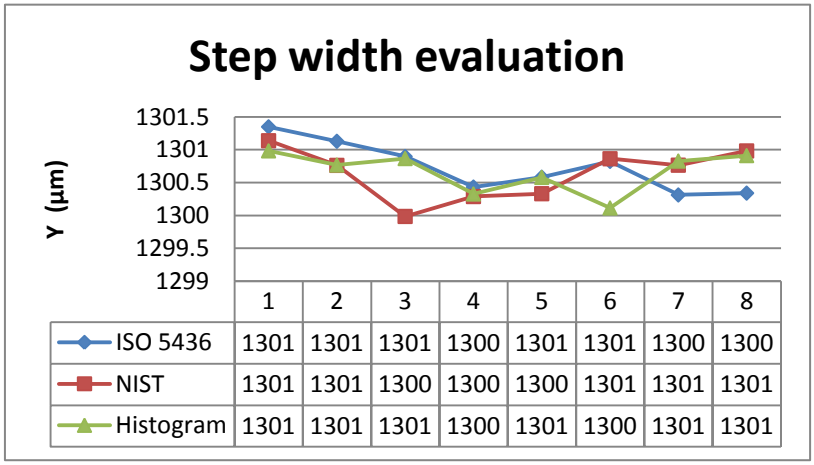

Figure 5-15 Results of step width based on ISO5436, NIST and histogram method

According to the measurement data and edge line roughness, the micro step side wall roughness is expressed by edge line roughness and line width roughness. The result is shown in Table 5-2.

Table 5-2 Micro step side wall roughness

	Edge line roughness	Line width roughness
Top left	5.428	5.524
Top right	5.619	
Bottom left	5.893	5.775
Bottom right	5.662	

As a standard gauge block, this sample is manufactured with a high precision. From the results it can be seen that the three different evaluation methods, including ISO 5436, NIST and histogram method have their own application scope. All these methods have the target to ensure the evaluation process is not affected by the error information from the step edge regions. To ensure the accuracy, it is also important to define the effective region to be as large as possible. Due to the size of this sample being relatively large compared to the some MEMS devices, the effective region is defined as larger as possible and hence less influence from the edge side error information.

Figure 5-16 shows a schematic diagram of a micro fluidic device. Micro fluidic devices have important application in biological research. Biological fluid samples can be loaded on the device which then flows through the channels and are separated into constituent parts allowing further extraction or analysis.

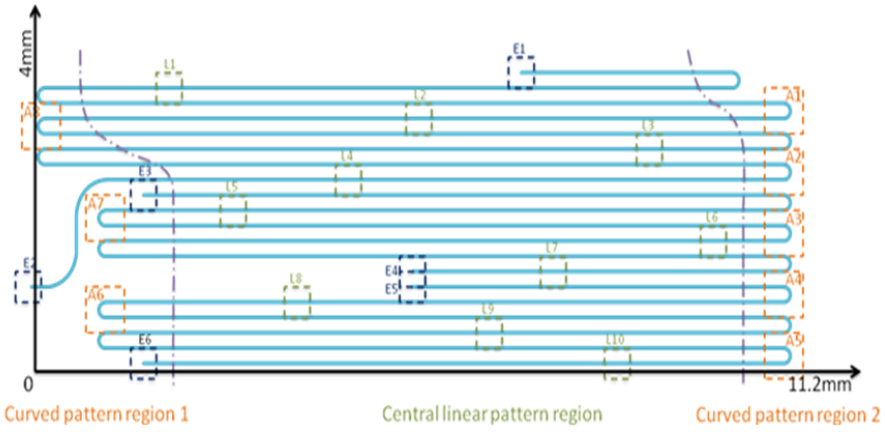

Figure 5-16 Schematic diagram of micro fluidic

As shown in figure above, the ending regions in the blue boxes are the key sections for the micro fluidic. The biological sample will become chaotic in terms of flow during these sections. The rest parts of micro fluidic are micro tunnels and its ending

sections. The lengths of micro tunnels are dependent on the stratification requirement. Figure 5-17 shows the measurement data from ending regions.

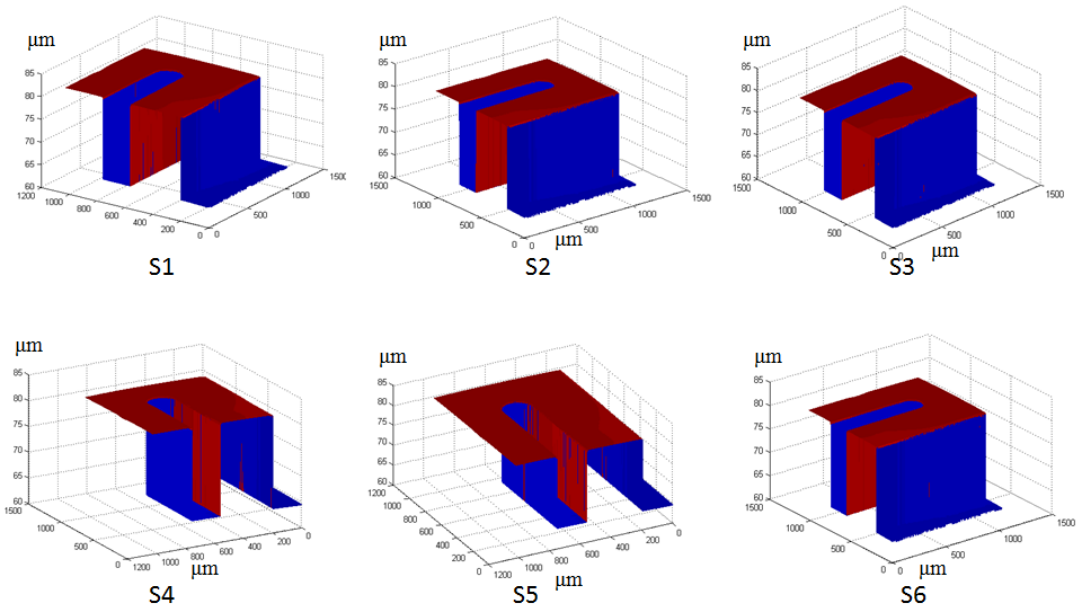

Figure 5-17 Measurement data of ending regions in micro fluidic

In the step height standard gauge block evaluation, three different methods for step height evaluation have been compared. NIST use parameter W/x to define regions on both top and bottom of the micro steps. Due to its flexibility, ISO 5436 method has the advantage to analyze samples has a micro steps down to a few micrometers. For the micro fluidic, $X = 10$, the results of all six ending regions are shown in Figure 5-18.

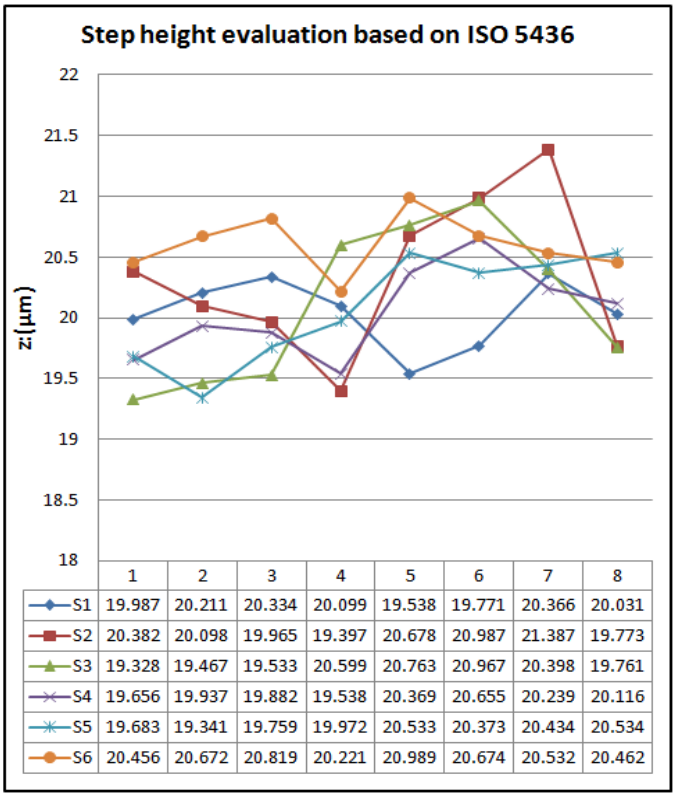

	1	2	3	4	5	6	7	8
S1	19.987	20.211	20.334	20.099	19.538	19.771	20.366	20.031
S2	20.382	20.098	19.965	19.397	20.678	20.987	21.387	19.773
S3	19.328	19.467	19.533	20.599	20.763	20.967	20.398	19.761
S4	19.656	19.937	19.882	19.538	20.369	20.655	20.239	20.116
S5	19.683	19.341	19.759	19.972	20.533	20.373	20.434	20.534
S6	20.456	20.672	20.819	20.221	20.989	20.674	20.532	20.462

Figure 5-18 Results of ending regions step height based on ISO5436

The micro fluidic width evaluation results are shown in Figure 5-19.

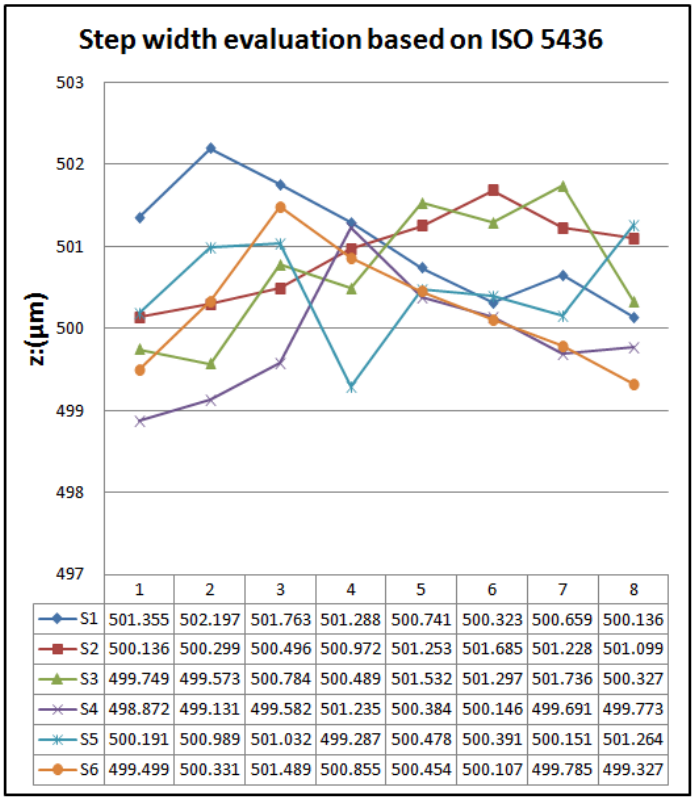

	1	2	3	4	5	6	7	8
S1	501.355	502.197	501.763	501.288	500.741	500.323	500.659	500.136
S2	500.136	500.299	500.496	500.972	501.253	501.685	501.228	501.099
S3	499.749	499.573	500.784	500.489	501.532	501.297	501.736	500.327
S4	498.872	499.131	499.582	501.235	500.384	500.146	499.691	499.773
S5	500.191	500.989	501.032	499.287	500.478	500.391	500.151	501.264
S6	499.499	500.331	501.489	500.855	500.454	500.107	499.785	499.327

Figure 5-19 Results of ending regions step width based on ISO5436

For micro fluidics, the maximum and minimum distance of micro tunnels are key parameters. It affects the micro biological sample mixing and diffusion. In some extremely compact fluidics for plasma testing, the width of micro tunnels can be a few µms [92,101]. If the minimum distance is representing tunnel's functionality, once the value is close to zero, it means one of the tunnels is disabled. Furthermore, the maximum distance is important, once the distance goes up to the threshold. It will cause the turbulent flow of the testing sample. Figure 5-20 shows the maximum and minimum distance of the micro tunnels.

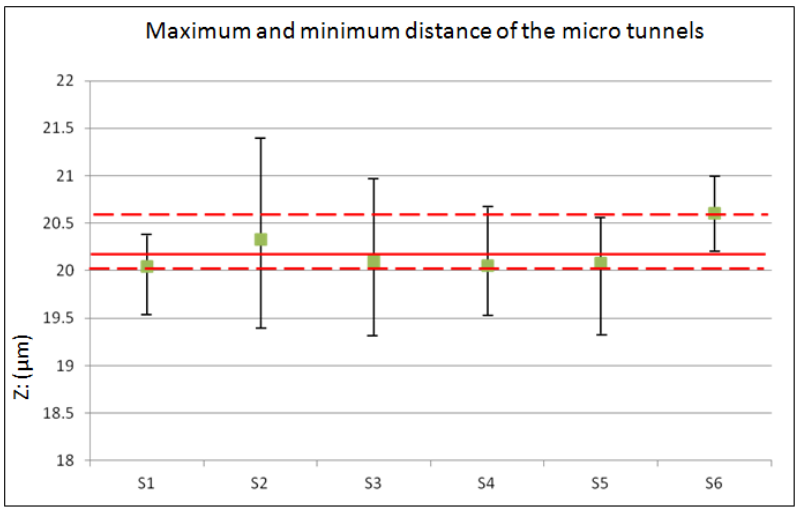

Figure 5-20 Maximum and minimum distance of six ending regions

5.6 Conclusions

In this chapter, the evaluation parameters including micro step height/groove depth, width of the step and approximate sidewall roughness have been studied. Evaluation methods for the micro structured features according to the classification have been developed. Case studies of the most significant applications, micro fluidics have been studied with experimental results.

Chapter 6 Pre-processing and feature extraction of structured surfaces

The objective of this chapter is to extract features from observed measurement data, as well as the data pre-processing. In this section, techniques of digital image processing are applied into measurement pre-processing, including denoising and data enhancement. This chapter also investigates both low-level algorithms and flexible methods for feature extraction. The results of them have been compared and discussed.

6.1 Measurement data Pre-processing

Due to the structural characteristics of structured surfaces, pattern recognition is an indispensable process in surface characterisation. For example, a micro sensor surface mentioned in Chapter 4, the key functional parameter of this device is the step height and groove width. Once a proper measurement work is done, a massive data of the whole structured surface is obtained. It will be much more difficult to analyse the whole surface with all the features mixed together, and it is not necessary. So, a process of pattern recognition for measurement data can extract the key features and make it possible to focus on the major functional parameters of the surface. In addition, once there are several types of structures on the same surface, pattern recognition can classify all the similar structures into a same category. It also will reduce the difficulty of surface characterisation [72,79].

Pattern recognition is a scientific discipline whose aim is the classification of the objects into categories or classes. Pattern recognition is also an integral part of most machine intelligence system built for decision making. Pattern recognition has its origins in engineering, with almost 40 year's history in industry. Pattern recognition now has a wide range of applications [76].

For structured surface characterisation, pattern recognition aims to classify measurement data based on either a priori knowledge or on statistical information extracted from the patterns. It is a technology that concerns the description or classification of measurements.

The typical process of pattern recognition includes a sensor to transfer the observed pattern p_i into measurement data m_i. In this study, the three major measurement instruments introduced above will be used, especially the TalySurf CCI 3000. To apply image-processing methods to surface characterisation, a part of measurement data is transferred to digital image formats. Preprocessing like de-noising and enhancement will help to extract the key features and improve the precision of the final results. There is no universal method for extraction of all the surface features. Different feature extraction algorithms have their own advantages and disadvantages with some algorithms only suitable for specific features. For example, because of the irregular shape and very limited interval distance, features of a chip pin surface cannot be extracted by some commonly used extraction algorithms. A classification and description of extracted features or primitives will be presented in this chapter. In Figure 6-1, a schematic diagram of pattern recognition demonstrates the process to be developed.

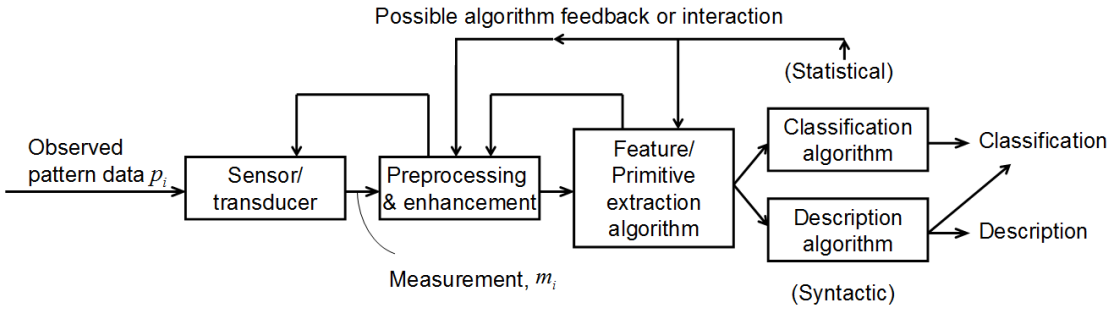

Figure 6-1 A schematic diagram of pattern recognition process for structured surfaces

6.2 Measurement data denoising

Denoising aims to remove measurement noise as much as possible while preserving useful information. An effective denoising method is a necessary preprocess for extraction of surface features, pattern classification and other analysis processes, and remains an ongoing challenge [94]. For different types of noise e.g. additive and multiplicative noise, several different denoising techniques can be applied. Denoising can remove noise from the measurement data, but normally some useful information will be lost after the denoising process. For some micro/nano scale structured surfaces measurement data, the contours of features are originally too small to be differentiated. After denoising it can be difficult to extract the contours as they can become discontinuous and lead to false results. So image enhancement is used to solve this problem to provide a better sample for the following feature extraction processes.

6.2.1 Gaussian noise and denoising

Gaussian noise is statistically random noise that is evenly distributed over the measurement data. This means that each pixel in the noisy image is the sum of the true pixel value and a random Gaussian distributed noise value. In other words, the values that the noise can take on are Gaussian-distributed [76]. So let g represent the

image gray level, m is the mean or average of the function and σ is the standard deviation of the noise, a Gaussian distribution is given by,

$$F(g) = \frac{1}{\sqrt{2\pi\sigma^2}} e^{-(g-m)^2/2\sigma^2} \tag{6.1}$$

Graphically, Gaussian distribution has a probability distribution, shape as shown in Figure 6-2.

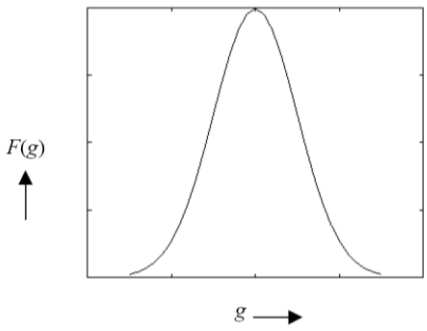

Figure 6-2 Gaussian distribution

Using a linear filtering method, a simple blurring is used to remove high frequencies caused by the noise. Two 1D signals with Gaussian noise added, and denoising applied are shown in Figure 6-3.

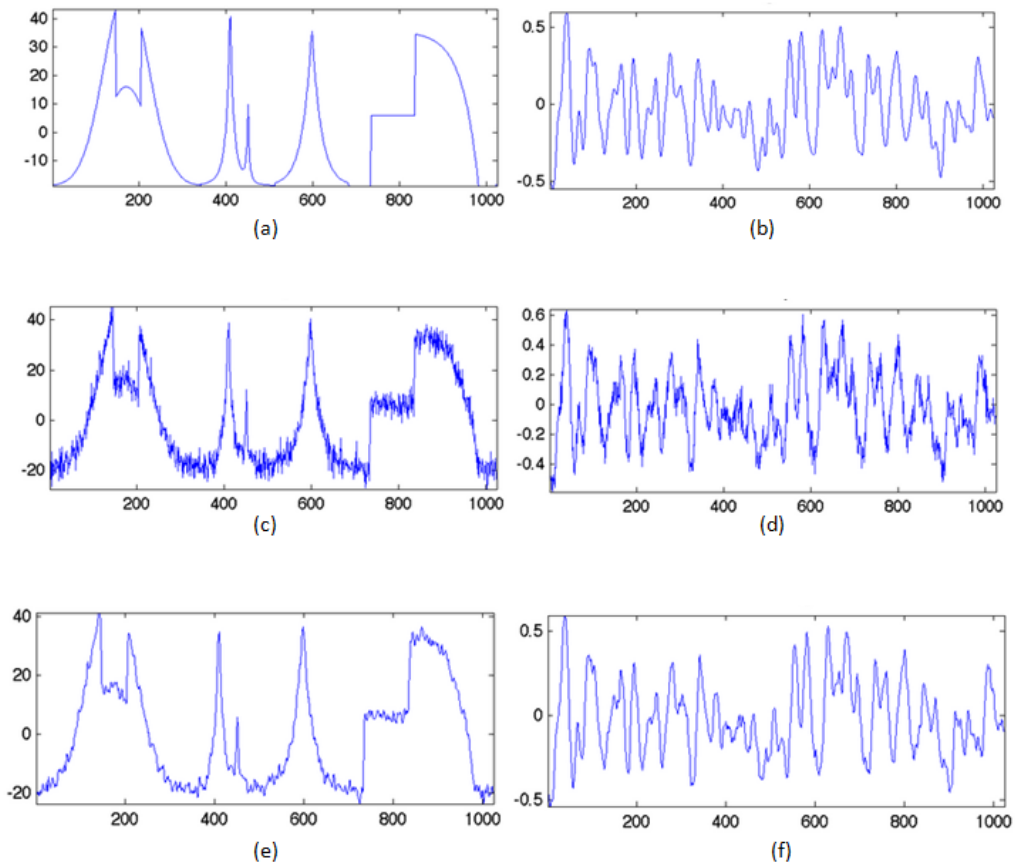

Figure 6-3 (a) and (b) are 1D signals, (c) is (d) with Gaussian noise added, (e) and (f) are corresponding denoising results of (c) and (d)

From the donoising results, blurring is well adapted to stationary signals such as filtered noise, but it tends to destroy singularities on the remaining data. Consequently, linear denoising is bound to fail on complex signals containing singularities. In the following section, a non-linear denoising method using wavelets is presented.

White Gaussian noise is defined as values at any pairs of space are statistically independent. A definition of white Gaussian noise is given. A random process $N(t)$ is white Gaussian noise if $N(t)$ satisfies $\mu_N = E[N(t)]$ and for any space instants, where $N(t_1), N(t_2), ...N(t_k)$ are independent Gaussian random variables. This noise accounts for measurement imperfections, for example, poor quality captured date can be

quantified as noise [74,75]. Gaussian noise is presented to demonstrate the denoising processes on micro sensor measurement data, as shown in Figure 6-4.

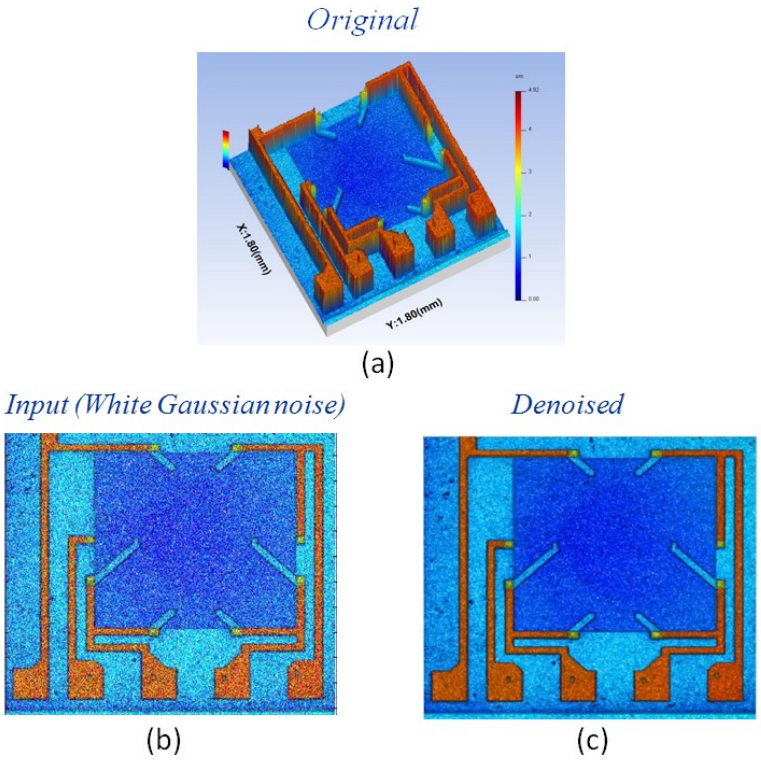

Figure 6-4 (a) original measurement data from a micro sensor (b) a image with white Gaussian noise added (c) the denoised data

The original data is from a micro acceleration sensor surface, measured by Talysurf CCI 3000. The lower-left picture is a local image of the acceleration sensor surface with a white Gaussian noise added, and the lower-right picture shows the denoised result.

6.2.2 Salt and pepper noise and median filter

Salt and pepper noise is a form of noise typically seen on camera based images [74]. It is an impulse type of noise. Intensity spikes are characteristics of this noise. It represents itself as randomly occurring white and black pixels. Salt and pepper noise

is generally caused due to errors in sensor data transmission. For images corrupted by salt and pepper noise, the so-called intensity spikes or noisy pixels take the maximum and the minimum values in the dynamic range, so it appears on the image as white and black pixels, as illustrated in Figure 6-5. However, if the values take a random value, it is a random-valued noise, also can be regarded as impulse noise [68,71].

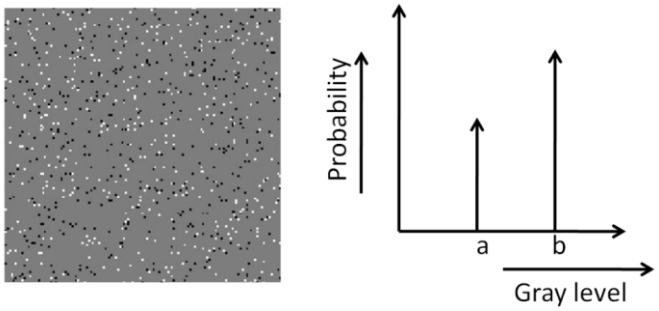

Figure 6-5 Salt and pepper noise and probability density function

Among numerous noises reducing algorithms, median filter is one of the most popular methods in reducing salt/pepper noise [78]. The median filtering is a nonlinear process that can suppress salt/pepper noise without blurring sharp edges of the micro/nano features. It works by arranging the pixels in a local window according to the size of their intensity values and replaces the value of the pixel in the result image by the middle value [75]. The median filter has three major advantages in noise removal. Firstly, it is more robust than the mean filter. The result of denoising will not be affected by outliers of the image. Secondly, compare to other conventional smoothing filters, the median filter does not shift the boundaries of the target features. Thirdly, the result has no reduction in contrast across steps. The median of n observations $x_i, i = 1,...n$ is denoted by $med(x_i)$ and it is given by:

$$med(x_i) = \begin{cases} x_{(v+1)} & n = 2v+1 \\ \frac{1}{2}\left(x_{(v)} + x_{(v+1)}\right) & n = 2v \end{cases} \quad (6.2)$$

Where $x_{(i)}$ denotes the $i-th$ order statistic. A 1-D median filter of size $n=2v+1$ can be defined as:

$$y_i = med\left(x_{i-v},...,x_i,...,x_{i+v}\right) \qquad i \in Z \tag{6.3}$$

A 2-D median filter defines the filter window, and it is given by:

$$y_{ij} = med\left(x_{i+r,j+s} \quad (r,s) \in A\right) \qquad (i,j) \in Z^2 \tag{6.4}$$

The set $A \subseteq Z^2$ defines a neighborhood of the central pixel (i,j) [131]. A median filter acts on an image by smoothing it. It reduces the intensity variation between adjacent pixels. The principle of the median filter is using a sliding window spatial filter that replaces the center value in the window with the average of all the neighboring pixel values. A 3×3, 5×5 or 7×7 kernel of pixels is scanned over the pixel matrix of the entire image. By this means, the noisy pixel is replaced. An example of median value of a pixel neighborhood is shown in Figure 6-6.

123	125	126	130	140
122	124	126	127	135
118	120	150	125	134
119	115	119	123	133
111	116	110	120	130

Figure 6-6 Median value of a pixel neighborhood

As seen in the figure above, the central pixel value of 150 is rather unrepresentative of the surrounding pixels and is replaced with the median value [77,83]. The mask or kernel is a square, if the coefficients of the mask sum up to one, it means the average brightness of the image remains the same. Once the coefficients' sum to zero, the average brightness is lost, and the image becomes dark. Hence, median filtering is

carried out by, first sorting all the pixel values from the surrounding neighborhood into numerical order and then replacing the pixel being considered with the middle pixel value. In practical applications, commonly, a 3×3 square neighborhood is applied in removing the salt and pepper noise. Larger square neighborhoods will produce more severe smoothing [89].

Compared to other denoising algorithms, like the mean filter, median filtering is much better at preserving sharp edges. A mean filter also can isolate the out-of-range noise, but it always blurs edges. The median filter does not change any out-of-range spots more than half of the window size, as the spot is large enough to be some legitimate feature in the image.

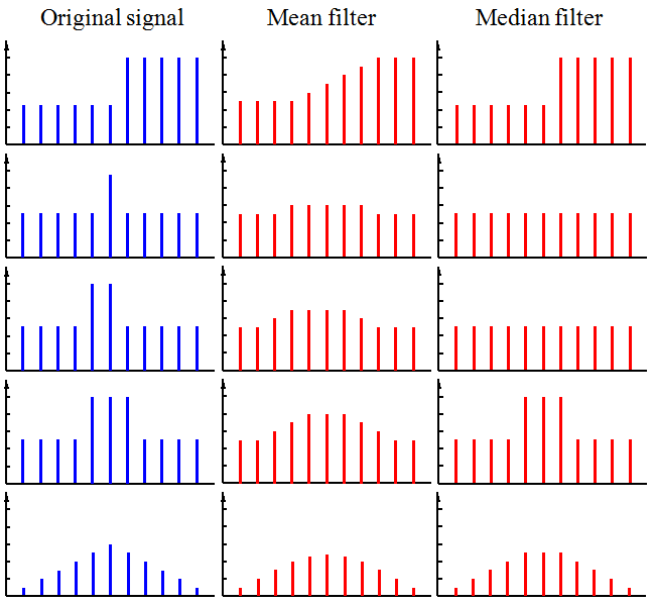

Figure 6-7 A comparison of denoising results of a 1D signal by a mean filter and median filter [73]

Figure 6-7 above shows a comparison of denoising results of 1D signal by a mean filter and median filter. The first columns in blue are five 1D signal. The second columns in red are the results by a mean filter and third column in red are the results

by a median filter. It is clear that median filter can preserve sharp edges much better than a mean filter.

The next section presents a case study concerning structured surface denoising and the result is shown in Figure 6-8. The original data is from a microlens array surface, measured by a Talysurf CCI 3000. (a) on top-left shows the measurement data, (b) on top-right is a local image of the micro sensor surface, (c) on lower-left is the image added with salt and pepper noise and (d) shows the final result of denoising. From the result, it is obvious all the out-of-range spots are removed by the median filter, and the edge of this micro-lens is relatively remained.

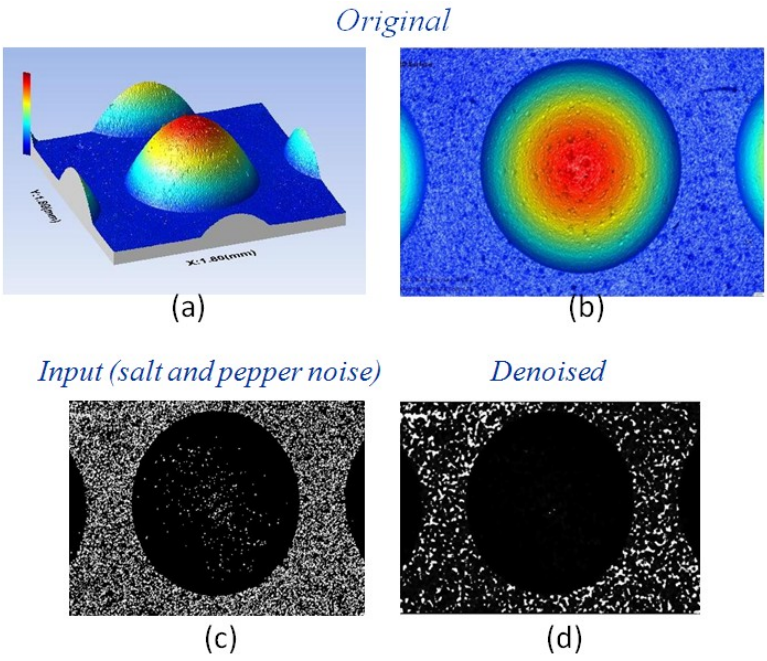

Figure 6-8 (a)micro sensor surface original measurement data (b)local image of the micro sensor surface (c) a image with white Gaussian noise added (d) the denoised data

6.2.3 Morphological filters

In the sections above, denoising methods for a linear system have been presented. These traditional approaches for denoising can solve the problem to a certain extent,

but also have their limitations. For instance, it is not suitable or even fails to solve problems of geometrical aspects of a data set [88]. Therefore, a nonlinear methodology is needed for geometric approaches. A powerful nonlinear tool for image denoising is the morphological filter. Mathematical Morphology (MM) is a theory for the analysis of geometrical structures and math is based on set theory, integral geometry and lattice algebra. MM aims at quantitatively describing the geometrical structure of image objects. The task of morphological filter includes cleaning the image from different types of noise, enhancing the contrast between adjacent surface features and selectively smoothing the features at a specific scale. A morphological filter can be defined as an operator φ, acting on a complete lattice T, which preserves the ordering $\leq$ of T

$$X \leq Y \Rightarrow \varphi(X) \leq \varphi(Y), X, Y \in T \tag{6.5}$$

Therefore,

$$\varphi(\varphi(X)) = \varphi(X), X \in T \tag{6.6}$$

In binary morphology, a probe called the structuring element is built to analyse the image. It is a pre-defined geometrical shape, and its size is smaller than the image, drawing conclusions on how this shape fits the shapes in a binary image [83,88]. The shape of the structuring elements can vary. For example, by letting $E = R^2$, the structuring element is an open disk of radius R. Two standard types of neighbourhoods N_4 and N_8 are shown in Figure 6-9.

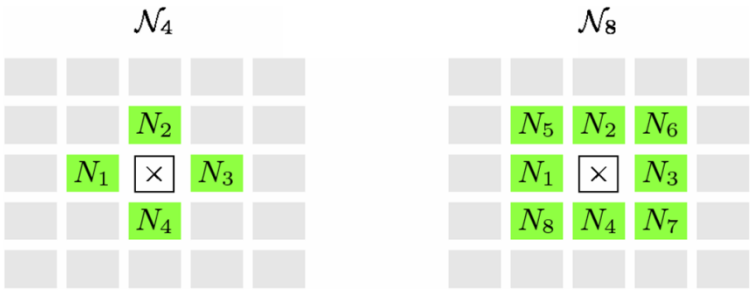

Figure 6-9 Four-neighborhoods structuring element and an eight-neighbourhoods structuring element

The use of sets to represent binary images is an important concept offered by mathematical morphology. Set operations also represent binary image transformations. There are four basic operators, including erosion, dilation, opening and closing, among them, erosion and dilation are the most two important operators. All the other operators are a composition of these two operators [81]. The erosion of the image A by the structuring element B is defined by,

$$A\Theta B = \left\{ z \in E \middle| B_z \subseteq A \right\} \tag{6.7}$$

Where B_z is the translation of B by the vector Z, $B_z = \left\{ b + Z \middle| b \in B \right\}, \forall Z \in E$.

The Dilation of A by the structuring element B is defined by,

$$A \oplus B = \left\{ z \in E \middle| \left(B^s \right)_z \cap A \neq \varnothing \right\} \tag{6.8}$$

Erosion and dilation create two other operations, the opening $X \cdot B\Theta\left(X\Theta B\right)$ and closing $X \cdot B\Theta\left(X \oplus B\right)$ of X by B. Figure 6-10 shows the four basic operations. The small disk is a structuring element with a round shape, the original image is shown as dark-coloured areas, and results after the operation are shown as light-coloured areas.

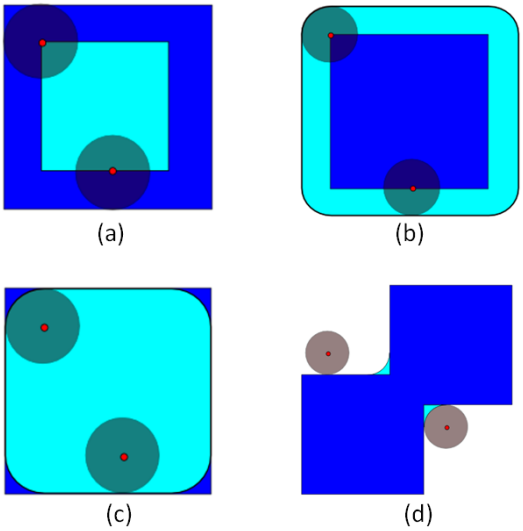

Figure 6-10 A schematic diagram of four operations, (a)erosion, (b)dilation, (c)opening, (d)closing [96]

Morphological filters are flexible techniques and with different filters many of image processing tasks can be achieved. For example, application at these filters can spread out and shrink image regions. This removes all small regions, probably created by noise, such as salt and pepper noise [84]. Also, application can fill up some unnecessary cavities and smooth boundaries. For structured surface measurement by Tylorsurf CCI, some error measurement point data caused by small cavities on the surface or non measured data points can be dealt with. Morphological filters are effective at removing these unnecessary cavities. Ten morphological filters and their descriptions are listed in Table 6-1.

Table 6-1 Morphological filters and descriptions

Morphological filter	Description
Smooth	$Smooth(S,F) = Close(Open(S,F),F) = E(D(D(E(S,F),F)F,)F,)$
Contrast	$Contrast(m,n) = \frac{D(m,n) - E(m,n)}{65535} \cdot (S(m,n) - E(M,N))$ Structural element F is used here during the calculation of dilation and erosion.
Min	The new value for the points is taken as minimal one among the value of this point and eight neighbor points. In the terms of morphological operations. This is an operation erosion with a structural element 3×3, where all the value are equal to zero.
Max	The new value for the points is taken as minimal one among the value of this point and eight neighbor points. In the terms of morphological operations. This is an operation dilation with a structural element 3×3, where all the values are equal to zero.
Dilation	Operation dilation with structural element F.
Erosion	Operation erosion with structural element F.
Open	$Open = D(E(S,F),F)$
Close	$Close = E(D(S,F),F)$
Gradient	$Gradient = \frac{1}{2}(D(S,F) - E(S,F)$
Laplace	$Laplac = \frac{1}{2}[(D(S,F) - S) - (S - E(S,F))]$ $= \frac{1}{2}[D(S,F) + E(S,F) - 2 \cdot S]$

To demonstrate morphological filter performance, the measurement data is transferred to a local binary image of twelve drop-shaped features as shown in Figure 6-13. It is clear that the original image contains many isolated pixels, similar to the salt and pepper noise. To remove this inconsequent information a morphological operation composed from two basic operation erosion and dilation is applied. Erosion is the reduction of ON regions and inversely dilation increases their size by adding ON value layers to the boundaries. A moving $k \times k$ window scans over the image and removes the noise. The size (k) of the window should be carefully chosen to match

the noise [86]. Noise is removed by filling the core, $(k-2)^2$ region. The neighborhood $4(k-1)$ pixels make the decision, whether or not to fill requires. Only when the following condition is met does filling occur.

$$(c=1) and \{(n>3k-4) or [(n=3k-4) and (r=2)]\} \tag{6.9}$$

c is the number of connected groups of ON(OFF) pixels, r is the corner pixels and n is the number of ON pixels. A flowchart of the whole process is shown in Figure 6-11.

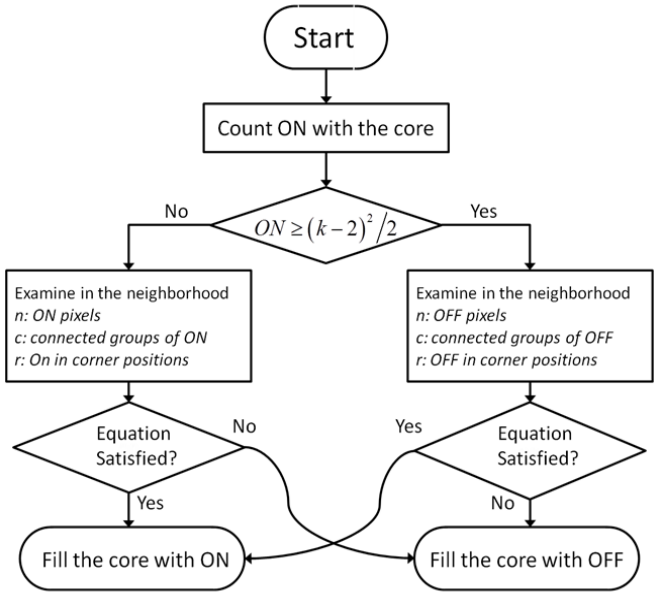

Figure 6-11 Flowchart of isolated pixels algorithm

An etched *Si* structured surface is shown in Figure 6-12. This sample has drop-shaped features on its surface, measured by Talysurf CCI 3000. In Figure 6-13, (a) is a local binary image of etched *Si* sample with isolated pixels, similar to the salt and pepper noise. A 3×3 structuring element is used. (b) shows the denoising result with a only single iteration, $k=4$. Comparing the results of (a) and (b), it is clear that the morphological filter can remove the inconsequent isolated pixels and leave more defined feature boundaries.

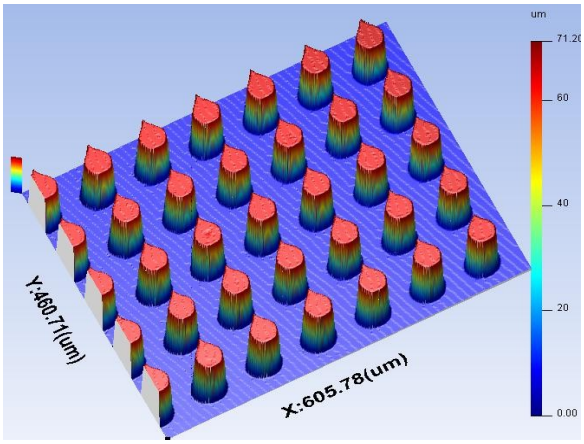

Figure 6-12 A etched Si sample with drop-shaped features on the surface

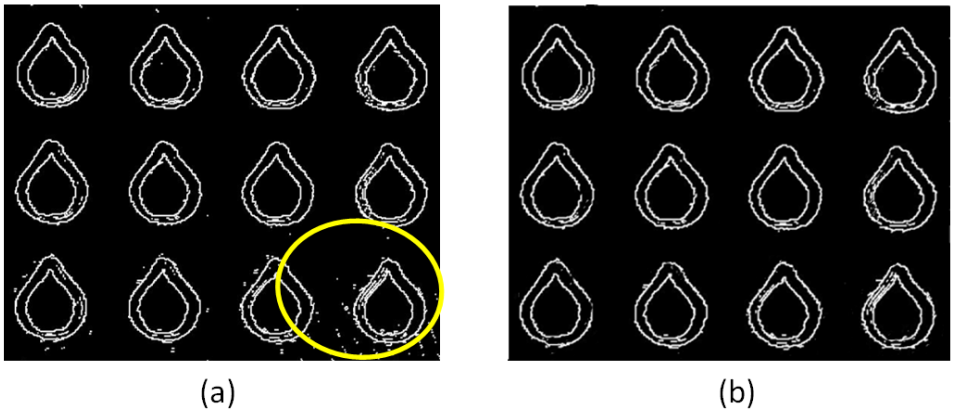

Figure 6-13 (a) A binary image of etched features with isolated pixels (b) A result of isolated pixels removed

6.3 Histogram equalization for image enhancement

Histogram equalization is a technique to analyse the surface based on their image information. It can adjust the specific grey scale of the image and mapped onto a uniform histogram. It uses a variable γ to represent the gray level of the measurement data. In the following equation, γ is continuous the value of γ s within the closed interval $[0:1]$. If the pixel of image is black, r=0. If it is white, r=1. A transformation for any γ is given by the equation below.

$$s = T(r) \tag{6.10}$$

Let the original and transformed grey levels be characterized by their probability density functions $P_r(r)$ and $P_s(s)$ respectively. Then from elementary probability theory, if $P_r(r)$ and $P_s(s)$ are known then the probability density function of the transformed grey level is given by:

$$p_s(s) = \left[p_r(r) \frac{dr}{ds} \right]_{r=T^{-1}(s)} \tag{6.11}$$

If the transformation is given by:

$$s = T(r) = \int_0^r P_r(w)\, dw \tag{6.12}$$

Then substituting $dr/ds = 1/P_r(r)$ in Eq. (6.9) $P_s(s) = 1$ can be obtained. Thus it is possible to obtain a uniformly distributed histogram of an image by the transformation described by equation above.

An algorithm to implement histogram equalization for a grey level image is given below. For every pixel in the image the grey level value is a variable i, $hist[i] = hist[i] + 1$ when $i = 0$ to $L-1$ for a L level image. From the histogram array, one can obtain a cumulative frequency of the histogram $hist_{cf}[i] = hist_{cf}[i-1] + hist[i]$. The generated equalized histogram is given as:

$$eqhist[i] = \frac{\left[L * hist_{cf}[i] - N^2 \right]}{N^2} \tag{6.13}$$

Where, L is the number of grey levels in the image, N^2 is the number of pixels in the $N \times N$ image, $[x]$ is the truncation of x to the nearest integer. Replacing the grey value i by $eqhist[i]$ for each i, then $eqhist$ contains the new mapping of grey values.

Figure 6-14 shows a different sample, measurement data of laser etched landing zones of a hard disk surface, measured by Tylorsurf CCI 3000. The surface has a donut-

shaped micro feature formed by laser texturing. Laser texturing processes allow production of patterned surfaces with precise and controllable topography. However, due to its high energy, focused laser is used to vaporize a microscopic area of the disk substrate rapidly and form this shape.

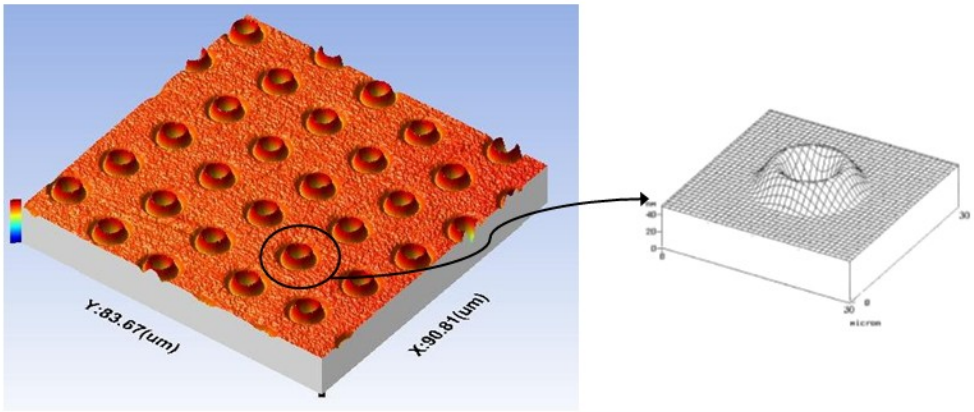

Figure 6-14 Measurement data of laser etched landing zone of hard disk surface with donut-shaped micro features

Figure 6-15 shows the result of enhanced measurement data by Histogram equalization. Considering the histogram of the original image is non-uniform, due to many surface undulations, the histogram of the equalized image has more or less a uniform density function. (a) and (b) are original images of laser etched landing zone of hard disk. (c) and (d) are the enhanced results and equalized histogram.

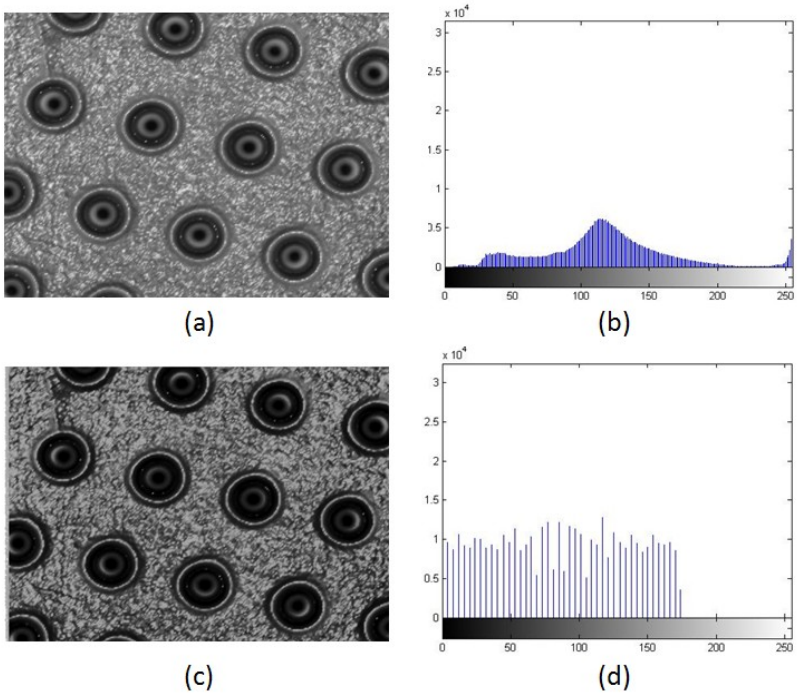

Figure 6-15 (a) original image of hard disk surface (b) histogram of the image (c) enhanced image of hard disk surface (d) equalized histogram

6.4 Feature extraction of structured surfaces

Feature extraction is a critical step of structured surface characterisation. Structured surface normally contains different functional regions and defined features. To define and identify these regions or stable features in observable measurements, an effective feature extraction technique is fundamental. In some cases, when measurement large data needs to be processed by an algorithm, it also needs feature extraction to transfer the input data into a reduced representation set of a feature. For structured surface measurement data, feature extraction will affect the follow-up analysis issues such as edge roughness and geometrical alignment. Feature extraction will extract the relevant information from the input data in order to perform the desired task instead of analyzing full-size measurement data. In this section developed feature extraction techniques used for structured surface are classified into two major types, low-level

feature extraction and flexible methods of feature extraction. Low-level feature extraction includes edge detection for step type microstructures, straight-line-based primitive extraction and rectangle detection. Compared to the former techniques an algorithm based on active contours is more flexible and is introduced. It can extract single or multiple features and is sensitive to the small concaves features of the boundary. Finally, a wavelet based feature extraction is used, using both the Dual-tree Complex Wavelet Transform (DTCWT) and Discrete Wavelet Transform (DWT), and a comparison of the results is presented.

6.4.1 Low-level feature extraction

Edges of micro/nano structures can be defined as an abrupt change, or sharp discontinuity when surface measurement data is transferred into an image. Normally, a grey level image is appropriate to provide all the edge information of the micro/nano structures. Edge detection performs a computation on an image pixel by pixel. In other words, many arithmetic operations performed on each pixel of the image. For data that has sharp intensity transitions and low noise, edge detection works fairly well. For example, a square shaped etched *Si* sample has a micro step feature on its surface and the sidewalls are almost vertical to the base. In this case the most commonly used edge detection operator is the Sobel operator, Prewitt operator and Roberts cross operator. Comparing these three methods, the Sobel operator is the most suitable one for feature edge detection, because of its smoothing and differencing effects and also the algorithm simplicity. The Laplacian operator or second-order derivative has a zero-crossing at the midpoint in any intensity change of an image. While, the first-derivative detection is different, it indicates the direction of change. Although the Laplacian operator is sensitive to noise, it is still more effective than the

gradient operator. For an image which contains blurred edges and low noise, the second derivative is more effective than the gradient operator for identifying the location of edges [92].

The Sobel operator is composed of two convolution masks. Respectively, these two masks are applied to detect the gradient horizontality and verticality. ∂x is the horizontal mask and ∂y is the vertical mask. In Figure 6-16 two convolution masks and 3×3 image block Z are presented.

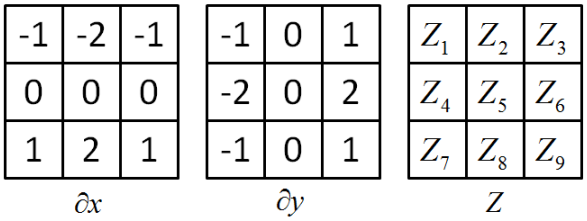

Figure 6-16 Sobel convolution masks

The measurement data of square-shape step etched *Si* sample is shown in Figure 6-17, as measured by Tylorsurf CCI 3000. (b) and (c) are respectively the X profile and Y profile, (d) shows the feature extraction result following Sobel operator application.

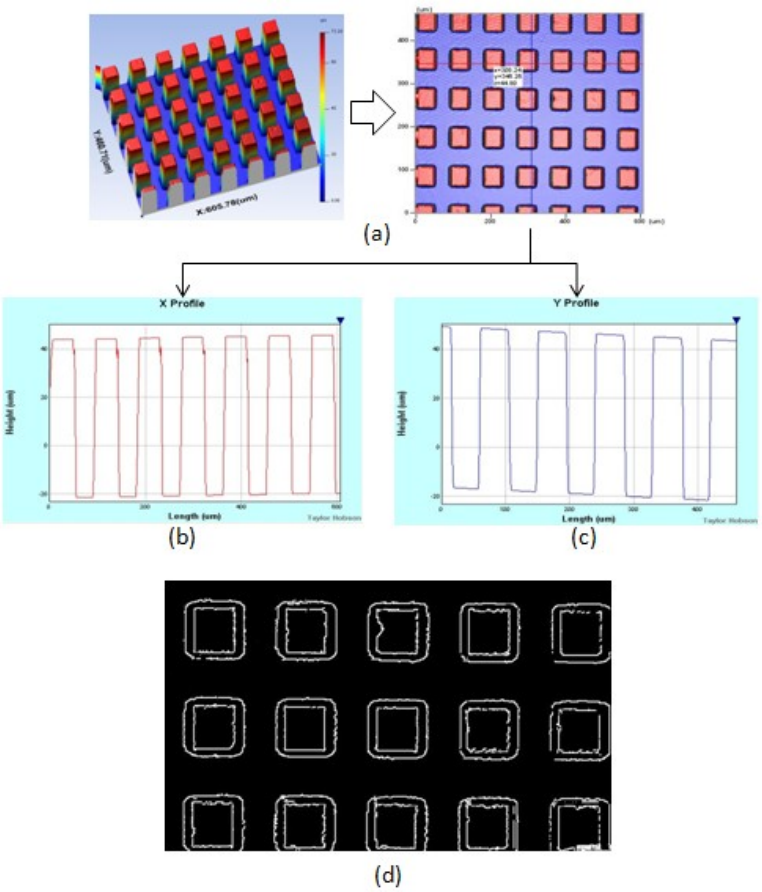

Figure 6-17 (a) measurement data of square-shape step etched Si sample (b) and (c) X profile and Y profile of the micro steps (d) extracted feature by sobel operator

Furthermore, Figure 6-18 shows a different sample, the measurement data of a laser etched landing zone of a hard disk surface, measured by CCI 3000. (b) and (c) are respectively the X profile and Y profile, (d) shows the feature extraction result by Sobel operator. Comparing these two figures of X and Y profiles it is clear micro steps of square-shape etched *Si* sample have a clear boundaries, and the sidewalls are almost vertical, so it means the image at this point changes "abruptly". For the laser etched landing zone of hard disk surface, the dominant features have a relatively "smooth" boundary. Because of the result of Sobel operator depends on the intensity change, so the result of latter is discontinuous and hard to recognized and is thus less useful.

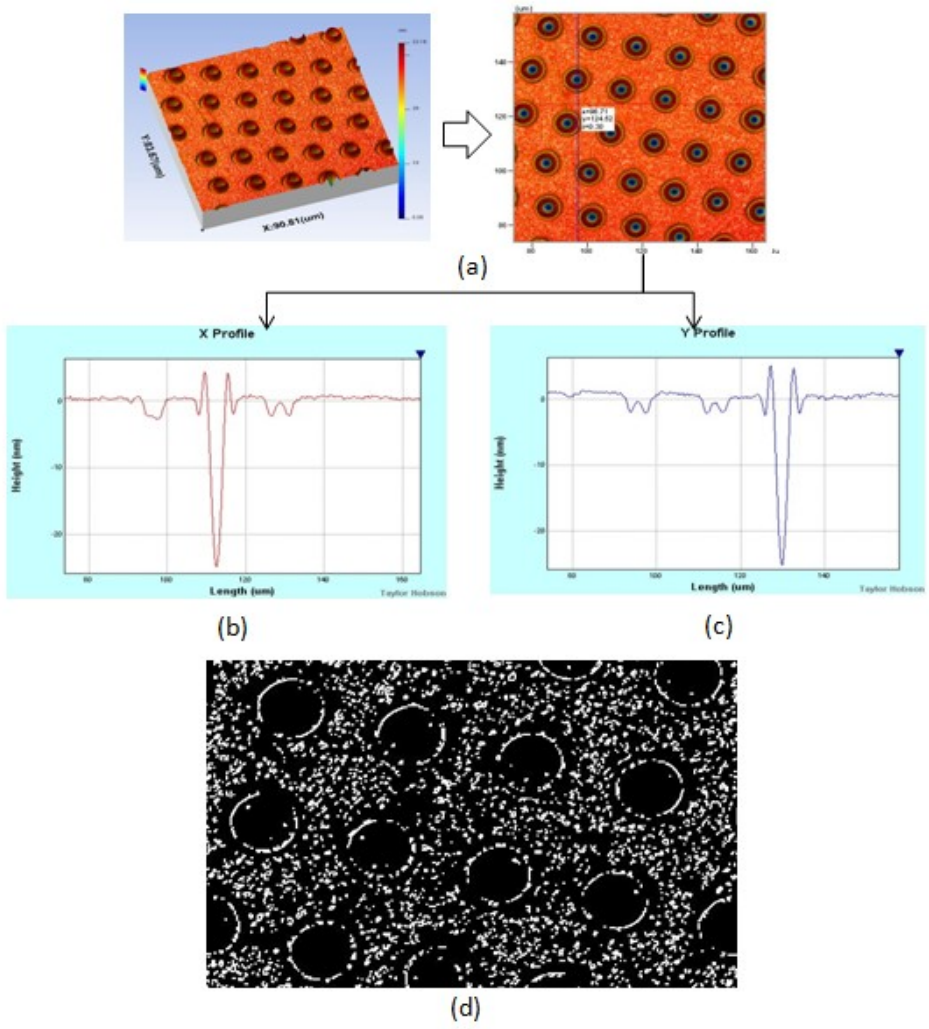

Figure 6-18 (a) measurement data of laser etched landing zone of hard disk surface (b) and (c) X profile and Y profile of the micro features (d) extracted feature by sobel operator

From the comparison, it is clear the Sobel operator is suitable to extract the micro step features and has difficulty when dealing with features which have a "smooth" boundary. In addition, edge detectors using the derivative will usually cause the noise. The Sobel operator has a smoothing effect. This means it has the ability to denoise. This property makes the Sobel operator one of the most commonly used edge detection methods for step type data sets.

For more complex data, it is necessary to extract the linear primitive shape from the edge detected image in locating a microstructure feature. Hough Transform (HT) is a

technique to find imperfect instances of objects within a certain class of shapes by a "voting procedure" [79]. Because of its global vision and robustness, it is recognized as a useful tool for graphic element extraction from images. The HT is not sensitive to noise, so it can be used in noisy data sets. Due to its heavy computation in the accumulation, HT has been used only in small-size images, but it is suitable for peak detection and line verification. It also can be used to extract straight-line-based primitives in images [79,103].

In a binary image, a contour line is defined as a linear primitive (LP) [97]. It can be seen as a continuous pixel wide line in an image. To extract these lines it is necessary first to know is their orientation. All the orientations of these linear primitive can be classified into horizontal, vertical and an undetermined classification. In Figure 6-19, a line segment is a line formed by LPs with similar features including orientation and length. Also, a straight line is considered as a straight-line segment that corresponds to a straight boundary of an object in the image [82].

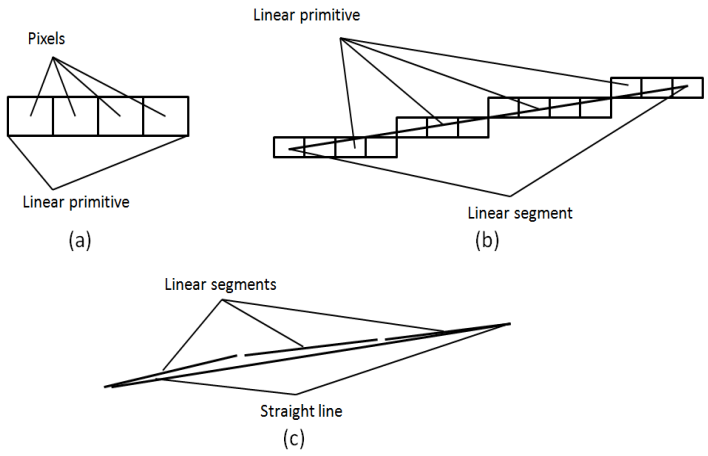

Figure 6-19 (a) linear primitive (b) line formed by LPs with similar features (c) straight line segment [82]

A cluster analysis method is applied to detect the linear primitives to line segments. Each line segment has a corresponding cluster. An LP with one neighboring LP is

considered as a start segment for cluster analysis. If an eight connected contour fragment has no such neighbors, the linear primitive with the max length will be chosen as the initial one. Linear primitives can be joined to the cluster when the following three conditions are satisfied. (1) Linear primitives are connected with cluster of line segment already found. (2) Linear primitives have the same orientation. (3) Deviation of their length from average LP length in a cluster does not exceed a given threshold. If the above conditions are not satisfied, then another cluster corresponding to another line is started. To reduce the sensitivity to noise, additional clustering conditions can be added to the algorithm. Finally, line segments can be extracted.

A linear least square algorithm is employed to optimize the extracted straight line. It will also decrease the random error of the merged neighboring linear primitives. Let S be a set of data points in the neighboring linear primitives. We denote the S to be of size K.

$$S = \left\{ \begin{pmatrix} x_i \\ y_i \end{pmatrix} l_i = 1, 2, ..., k \right\} \tag{6.14}$$

Based on the Hough transform, calculate the quadratic sum of distance between all points of the set and the rough straight line.

$$D = \sum_{i=1}^{k} \left(x_i \cdot \cos\theta + y_i \cdot \sin\theta - P \right)^2 \tag{6.15}$$

In the equation above, P is the normal length and θ is the included angle between the normal and the x axle. Minimize the error sum of squares, and the algorithm extracts the parameter θ and P to make the value of D to be minimal. Let

$$\frac{dD}{dP} = -2\sum_{i=1}^{k} \left(x_i \cdot \cos\theta + y_i \cdot \sin\theta \right) = 0 \tag{6.16}$$

$$\frac{dD}{d\theta} = -2\sum_{i=1}^{k}\left(x_i \cdot \cos\theta + y_i \cdot \sin\theta - p\right)\cdot\left(-x_i \cdot \cos\theta + y_i \sin\theta\right) \tag{6.17}$$

Then,

$$P = \bar{x} \cdot \cos\theta + \bar{y} \cdot \sin\theta \tag{6.18}$$

Where, $\bar{x}, \bar{y}$, are areal coordinates of the points-data set S , $\bar{x} = \frac{1}{k}\sum_{i=1}^{k} x_i, \bar{y} = \frac{1}{k}\sum_{i=1}^{k} y_i$.

Thus, $\frac{dp}{d\theta}$ is,

$$\begin{aligned}\frac{dP}{d\theta} &= \left(\sum_{i=1}^{k}\left(y_i^2 - x_i^2\right) - k\left(\bar{y}^2 - \bar{x}^2\right)\right)\cdot\sin\theta \\ &+\left(2\left(\sum_{i=1}^{k}\left(x_i \cdot y_i\right) - k\cdot\bar{x}\cdot\bar{y}\right)\right)\cdot\cos 2\theta = 0\end{aligned} \tag{6.19}$$

Let $u_i = \sum_{i=1}^{k}\left(y_i^2 - x_i^2\right) - k\left(\bar{y}^2 - \bar{x}^2\right), u_2 = 2\left(\sum_{i=1}^{k}\left(x_i y_i\right) - k\overline{xy}\right)$, then,

$$\theta = \begin{cases} \frac{1}{2}\tan^{-1}\left(-\frac{u_2}{u_1}\right), |u_1| \le |u_2| \\ \frac{1}{2}\tan^{-1}\left(-\frac{u_2}{u_1}\right), |u_1| \ge |u_2| \end{cases} \tag{6.20}$$

The parameter p can be obtained by substituting θ , thus the precise normal formula of the accurate straight line is obtained.

It should be noticed even small errors in the line extraction process will lead to a deviation in collinearity of extracted lines. Meanwhile, most structured surface features like the etched *Si* sample and micro MEMS sensor surface have rectangular features. Therefore, it is more reasonable to view the extracted objects as a rectangle represented by pairs of almost parallel lines. To do so, the first step is to define a rectangle in an image. A rectangle consists of pairs of parallel lines, or so-called quadrangles. The extracted quadrangles are approximated by rectangles or can be considered as potential rectangles of an image and four straight-lines can form a

quadrangle. Edge detectors mentioned above cannot ensure the contour connectivity at the corners and sometimes the two extracted lines do not intersect. Due to small deviations of straight-line extraction, the lines may not be parallel after extraction. So, rectangular objects of images can be recognized as two pairs of parallel lines, quadrangles or so called potential rectangles need to be replaced by a rectangle. For instance, there are two pairs of lines a and b, both of them are consist of almost parallel lines to form a quadrangle if the following conditions are satisfied. (1) Two straight lines are approximatly parallel. (2) The lengths are almost equal. (3) The perpendicular bisector should nearly be an identical straight line. In Figure 6-20, three parameters of vector p are presented. Let M be a linear vector space of all straight-line vectors p, and denote $p_i = (\theta_i, L_i, H_i)$. Respectively, θ is the slope of the straight line, L is the length of straight line and H is the distance from origin to the intersection between the x-axis and the perpendicular bisector.

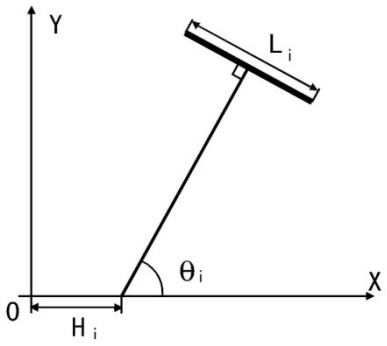

Figure 6-20 Three Parameters of vector P

Define a parameter vector D_{vector}, the distance between various vectors in vector space M is,

$$D_{vectors} = (P_i - P_j)^2 = (A_i - A_j)^2 + (L_i - L_j)^2 + (H_i - H_j)^2 \quad (6.21)$$

If the distance of two parameter vectors is smaller than a hypothesis threshold value, these two straight lines should be a pair of rectangular opposite sides.

To improve the precision of rectangular detection, the mutual spatial relationship of detected pairs of lines needs to be considered, also the rectangularity value needs to be calculated. It is the maximum value among distances between the intersection points and the closest endpoint of a corresponding line. Rectangularity values will be obtained for all intersections. The set of lines can be considered as a quadrangle only when the rectangularity value is less than the preset threshold. Average gap values and average distances between neighboring rectangular objects control the rectangularity value. In Figure 6-21, two parallel straight lines have been built. These lines pass the centre points of the original ones, and use the average slope of the original lines.

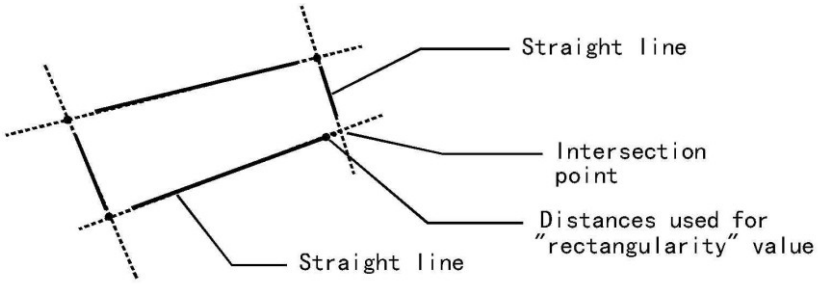

Figure 6-21 Calculation of rectangularity value

Figure 6-22, is a MEMS structured surface image, measured by a CCI 3000 and transferred to a grey-scale image. (b) shows the edges extracted by Sobel operator, obviously the edges of these surface features are clear but also leave some small curves and concaves. To effectively distinguish the functional area, it is necessary to extract straight lines in the image. (c) shows the result of topology detection, straight-line and rectangular areas have been detected and extracted.

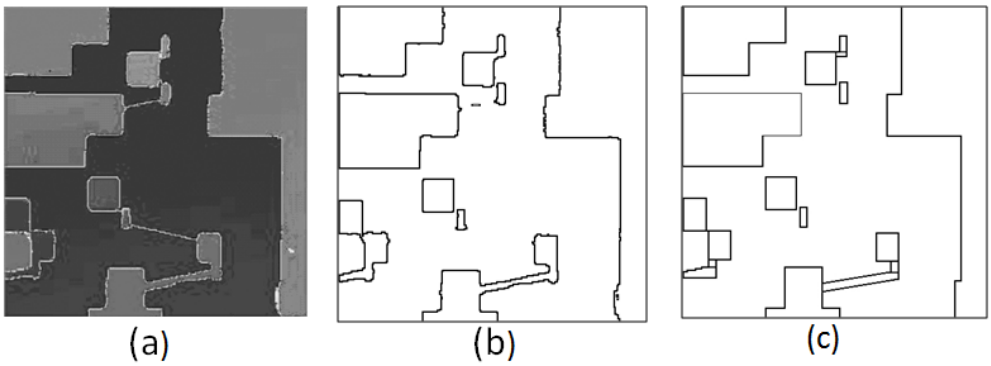

Figure 6-22 (a) Original grey-scale image of MEMS structured surface (b) Edges of micro features extracted by Sobel operator (c) Results of line merging and rectangular detection

6.4.2 Flexible methods of feature extraction

Flexible methods of feature extraction are based on different principles compare to low-level feature extraction techniques mentioned in section 6.4.1. For some of the micro/nano structured surface samples, the feature is far more complex than the others. To extract these features accurately and reliably, an initial scope setting and controllable processing are vital. Although, the low-level feature extraction approaches have the advantage of computation simplicity, but only image information can be obtained during the process. Therefore, features can be extracted by the low-level methods without any defined spatial relationships or shape information. Flexible methods use higher level information during the feature extraction process, for example, finding shapes by matching. However, this implies knowledge of a model, mathematical or template of the target feature. For some micro-scale features, it might be that the exact shape is unknown or that shape is difficult to parameterize, for example a chip pin surface. In this case, the flexible techniques based on active contours or so-called snake algorithm can evolve to the target solution [96].

Active contour algorithm uses a set of dynamic points to extract features. These points have been initially defined to enclose the target features. The whole process is

analogous to using a balloon to find a target feature. The balloon is placed to surround the feature. An initial contour is placed outside the target feature, and is then evolved to enclose it. After that, by taking air out of the balloon, making it smaller, the shape is found when the balloon stops shrinking, i.e. it fits the target shape. In this way, active contours arrange a set of points to describe a target feature, by enclosing it. Active contour method is expressed by an energy minimization process. The final result of feature extraction by this method will be a minimum of a formulated energy function with initial parameters [85]. The initial parameters will control the contour stretch and curve to fit the target features obtaining the edge information. Especially, it can deal with the small concaves which low-level feature extraction methods are not available.

An active contour represents a compromise between its own properties and image properties. The active contour own properties include the bend and stretch ability of contour. The major image property is the edge magnitude [90]. Respectively, the energy function is the addition of a function of the contour's internal energy, its image energy and the constraint energy. The energy functional E_{snake} is expressed as below.

$$E_{snake} = \int_{s=0}^{1} \left(E_{\text{int}}\left(v(s)\right) + E_{image}\left(v(s)\right) + E_{con}\left(v(s)\right) \right) ds \tag{6.22}$$

In the equation above, the energy functional consists of three parts, internal energy, image energy and constraint energy. E_{int} is determined by the initial parameter and the original arrangement of the contour points. Furthermore, it controls the behavior of the contour during the processing. E_{image} attracts the points close to the target feature to find the edge information. E_{con} allows higher-level information to control the snake's evolution, it also will affect the iterations and computation time of the whole

processing. The aim of the active contours is to evolve by minimizing the equation above. New contours are those with lower energy and are a better match to the target feature. A set of points $v(s)$ is expressed by the following equation.

$$\frac{dE_{snake}}{dv(s)} = 0 \tag{6.23}$$

The energy functionals are expressed in terms of functions of the active contours. The functions contribute to the snake energy according to values chosen for respective weighting coefficients. In this manner, the internal image energy, E_{int} can be defined as a weighted summation of first and second order derivatives around the contours.

$$E_{\text{int}} = \alpha(s)\left|\frac{dv(s)}{ds}\right|^2 + \beta(s)\left|\frac{d^2v(s)}{ds^2}\right|^2 \tag{6.24}$$

In the equation (6.22), $dv(s)/ds$, the first-order differential measures the energy due to contour stretching. $dv(s)/ds$ is the flexible energy. It implies a high rate of change in a specific region of the active contour. Meanwhile, $d^2v(s)/ds^2$, the second-order differential measures the energy due to bending. It is the curvature energy. In the equation, $dv(s)/ds$ is weighted by $\alpha(s)$. It controls the contribution of the flexible energy based on the initial parameters $d^2v(s)/ds^2$. The second-order differential is weighted by $\beta(s)$, which controls the contribution in the curvature energy due to point variation [76].

The image energy, E_{image} attracts the contour to target features using the low-level information, for example, the edge data and image brightness. It aims to pick the points with least contribution. The original formulation proposed energies are denoted

E_{line}, E_{edge} and E_{term}. It is means that lines, edges and terminations could contribute to the energy function. E_{line}, E_{edge} and E_{term} are respectively weighted by coefficients w_{line}, w_{edge} and w_{term}. The E_{image} is expressed by following equation.

$$E_{image} = w_{line}E_{line} + w_{edge}E_{edge} + w_{term}E_{term} \tag{6.25}$$

In the equation (6.23), E_{line}, the line energy can be initially defined as the image intensity at some specific points. For example, if black has a lower value than white, then the contour will be extracted to dark features. Altering the sign of w_{line} will attract the contour to brighter features. The edge energy can be calculated by an edge detection operator. The termination energy E_{term} can include the curvature of level image contours.

The greedy algorithm based snake method has the advantage of its simplicity and efficiency by its competitive performance. This greedy algorithm works directly in the energy term space of the snakes [91].

The greedy algorithm evolves the contour by repeatable iterations. The iteration is determined by the initial parameter setting. It uses a local neighborhood search around the contour points to pick new ones. The new points will have lower contour energy after iteration. By this manner, all the contour points have been evolved, until the final target feature is found. The greedy algorithm implements the energy minimization process as a purely discrete algorithm. The flowchart of greedy algorithm is illustrated in Figure 6-23.

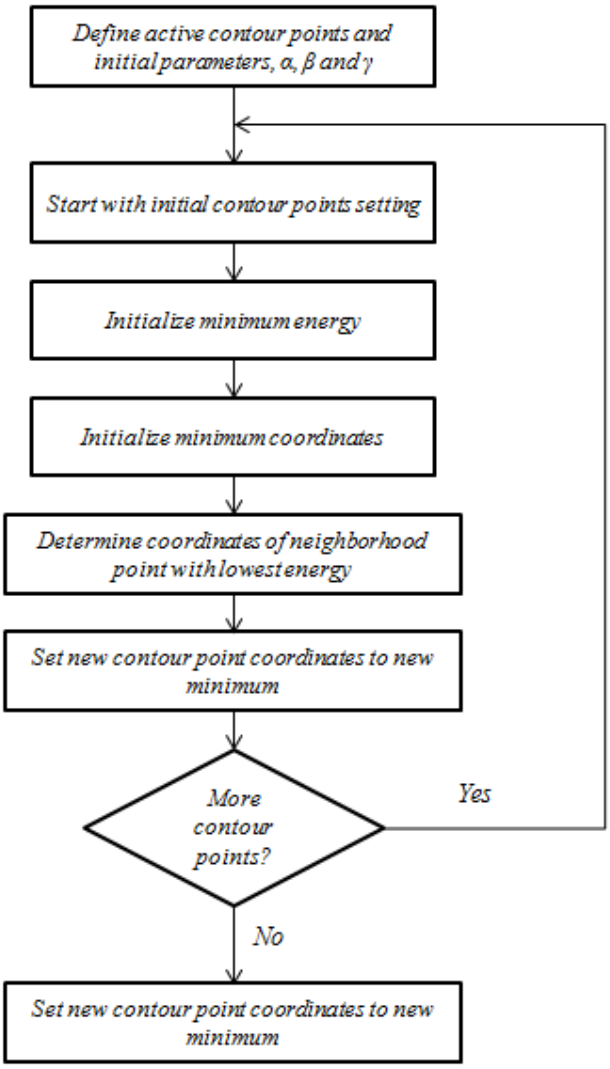

Figure 6-23 Flowchart of the greedy algorithm

According to the greedy snake proceedure, a deformable contour $V(s)$ has length s as a parameter under regular mapping as follows [95]. $V(s)=[x(s),y(s)]$ where $s\in\Omega$, the energy function has the form is expressed below.

$$E_{snake}[V(s)]=\int_{\Omega}\{E_{\text{int}}[V(s)]+P_{image}[V(s)]\}ds \tag{6.26}$$

The internal resistance term, E_{int} controls the regularity on the active contour by bending and stretching. It is defined as below [71].

$$E_{\text{int}}[V(s)]=\alpha(s)E_{cont}[V(s)]+\beta(s)E_{curv}[V(s)] \tag{6.27}$$

Where E_{cont} corresponds to a normalized first order continuity of the snake which makes it act like a membrane and encourages even spacing of its control points. E_{curve} corresponds to a normalized second order curvature of the snake which makes it act like a thin plate and discourages excessive bending of the curve. Adjusting the weights $\alpha(s)$ and $\beta(s)$ can control the mechanical properties. Setting $\beta(s)$ to zero at a point allows the snake to develop a corner [92,96]. Also, the image attraction term p_{image} will attract the active contour towards the micro surface features of interest. Lines, edges, and regions can be extracted, it is defined as following.

$$P_{image}\left[V(s)\right] = \gamma(s) P_{feature}\left[V(s)\right] \tag{6.28}$$

Where $p_{feature}$ corresponds to the desired features and is also to be normalized. $\gamma(s)$ is the weight that controls the attraction from the desired feature. However, there is no term for external although it would be possible to do so.

The deformable curve is then changed iteratively by minimizing its energy function E_{snake}. The final position corresponds to the minima E^*_{snake} of E_{snkae}

$$E^*_{snake} = \min\left\{E_{snake}\left[V(s)\right]\right\} = \min\int_{\Omega}\left\{E_{\text{int}}\left[V(s)\right] + P_{image}\left[V(s)\right]\right\} ds \tag{6.29}$$

Under the searching strategy based on the connective property of the eight neighbours of an image point, the greedy algorithm iteratively examines the neighbourhood of each contour point. It chooses the points in the neighbourhood having the minimum value for the energy as the new location of the point.

The greedy algorithm and its variation can be considered as a first attempt at achieving segmentation in a highly intuitive and efficient way. As illustrated in Figure 6-24, two micro-scale etched *Si* samples are extracted using the active contour based

on the greedy algorithms. Both of these samples are measured by Taylorsurf CCI 3000. (a), (d) is, respectively the raindrop-shaped micro features and rectangular-shaped micro features. (b), (e) shows the original input image, and (c) and (f) show the final result of an extracted feature after 800 iterations.

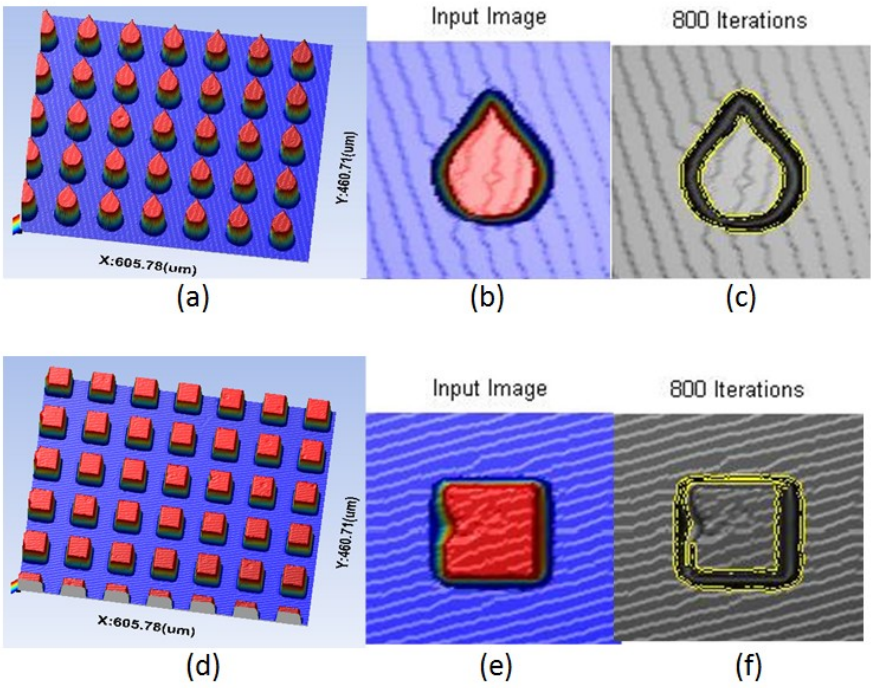

Figure 6-24 Two micro-scale features extracted by active contour based on greedy algorithm

Nevertheless, the greedy snake still has some of the same drawbacks as those of the original snakes. The energy minimization of the snake does not work properly if an initial contour is not close enough on its target feature in both position and shape. Due to its own internal resistance, the snake is prone to shrink if it is placed within a landscape that lacks image attracting forces, and it cannot extract small concave contours effectively.

The Geometric active contour (GAC) model is a further development of snake method. It is a combination of active contour and level set functions. Compared to active contour model, the GAC model is less sensitive to the initial contour point setting,

more anti-noising. Furthermore, it can extract surface features with blurred boundaries, especially for small concaves. The basic idea of GAC is to represent curve implicitly in a level set function. A contour of GAC is evolved by the level set function, this leads to contour attract on to the micro surface features of interest efficiently. Mathematically, a closed planar curve is defined as the zero level set of two-notional surface functions, or so-called level set functions. That is a point set with same function value. As the curve evolves, the topological changes can be automatically handled, so the contour may stretch or curve to fit the target features. Furthermore, the GAC model has a stable numerical result to improve the efficiency.

The level set formulation of active contour can be represented by following equation.

$$C(t) = \left\{ (x, y) \middle| \Phi(t, x, y) = 0 \right\} \tag{6.30}$$

The level set formulation is denoted by C. $\Phi(t, x, y)$ is the level set function. The evolution equation of Φ is expressed by the following equation [98]. F is the speed function. It is a key factor of contour evolution in surface feature extraction. It depends on level set function F and corresponding measurement data.

$$\frac{\partial \Phi}{\partial t} + F\left|\nabla \Phi\right| = 0 \tag{6.31}$$

Compared to the greedy algorithm, GAC has a better performance for the details of feature extraction due to its combination of level set function. During each evolution, the level set function Φ causes sharp shape points on the active contour. This leads to computation inaccuracies and to solve the problem. The function Φ can be defined as a signed distance function before evolution by a numerical scheme. This means the function F needs to be periodically re-initialized at every iterations. The re-initialization is a decision process of the level set method.

The re-initialization process is expressed by the following equation [21].

$$\frac{\partial \Phi}{\partial t} = sign(\Phi o)(1 - |\nabla \Phi|) \tag{6.32}$$

In the equation above, Φo is the original function before re-initialization while $sign(\Phi)$ is the sign function. During the evolution, if the original function is too "abrupt" on one side of the interface compared to the other side, the function Φ will move in the wrong direction from original function Φo. On the other hand, if the level set function is too far away from the $sign(\Phi)$, it is impossible to re-initialize the level set function by the $sign(\Phi)$.

In practical surface feature extraction, if the value of time step is not set small enough, it will cause great deviation from its value. The re-initialization process has been wildly used as a numerical control for curve evolution. It ensures the stability of contour during the iteration, meanwhile it makes the contours curve move towards the target features. However, the re-initialization process also brings about several problems. First of all, it is complicated in term of computation. Secondly, adjustments need to be carried out to re-initialize the level set function to a signed distance function according to different measurement samples. To overcome these disadvantages, the re-initialization process needs to be removed. To successfully extract features from the sample without any re-initialization, it is necessary to define an external energy. It controls the zero level contour curve movement toward the target feature. The external energy of a function $\Phi(x, y)$ can be defined by following equation.

$$\varepsilon_{g,\lambda,\nu}(\Phi) = \lambda L_g(\Phi) + \nu A_g(\Phi) \tag{6.33}$$

Where g is the edge indicator function, let I be the measurement sample, the definition is given below. G_σ is the Gaussian kernel with standard deviation σ.

$$g = \frac{1}{1+\left|\nabla G_\sigma * I\right|^2} \tag{6.34}$$

In equation (6.31), the term $L_g(\Phi)$ and $A_g(\Phi)$ are defined by the following equations.

$$L_g(\Phi) = \int_\Omega g\delta(\Phi)\left|\nabla\Phi\right| dxdy \tag{6.35}$$

And

$$A_g(\Phi) = \int_\Omega gH(-\Phi)\, dxdy \tag{6.36}$$

Therefore, the total energy function is given below.

$$\varepsilon(\Phi) = \mu P(\Phi) + \varepsilon_{g,\lambda,\nu}(\Phi) \tag{6.37}$$

The external energy $\varepsilon_{g,\lambda,\upsilon}$ controls the zero level set moving toward the features of interest. $\mu P(\Phi)$ is the internal energy, during the contour curve evolution, $\mu P(\Phi)$ reduces the deviation of the level set function from a signed distance function.

The steepest descent process for minimization of the functional ε is the following gradient flow [21].

$$\frac{\partial\Phi}{\partial t} = \mu\left[\Delta\Phi - div\left(\frac{\nabla\Phi}{\left|\nabla\Phi\right|}\right)\right] + \lambda\delta(\Phi)\, div\left(g\frac{\nabla\Phi}{\left|\nabla\Phi\right|}\right) + \nu g\delta(\Phi) \tag{6.38}$$

This gradient flow is the evolution equation of the level set function in this method. The time step parameter can be chosen to be much larger than the traditional level set methods. A greater time step parameter will reduce the computation time and speed up the contour curve evaluation. Meanwhile, if it is too large, it may cause inaccuracy in the target feature location. Therefore, the balance lies between the speed of the evolution and accuracy in boundary location [98,100].

Firstly, a chip pin structured surface feature extracted by the greedy algorithm is presented. Compared to the other structured surface, like drop-shaped and square-shape etched *Si* samples, chip pin surface has an irregular shape, and more importantly, most pin features have a blurry boundary and many of them are connected to the adjacent features. So, this specific property of chip pin surface leads to a great challenge for feature extraction and subsequent analysis for the single features on the surface. Low level feature extraction methods can hardly accomplish the extraction task for a chip pin surface. Figure 6-25 shows the extraction result using Sobel operator.

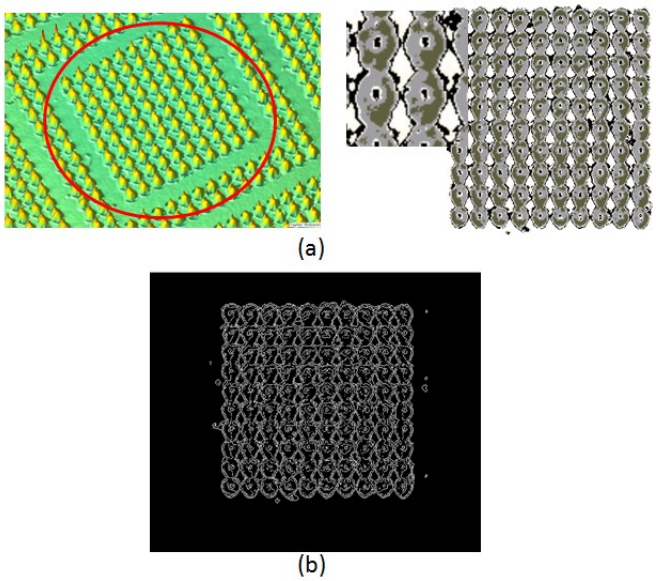

Figure 6-25 (a) Chip pin surface and local details of the features (b) Feature extraction result by Sobel operator

From the result, it is obvious that the extracted edges are connected. The active contour method has a more flexible technique to extract a single feature by defining the initial parameters before extraction. Figure 6-26 shows the same chip pin surface extracted by the greedy algorithm, (a) is the original measurement data and (b)-(d) are the results respectively after 20, 200 and 360 iterations. Compared to the Sobel

operator, the greedy algorithm has an ability to separate connected features and get a clear edge. So, it is useful for the chip pin surface and may be applicable to other complex feature extraction tasks.

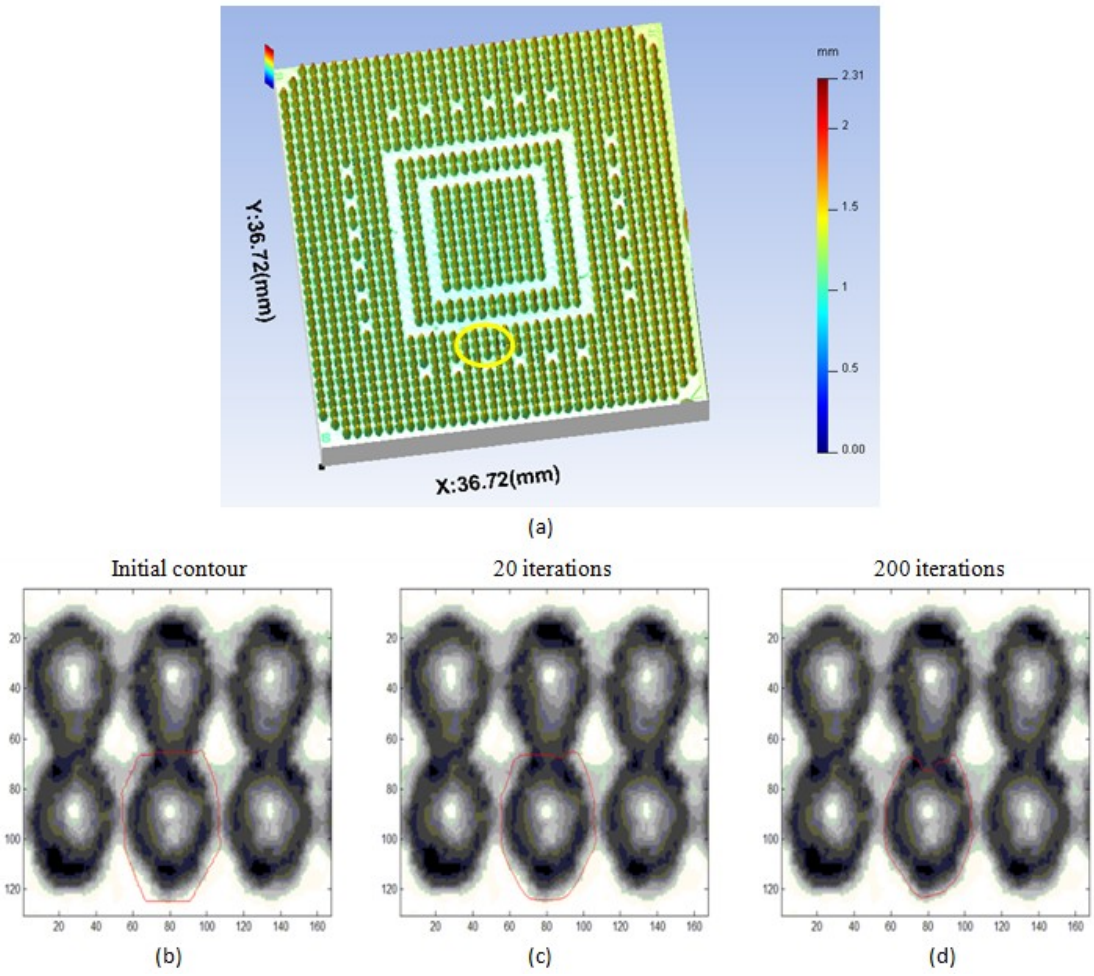

Figure 6-26 (a) Original measurement data micro-chip pin surface (b)-(d) Analysis results based on greedy algorithm, respectively after 20, 200 and 360 iterations

Another experiment result concerning laser etched landing zone shows the flexibility of the active contour method. The red pentagon in Figure 6-27 is firstly defined, and then the result after 310 iterations and the final result shown in (d).

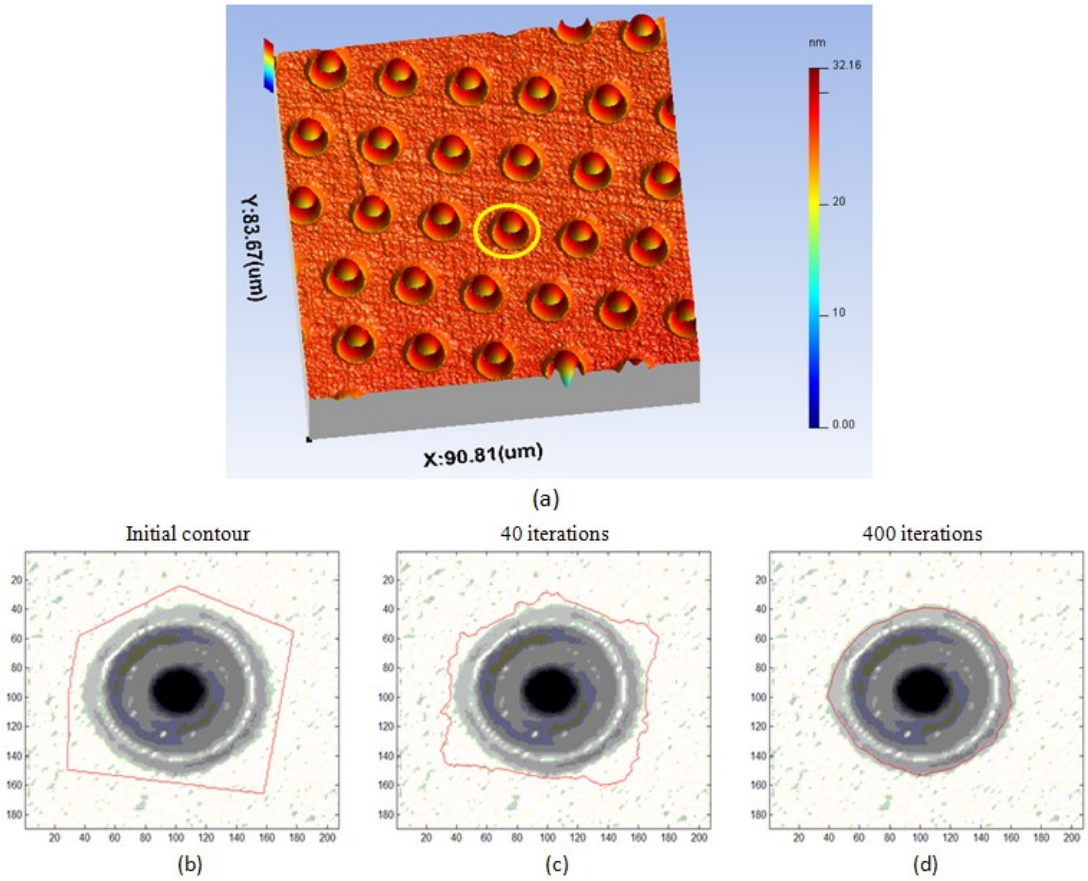

Figure 6-27 (a) Laser etched landing zone of hard disk surface (b-(d) Results respectively after 0, 150 and 310 iterations

As pointed out earlier, the GAC algorithm has its own advantages when compared to the greedy algorithm. Namely that is can handle small concaves of the features.

In Figure 6-28, a comparison of these two methods is shown. (a) is the measurement data of a square-shaped *Si* etched sample, notice the small concave in the yellow circle. (b) shows the result of greedy algorithm and (c) shows the result of GAC algorithm. From the experimental result, both greedy algorithm and GAC algorithm can extract the feature, and the latter is more precise at the small concave feature. A clear feature edge is obtained by GAC.

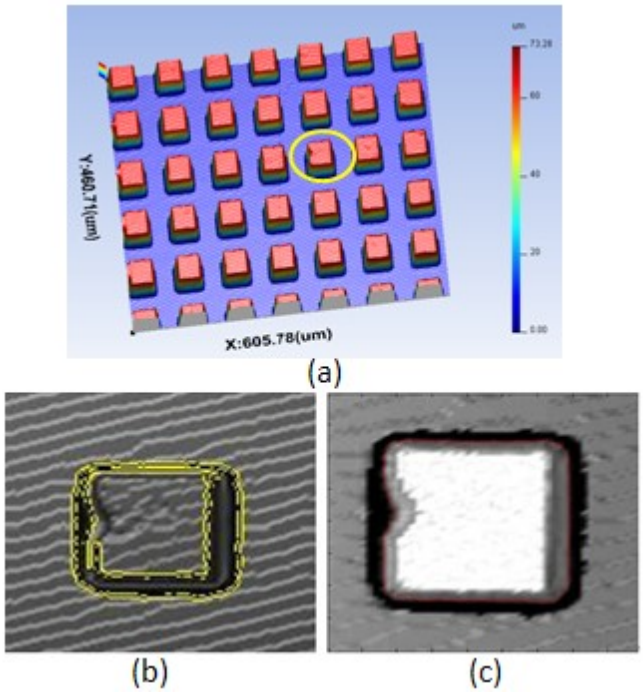

Figure 6-28 Comparison between the features extracted (a) measurement data of a square shaped Si etched sample (b) and (c) are the results extracted by greedy algorithm and GAC

As a hige-level feature extraction method, the active contour can also apply multi-feature extraction. However, more time is needed due to the complex computation. Firstly, an experimental result is shown in Figure 6-29, to extract two triangle-shaped *Si* etched features, the GAC algorithm needs 500 iterations. In (c) the red line shows the initially defined starting points, forming a square to frame the features which is selected. Furthermore, a larger area can be initially defined if more features are selected, and that will lead to more iterations. In the experiment, just two features need to demonstrate the multi-feature extraction ability of GAC algorithm. (d)-(f) shows the results respectively after 10, 200, 360 and 500 iterations.

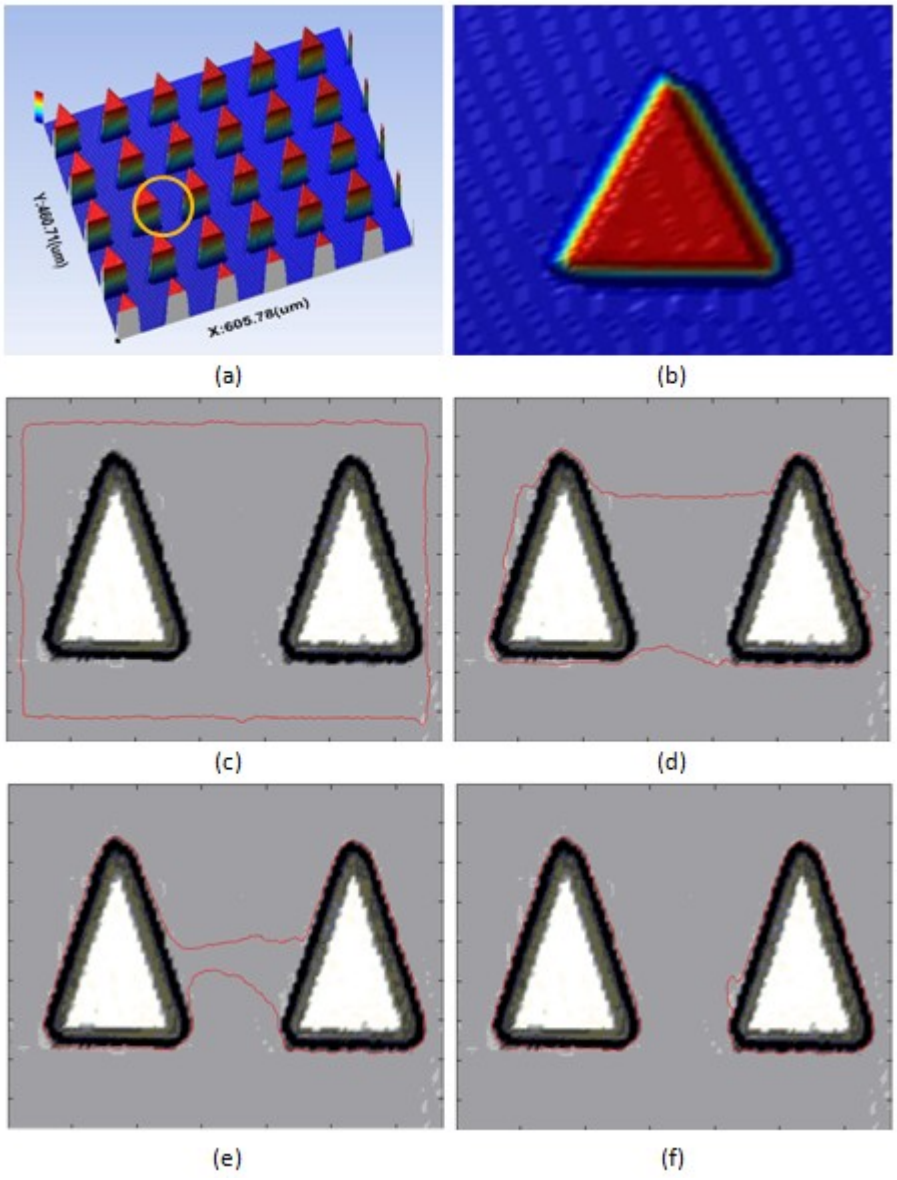

Figure 6-29 (a) Measurement data of an etched Si microstructure (b) Single triangular microstructure (c-f) Results of GAC, respectively after 20, 200, 360 and 500 iterations

Due to the algorithm simplicity of the low-level feature extraction technique, computation is not an important issue. However, for active contour based methods, computation must be considered before the algorithm applied, especially, for the multi-feature extraction. Until now, it is still a limitation of this method. In Table 6-2, triangular shaped etched *Si* sample is used for multi-feature extraction, iterations and computation time is listed below.

Table 6-2 Iterations and computation time for multi-feature extraction based on GAC algorithm

Feature amount	Iterations- GAC algorithm	Computation time- GAC algorithm
2	500	19s
5	1320	52s
10	2950	73s
20	6300	137s
50	14500	295s

Meanwhile, five different samples including triangular-shaped, square-shaped, octagon-shaped, drop-shaped etched *Si* sample have been used to test iterations and computation time based on GAC algorithm, as shown in Figure 6-30. Though the sharpes of these micro features are different, but the final results are similar. Iterations and computation time appears mainly dependent on the amount of the features to be extracted.

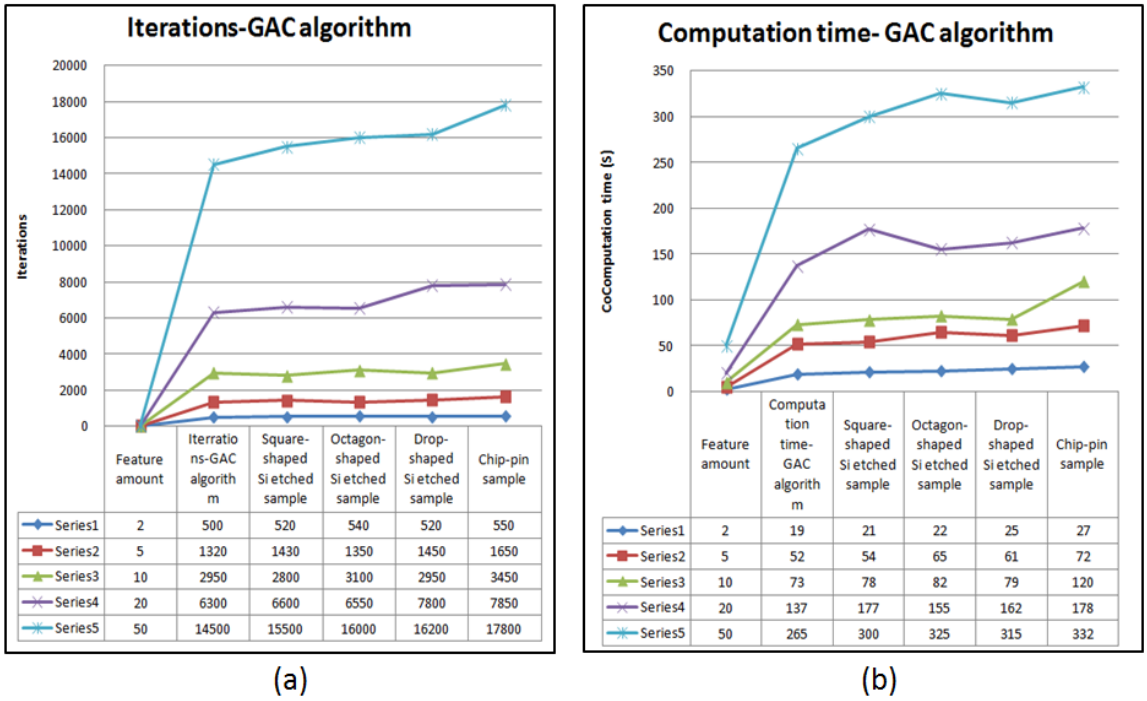

Figure 6-30 Iterations and computation time based on GAC algorithm

6.5 Conclusions

In this chapter, research concerning of surface data pre-processing processes has been presented and developed. Techniques of digital image processing have been successfully applied. For different noise types, complete denoising and data enhancement algorithms have presented. To extract the primaries of the surface, both low-level feature extraction algorithms and flexible methods of feature extraction have been studied and presented. A novel feature extraction technique based on active contour has been firstly developed for topography extraction and compared to the low-level feature extraction techniques. Furthermore, the results have been illustrated with case studies.

Chapter 7 Conclusions and future work

To fulfil the aim and objectives of this research project, several novel methods and techniques have been developed and applied. A number of theoretical analyses with experimental studies are presented. This chapter summarizes the major contributions of this project. The main conclusions from the work are summarized. Future work on micro/nano scale structured surface measurement and charaterisation is also discussed.

7.1 Summary of contributions

The primary contribution of this project is developing a novel flexible method of feature extraction. The traditional low-level feature extraction methods have clear disadvantages in complex micro feature analysis. Meanwhile, the flexible methods based on active contours are more sensitive to the details of micro features. The major superiorities of this technique are listed below.

- It is more sensitive compared to low-level feature extraction techniques and can handle small concaves of the surface structures.

- The starting regions can be flexibly divided by delimiting the original parameters. Also the extraction process is controllable by setting the numbers of iterations. It is effective in extracting the target features with non distinct boundaries.

The second contribution of this project is the development of a new micro structured surface classification system according to its functional properties and evaluation

requirements. Micro structured steps surfaces are presented in most of MEMS devices. Geometrical parameters have been developed and evaluation methods have been established for the micro structured steps according to the classification. For representative structured surface applications, micro fluidics, an evaluation framework is established. The evaluation methods and analysis techniques in this project have significance for micro structured surfaces manufacturing. The geometrical parameters can be used as the functional evaluation index. These methods are also applicable to other devices which have similar structured features.

7.2 Conclusions

In order to fulfill the aims and objectives of this project, a number of issues have been investigated and studied, including the establishment of metrology strategy and development of methodology for characterisation and evaluation of micro/nano scale structured surfaces. Experimental studies associated with theoretical analysis were performed. The main conclusions from this work are summarised in the following section.

The key factor of structured surfaces is their specific functions. A definite surface classification based on the survey of surface applications is necessary for the following measurement, characterisation and evaluation of micro/nano scale structured surfaces.

For structured surface measurement, the material, fabrication techniques, feature shape and dimensions of structured surface need to be investigated associated with the measurement range and resolution of surface measurement instruments.

Surface measurement instruments based on different principles have their advantages and limitations. A practical guide of measurement should consider both samples and instruments. Although most structured surfaces can be effectively measured by contacting stylus instruments, non-contacting optical method and scanning probe microscopes, there still are still many challenges in specific samples.

Establishment of a datum plane is the fundamental analysis for the following microstructure characterisation and evaluation. It is the identification of characteristic functional regions.

Geometrical parameters and evaluation methods for micro/nano scale structured surfaces have been developed associated with experimental analysis for micro fluidics. The methods are practicable to other structured surface applications in the same classification.

Flexible feature extraction algorithms based on active contours has better performance than conventional low-level feature extraction algorithms. It is more precise for small concave feature extraction. It can deal with both single feature and multiple features by its flexible initial region definition.

7.3 Future work

The research work presented in this thesis point to several directions for future work. Some issues need to be pursued are listed below for further investigation.

In this project, there are still a number of issues have not been completely studied. Some of the issues are listed below and needs further investigations.

As a new method to extract features form surface, active contour has a disadvantage of complex computation, especially for the multiple feature extraction. A more efficient initial region definition needs to be developed to meet the requirement of a practical analysis process. Testing of the algorithms against synthetically generated data sets, thus, allowing the techniques to be tested under extreme conditions.

As structured surface uses are developing rapidly, especially for MEMS applications, a large number of sample surfaces with different structured features need to be investigated. This will test the robustness and efficiency of the suggested methodologies.

More research studies need to be completed to establish a close relationship between evaluation parameters and surface manufacturing process to improve its functional performance. This could be especially true for large area structured surfaces produced by roll-to-roll techniques. Incorporate the developed active contour algorithms into user friendly software.

Reference

1. Whitehouse, D. J. (2003) *Handbook of Surface and Nanometrology*, pp:1-7.
2. Köhler, M and Fritzsche. W (2008). *Nanotechnology: An Introduction to Nanostructuring Techniques Nanotechnology,* pp:23-25.
3. Blunt, L., Jiang, X. and Scoott, P. (2005). *Advances in micro and nano-scale surface metrology. Key Engineering Materials*, ISSN 1013-9826, pp. 431-436.
4. Evans, C.J. and Bryan, B. J. (1999). "Structured", "Textured" or "Engineered" Surfaces. *CIRP Annals. Manufacturing Technology,* 48 (2) pp: 541-556.
5. P.M. Lonardo, D.A. Lucca and L.De Chiffre (2002). Emerging Trends in Surface Metrology. CIRP Annals. *Manufacturing Technology*, 51(2) pp:701-723.
6. Stout, K.J. and Blunt, L. (2001). A contribution to the debate on surface classifications random systematic, unstructured, structured and engineered. *International Journal of Machine Tools and Manufacture*, 41(13-14), pp. 2039-2044.
7. Grieve, D. J., Kaliszer, H. & Rowe, G. W. 1970 A "normal wear" process examined by measurements of surface topography. *CIRP Annals* 18(4), pp585 – 592.
8. Zorman, A.C. and Mehregany, M. (2004) Materials Aspects of Micro- and Nano-electromechanical Systems. *Handbook of Nonotechnology*, pp203.
9. Varadan, K.V., Vinoy, K. J. and Jose K.A. (2002) Chapter 2. MEMS Materials and Techniques. *RF MEMS and Their applications*, pp45-48.
10. Dorozhkin V.S. Bioceramics of calcium orthophosphates. (2009) *Biomaterials*, 31(7), pp1465-1485
11. Teague, E. C., Scire, F. E., Baker, S. M. & Jensen, S. W. 1982 Three-dimensional stylus profilometry. *Wear* 83, pp1-12.
12. C. Liu, Recent Developments in Polymer MEMS. (2007) *Advanced Materials*, 19(22), pp: 3783-3790.
13. E.A. Montanha, F.J. Pavinatto and Caseli (2010) Properties of lipophilic nucleoside monolayers at the air-water interface. *Colloids and Surfaces B: Biointerfaces*. 77(2), pp: 161-165.
14. Chen J., Li Q., Meng L. and Shuai Z. (2010) Theoretical study on self-assembly in materials. *Frontiers of Chemistry in China*. 5(1), pp 34-32.
15. Robert A. and Freitas J. (2008) Molecular Assembler. www.molecularassembler.com (09-11-2009).

16. Robert B. (2009) The fast-moving world of MEMS technology. *Assembly Automation*. 29(4), pp:313.
17. McCracken, W.J. (2008) Surface Characterization of Ceramed Composites and Environmental Sensitivity. *Ceramic Engineering and Science Proceedings*. 11(2), pp23-24.
18. R. Isermann, P. Balle. (1997) Trends in the application of model-based fault detection and diagnosis of technical processed. *Control Engineering Practice*. 5, pp:709-719
19. Lagunovshy, D. and Ablameyko, S. (1999) *Straight-line-based Primitive Extraction in Gray Scale Object Recognition,* pp:1005-1014
20. T. Ogino, (1997) Self-organization of nanostructures on Si wafers using surface structure control, *Surface Science*, 386, pp137.
21. X.M. He, H.D. Li, C.H. Liu, W.Z. Li, IBAD (1997) Processing of surface Coatings and Nanocrystalline Multi-layers, *Journal of Materials Processing Technology*, 63(12), 902-907.
22. A.M. Contreras, J. Grunes, X.-M. Yan, A. Liddle, G.A. Somorjai, (2005) Fabrication of platinum nanoparticles and nanowires by electron beam lithography (EBL) and nanoimprint lithography (NIL):compareison of ethylene hydrogenation kinetics, *Catalysis Letters*, 3(4), pp115-125.
23. M. Kass., A. Witkin, and D. Terzopoulos, Snakes: Active contour models (1988) *Int. J. Comput Vision*, 1(4), pp. 321-331.
24. D.Cremers, M. Rousson and R. Deriche, Areview of statistical approaches to level set segmentation: Integrating color, texture, motion and shape (2007) *Int. J. Comput. Vision*, 72(2), pp. 295-313.
25. L.D. Cohen and I. Cohen, (1993) Finite-element methods for active contour models and balloons for 2-D and 3-D images IEEE Trans. *Pattern Anal. Mach. Intell*. 15(11),pp:1131–1147.
26. R. Ronfard, (1994) Region-based strategies for active contour models, *Internat J. Comput. Vision* 13 (2), pp.229–251.
27. D.J. Williams, M. Shah, A fast algorithm for active contours and curvature estimation, *CVGIP: Image Understanding* 55 (1), pp.14–26. 1992.
28. Y.Y. Wong, P.C. Yuen, C.S. Tong, (1998) Segmented snake for contour detection, *Pattern Recognition* 31 (11), pp.1669–1679.
29. S. Osher, J. A. Sethian (1998) Fronts propagating with curvaturedependent speed: algorithms based on Hamilton-Jacobi formulations, *J. Comp. Phys.*,79, pp.12-49.
30. J. A. Sethian, (1999) Level set methods and fast marching methods, Cambridge: Cambridge University Press, pp:122-132.
31. F. Leymarie, M.D. Levine, (1993) Racking deformable objects in the plane using an active contour model, IEEE Trans. *Pattern Anal. Mach. Intell.* 15 (6), pp.617–634.

32. Blunt, L.A., Jiang, X.Q. (2000) Three dimensional measurement of the surface topography of ceramic and metallic orthopaedic joint prostheses, *Journal of Materials Science: Materials in Medicine*, 11 (4), pp. 235–246.
33. X.Q. Jimg, L. Blunt and K.J. Stout. (2000) Development of a lifting wavelet representation for surface characterisation, *Proc. Roy. Soc. Lond*. A 456 (2000) pp1–31.
34. Jiang Xj, Whthehouse DJ. (2010)Technological shifts in surface metrology. *CIRP Annals - Manufacturing Technology*, pp:3-4.
35. X.Q. Jimg and L. Blunt. (2004) Third generation wavelet for the extraction of morphological features from micro and nano scalar surfaces, *Wear,* 257 pp:1235–1240.
36. De Chiffre L, Kunzmann H, Peggs GN, Lucca DA (2003) Surfaces in Precision Engineering, Microengineering and Nanotechnology. *Annals of the CIRP,* 52(2), pp:561–578.
37. Kingsbury N (2001) Complex Wavelets for Shift Invariant Analysis and Filtering of Signals. *Journal of Applied and Computational Harmonic Analysis* 10(3) pp:234–253.
38. Goupillard, P., Grossmann, A. and Morlet, J. (1984). Cycle-Octave and related transforms in seismic signal analysis. *Geoexploration*, 23, pp:85-102.
39. Yamada, M. and Ohkitani, K. (1991). An identification of energy cascade in turbulence by orthonormal wavelet analysis. *Prog. Theor. Phys.* 86(4), pp799-8.
40. Lonardo P.M. (1996) Progress in 3D Surface Microtopography Characterization, *Annals of the CIRP*, 45(2) pp589-598.
41. Blunt, L., X. Jiang, and P.J. Scott, Advances in micro and nano-scale surface metrology. Key Engineering Materials, 2005. 295: pp. 431-436.
42. ISO 17450-1. (2011) Geometrical Product Specification (GPS) – General Concepts – Part 1: Model for Geometrical Specification and Verification, *International Organization for Standardization*, pp345-356.
43. Jiang, JB, CE Cheung, S. To, KW Cheng, K. Wang, and WB Lee. (2006) Design and fabrication of freeform reflector for automotive headlamp. Pp:232-234.
44. Taylor, W., (1905), An Improvement in Golf Balls, British Patent Office, *British Patent* No. 18 688, pp2-4.
45. Yamaguchi, T., H. Namatsu, M. Nagase, K. Yamazaki, and K. Kurihara, Nanometer-scale linewidth fluctuations caused by polymer aggregates in resist films. *Applied Physics Letters*, 1997. 71: pp. 2388.
46. Suh NP, Saka N (1987) Surface Engineering. *CIRP Annals Manufacturing Technology* 36(1), pp:403–408.
47. Stout KJ (1998) Engineering Surfaces – a Philosophy of Manufacture (a Proposal for Good Manufacturing Practice). Proceedings of the Institution of Mechanical Engineers Part B *Journal of Engineering Manufacture* 212(3), pp:169–174.

48. Moon, S., N. Lee, and S. Kang, (2003) Fabrication of a microlens array using micro-compression molding with an electroformed mold insert. *Journal of Micromechanics and Microengineering*, 13, pp. 98.
49. Minsky, M. (1988) Memoir on inventing the confocal microscope. *Scanning*, 10, pp:128-138.
50. Shin, J., G. Han, Y. Ma, K. Moloni, and F. Cerrina, (2001) Resist line edge roughness and aerial image contrast. *Journal of Vacuum Science & Technology B: Microelectronics and Nanometer Structures*, 19, pp: 2890.
51. Vernhes, P., J. Bloch, C. Mercier, A. Blayo, and B. Pineaux, (2008) Statistical analysis of paper surface microstructure: A multi-scale approach. *Applied Surface Science*, 254(22), pp. 7431-7437.
52. Kang, W.J., E. Rabe, S. Kopetz, and A. Neyer, (2006) Novel exposure methods based on reflection and refraction effects in the field of SU-8 lithography. *Journal of Micromechanics and Microengineering*, 16: pp: 821.
53. Rubin, D.M., (2004) A simple autocorrelation algorithm for determining grain size from digital images of sediment. *Journal of Sedimentary Research*, 74(1): p:160.
54. Zhang, J., M.B. Chan-Park, and S.R. Conner, (2004) Effect of exposure dose on the replication fidelity and profile of very high aspect ratio microchannels in SU-8. Lab Chip, 4(6), pp: 646-653.
55. Salonen, I., C. Icheln, and P. Vainikainen. A New Method for Array Pattern Correction, *Journal of Sedimentary Research*, 72(1): p:230-232.
56. Nguyen, N.T. and S.T. Wereley, (2002) *Fundamentals and applications of microfluidics*. Artech House Publishers, pp: 118-121.
57. Kittilsland, G., G. Stemme, and B. Norden, (1990) A sub-micron particle filter in silicon. *Sensors and Actuators A: Physical*, 23(1-3): pp: 904-907.
58. Kim, D.S., I.C. Chang, and S.W. Kim, (2002)Microscopic topographical analysis of tool vibration effects on diamond turned optical surfaces. *Precision Engineering*, 26(2), pp: 168-174.
59. Ballard, D.H., (1998) Generalizing the Hough transform to detect arbitrary shapes. *Pattern recognition*, 13(2): pp: 111-122.
60. Xu, L., E. Oja, and P. Kultanen, (2001) A new curve detection method: randomized Hough transform (RHT). *Pattern Recognition Letters*, 11(5), pp: 331-338.
61. Chen, Jackie, Weisong Wang, Ji Fang, and Kody Varahramyan, (2004) Variable-focusing microlens with microfluidic chip. *Journal of Micromechanics and Microengineering*, 14(5), pp: 675-680.
62. Misumi, Ichiko, Gaoliang Dai, Mingzi Lu, Osamu Sato, Kentaro Sugawara, Satoshi Gonda, Toshiyuki Takatsuji, Hans-Ulrich Danzebrink, and Ludger Koenders, (2002) Bilateral comparison of 25 nm pitch nanometric lateral scales for metrological scanning probe microscopes. *Measurement Science and Technology*, 21(3): pp: 035105.

63. Dai, G, H Wolff, F Pohlenz, HU Danzebrink, and G Wilkening, (2006) Atomic force probe for sidewall scanning of nano-and microstructures. *Applied Physics Letters*, 88, pp: 171.
64. Lounaci, Malika, Yong Chen, and Pascal Rigolet, (2010) Channel height dependent protein nucleation and crystal growth in microfluidic devices. *Microelectronic Engineering*, 87(5-8), pp: 750-752.
65. Wunnicke, O., A. Hennig, K. Grundke, M. Stamm, and G. Czech. (2002) *Surface properties and topography of 193-nm resist after exposure and development*, pp: 45-48.
66. Li, S., Z. Xu, A. Mazzeo, D.J. Burns, G. Fu, M. Dirckx, V. Shilpiekandula, X. Chen, N.C. Nayak, and E. Wong. (2008) *Review of production of microfluidic devices: material, manufacturing and metrology*,pp:119-121.
67. Bora, CK, EE Flater, MD Street, JM Redmond, MJ Starr, (2005) RW Carpick, and ME Plesha, Multiscale roughness and modeling of MEMS interfaces. Tribology Letters, 19(1), pp: 37-48.
68. Karrholm, J., Nivbrant, B., Thanner, J., Anderberg, C. (2000) *Radiostereometric evaluation of hip implant design and surface finish: micromotion of cemented femoral stems*. Scientific exhibit presented at the 67th Annual Meeting of the American Academy of Orthopaedic Surgeons, Orlando, USA, March 2000, pp. 1–14.
69. Salonen, I., C. Icheln, and P. Vainikainen. A New Method for Array Pattern Correction, *Journal of Sedimentary Research*, 72(1), p:235-238.
70. Majumdar, A. and B. Bhushan, (1990) Role of fractal geometry in roughness characterization and contact mechanics of surfaces. *Journal of Tribology*,112, pp: 205.
71. Kittilsland, G., G. Stemme, and B. Norden, (1990) A sub-micron particle filter in silicon. *Sensors and Actuators A: Physical*, 23(1-3), pp: 904-907.
72. Korniss, G., MA Novotny, H. Guclu, Z. Toroczkai, and P.A. (1990) Rikvold, Suppressing roughness of virtual times in parallel discrete-event simulations. *Science*, 299(5607), pp: 677.
73. Whitehouse, DJ and MJ Phillips, (1992) Two-dimensional discrete properties of random surfaces. Philosophical Transactions of the Royal Society of London. Series A, *Mathematical and Physical Sciences*, 305(1490): pp: 441.
74. Peucker, T.K. and D.H. Douglas, (1975) Detection of surface-specific points by local parallel processing of discrete terrain elevation data. Computer Graphics and Image Processing, 4(4), pp: 375-387.
75. Lee, T.W. and S.V. Pabbisetty, (1997) Microelectronic failure analysis: Desk reference. 3, *ASM International*, pp:21-23.
76. Fu, J and V Tsai, (1999) Algorithms for calculating single-atom step heights. *Nanotechnology*, 10, pp: 428.
77. ISO 5436:1985. Calibration specimens stylus instruments types，calibration and use of specimens. Pp:21.

78. Cohen, I., L.D. Cohen, and N. Ayache, (1991) Introducing deformable surfaces to segment 3D images and infer differential structures. *Microelectronic Engineering*, 87(5-8), pp:21-24.
79. Cohen, I., L.D. Cohen, and N. Ayache, (1992) Using deformable surfaces to segment 3-D images and infer differential structures. *CVGIP: Image understanding*, 56(2), pp: 242-263.
80. Scott, P.J., (2001) An algorithm to extract critical points from lattice height data. *International Journal of Machine Tools and Manufacture*, 41(13-14), pp: 1889-1897.
81. Scott, P.J., (2004) Pattern analysis and metrology: the extraction of stable features from observable measurements. *Proceedings of the Royal Society of London. Series A: Mathematical, Physical and Engineering Sciences*, 460(2050), pp: 2845.
82. Loughin, S., RH French, LK Noyer, WY Ching, and YN Xu, (1996) Critical point analysis of the interband transition strength of electrons. *Journal of Physics D: Applied Physics*, 29, pp: 1740.
83. Morse, S.P., (1968) A mathematical model for the analysis of contour-line data. *Journal of the ACM (JACM)*, 15(2), pp: 205-220.
84. Bennett, J.M., (1985) Comparison of instruments for measuring step heights and surface profiles. *Applied Optics*, 24(22), pp: 3766-3772.
85. Koening, RG, RG Dixson, J Fu, BT Renegar, TV Vorburger, VW Tsai, and MT Postek Jr. (1999) Step-height metrology for data storage applications. *Nanotechnology*, 15, pp: 34-42.
86. Muralikrishnan, B. and J. Raja, (2009) Computational surface and roundness metrology. *Journal of Sedimentary Research*, 79(2), pp:25-38.
87. Schröder, P. and W. Sweldens. (1995) Spherical wavelets: Efficiently representing functions on the sphere. *Microelectronic Engineering*, 57(5), pp:23-24.
88. Hu, S., E.A. Hoffman, and J.M. Reinhardt, (2006) Automatic lung segmentation for accurate quantitation of volumetric X-ray CT images. *Medical Imaging*, 20(6), pp: 490-498.
89. Goo, J.M., T. Tongdee, R. Tongdee, K. Yeo, C.F. Hildebolt, and K.T. Bae, (2005) Volumetric Measurement of Synthetic Lung Nodules with Multi–Detector Row CT: Effect of Various Image Reconstruction Parameters *Journal of Sedimentary Research*, 56(1): p:235-238.
90. Precioso, F., M. Barlaud, T. Blu, and M. Unser, (2005) Robust real-time segmentation of images and videos using a smooth-spline snake-based algorithm. *Image Processing*, 14(7), pp: 910-924.
91. Bode, W., F.X. Gomis-Rüth, and W. Stöckler, Astacins, serralysins, (1993) snake venom and matrix metalloproteinases exhibit identical zinc-binding environments and topologies and should be grouped into a common family, the metzincins'. FEBS letters, 331(1), pp:134-140.
92. Vincent, L. and P. Soille, (1991) Watersheds in digital spaces: an efficient algorithm based on immersion simulations. IEEE transactions on pattern analysis and machine intelligence, 13(6), pp: 583-598.

93. Stauffer, J.M., (2003) Network of Excellence in Multifunctional Microsystems Europractive-Microsystems Service, *MEMS Accelerometers for Production Applications*, 232(1-2) pp: 16.
94. Blunt, Liam and Xiangqian Jiang, (2003) *Advanced techniques for assessment surface topography*, pp:355.
95. Xu, L., E. Oja, and P. Kultanen, (2001) A new curve detection method: randomized Hough transform (RHT). *Pattern Recognition Letters*, 11(5), pp: 331-338.
96. Zahouani, H., (1998) Spectral and 3D motifs identification of anisotropic topographical components. Analysis and filtering of anisotropic patterns by morphological rose approach. *International Journal of Machine Tools and Manufacture*, 38(5-6), pp: 615-623.
97. Barré, F. and J. Lopez, (2000) Watershed lines and catchment basins: a new 3D-motif method. *International Journal of Machine Tools and Manufacture*, 40(8): pp: 1171-1184.
98. Barré, F. and J. Lopez, (2001) On a 3D extension of the MOTIF method (ISO 12085). *International journal of machine tools & manufacture*, 41(13-14), pp: 1873-1880.
99. Mezghani, S. and H. Zahouani, (2004) Characterisation of the 3D waviness and roughness motifs. *Wear*, 257(12): pp: 1250-1256.
100. Scott, P.J., (2003) Novel area characterisation techniques. Advanced Techniques for Assessment Surface Topography: Development of a Basis for 3D Surface Texture Standards *International Journal of Machine Tools and Manufacture*, 41(13-14), pp: 1889-1897.
101. Edenfeld, D, AB Kahng, M Rodgers, and Y Zorian, (2003) Technology roadmap for semiconductors. *Microelectronic Engineering,* 37(1), pp: 47-56.
102. Meli, F. and R. Thalmann, (1998) Long-range AFM profiler used for accurate pitch measurements. *Measurement Science and Technology*, 9, pp: 1087.
103. Bhushan, Bharat and Yong Chae Jung, (2006) Micro- and nanoscale characterization of hydrophobic and hydrophilic leaf surfaces. *Nanotechnology*, 17(11), p. 2758-2772.
104. Hansen, H.N., K. Carneiro, H. Haitjema, and L. De Chiffre, (2006) Dimensional micro and nano metrology. *CIRP Annals-Manufacturing Technology*, 55(2), pp: 721-743.
105. Chen, X., J. Raja, and S. Simanapalli, (1995) Multi-scale analysis of engineering surfaces. *International Journal of Machine Tools and Manufacture*, 35(2), pp: 231-238.
106. Jiang, XQ, L. Blunt, and KJ Stout, (2000) Development of a lifting wavelet representation for surface characterization. *Proceedings of the Royal Society of London. Series A: Mathematical, Physical and Engineering Sciences*, 456(201), pp: 2283.
107. Jiang, XQ, L. Blunt, and KJ Stout, (1999) Three-dimensional surface characterization for orthopaedic joint prostheses. *Proceedings of the Institution of Mechanical Engineers, Part H: Journal of Engineering in Medicine*, 213(1), pp: 49-68.
108. Maboudian, R., (1998) Surface processes in MEMS technology. *Surface Science Reports*, 30(6-8), pp: 207-269.
109. Brown, G.C. and R.J. Pryputniewicz, (2000) New test methodology for static and dynamic shape measurements of microelectromechanical systems. *Optical Engineering*, 39, pp: 127.

110. Dai, Gaoliang, Helmut Wolff, Thomas Weimann, Min Xu, Frank Pohlenz, and Hans-Ulrich Danzebrink, (2007) Nanoscale surface measurements at sidewalls of nano- and micro-structures. 2004
111. Garnaes, J, N Kofod, A Kühle, C Nielsen, K Dirscherl, and L Blunt, (2003) Calibration of step heights and roughness measurements with atomic force microscopes. *Precision Engineering*, 27(1): pp: 91-98.
112. Nussbaum, P., R. Völkel, H.P. Herzig, M. Eisner, and S. Haselbeck, (1997) Design, fabrication and testing of microlens arrays for sensors and microsystems. Pure and Applied Optics, *Journal of the European Optical Society Part A*, 6: pp: 617.
113. Jean-Michel, S. (2004) Market opportunities for advanced MEMS accelerometers and overview of actual capabilities vs. required specifications. *Microelectronic Engineering,* 37(1), pp: 47-56.
114. Tanaka, M., (2007) An industrial and applied review of new MEMS devices features. *Microelectronic Engineering*, 84(5-8), pp: 1341-1344.
115. Komori, M., H. Uchiyama, H. Takebe, T. Kusuura, K. Kobayashi, H. Kuwahara, and T. Tsuchiya, (2008) Micro/nanoimprinting of glass under high temperature using a CVD diamond mold. *Journal of Micromechanics and Microengineering*, 18, pp: 53.
116. Knauss, W.G., I. Chasiotis, and Y. Huang, (2003) Mechanical measurements at the micron and nanometer scales. *Mechanics of materials*, 35(3-6), pp: 217-231.
117. McWaid, TH, TV Vorburger, J. Fu, JF Song, and E. Whitenton, (1994) Methods divergence between measurements of micrometer and sub-micrometer surface features. *Nanotechnology*, 5, pp: 33.
118. Misumi, Ichiko, Satoshi Gonda, Qiangxian Huang, Taeho Keem, Tomizo Kurosawa, Akihiro Fujii, Nahoko Hisata, Takeshi Yamagishi, Hirohisa Fujimoto, Ken Enjoji, Sunao Aya, and Hiroaki Sumitani, (2005) Sub-hundred nanometre pitch measurements using an AFM with differential laser interferometers for designing usable lateral scales. Measurement Science and Technology, 16(10): pp: 2080-2090.
119. Nussbaum, P., R. Völkel, H.P. Herzig, M. Eisner, and S. Haselbeck, (1997) Design, fabrication and testing of microlens arrays for sensors and microsystems. *Pure and Applied Optics: Journal of the European Optical Society Part A*, 6, pp: 617.
120. Jean-Michel, S.(2004) Market opportunities for advanced MEMS accelerometers and overview of actual capabilities vs. required specifications. *Precision Engineering*, 27(1): pp: 91-98.
121. Tanaka, M., (2007) An industrial and applied review of new MEMS devices features. *Microelectronic Engineering*, 84(5-8), pp: 1341-1344.
122. Komori, M., H. Uchiyama, H. Takebe, T. Kusuura, K. Kobayashi, H. Kuwahara, and T. Tsuchiya, (2008) Micro/nanoimprinting of glass under high temperature using a CVD diamond mold. Journal of Micromechanics and Microengineering, 18, pp: 13.

123. Silverbrook, K., (2001) Inkjet printhead having a self aligned nozzle. *Journal of Micromechanics and Microengineering*, 18, pp: 53.
124. Wicht, H. and J. Bouchaud, (2009) NEXUS market analysis for MEMS and microsystems III 2005-2009. *Setting the pace for micro assembly solutions*, pp 33.
125. Gupta, T. and AH Jayatissa. (2003) Recent advances in nanotechnology: key issues & potential problem areas. *Wear*, 257(12): pp: 1250-1256..
126. Leach, Richard, Derek Chetwynd, Liam Blunt, Jane Haycocks, Peter Harris, Keith Jackson, Simon Oldfield, and Simon Reilly, (2006) Recent advances in traceable nanoscale dimension and force metrology in the UK. *Measurement Science and Technology*, 17(3), pp: 467-476.
127. Bao, M. and W. Wang, (1996) Future of microelectromechanical systems (MEMS). S*ensors and Actuators A: Physical*, 56(1-2): pp: 135-141.
128. Eloy, JC, (2007) Status of the MEMS Industry: Evolution or MEMS Markets and of the Industrial Infrastructure. *Sensors & Transducers Journal*, 86(12): pp: 1771-1777.
129. Maboudian, R., (1998) Surface processes in MEMS technology. *Surface Science Reports*, 30(6-8), pp: 207-269.
130. Jiang, Xiang, Scott, Paul J., Whitehouse, D.J. and Blunt, Liam (2007) Paradigm shifts in surface metrology. Part II. The current shift**.** *Proceedings of the Royal Society, A*, 463 (2085). pp. 2071-2099.
131. Loannis Pitas, Anastasios N. Venetsanopouls (2001) Nonlinear Digital Filters: Principles and Applications. *The Springer International Series in Engineering and Computer Science*, 84, pp 63-64.